Development and Application of Simplified Methods for Analysis of Floors under Human-induced Vibrations

by

Rahul Saini

A thesis submitted to the Faculty of Graduate and Postdoctoral Affairs in partial fulfillment of the requirements for the degree of

Master of Applied Science

in

Civil Engineering

Carleton University
Ottawa, Ontario

Abstract

This study presents a rational simplified model for vibration assessment of floors under walking load. The model is developed by converting the floor system into an equivalent SDOF model using appropriate transformation factors and applying simplified forcing functions to simulate the walking load. The accuracy of the proposed model is verified against experimental tests and detailed FE analyses. A parametric study is also carried out on 67 floors with a wide range of design parameters. The results show that, unlike most existing simplified vibration analysis methods which have a limited application range, the proposed model is able to accurately capture the peak acceleration of floors with different frequencies and structural systems. The model is then used for the vibration design of floors of modular hospitals. It is demonstrated that the proposed SDOF model greatly facilitates the design of modular floors with high natural frequencies, which is almost impractical to do with existing simplified vibration analysis methods.

Acknowledgements

I want to express my sincere gratitude towards Dr. Vahid Sadeghian and Dr. Jeffrey Erochko for mentoring me and guiding me throughout the project. Dr. Sadeghian has been a guiding force for me throughout my graduate studies. This study would not have been completed without his invaluable inputs. I would also like to thank Mr. Robert Erochko for his guidance from an industrial perspective. I would like to also thank the examiners, Dr. David Lau and Dr. Beatriz Martin-Perez, for taking the time and reviewing the thesis.

I would like to thank my friends for their constant support and encouragement throughout the project. Finally, I would like to thank my parents and my sister for supporting me throughout my study, especially my parents, who encouraged me to glide through tough times.

Table of Contents

List of Tables

List of Figures

Chapter 1: Introduction

1.1 Background

Over the last few decades, many structures have experienced major serviceability issues due to walking-induced vibration. London Millennium Bridge and Pont De Solferino Footbridge are two well-known examples that were forced to close within the first few days of their openings because of their excessive swaying motions under walking loads due to insufficient vibration design. Reopening of these structures required significant repair costs in order to mitigate the excessive vibration to acceptable limits. In the past few years, because of advances in modern construction, which allows lighter, slender, and longer structures, the floor vibration due to human activity has become an increasing serviceability concern that needs to be carefully considered in the design process.

Performance of structural floors under walking-induced vibration depends on three major parameters: 1) the footstep force applied on the floor, 2) dynamic properties of the floor, and 3) human perception of vibration. The magnitude and pattern of dynamic forces induced by walking can be influenced by several factors such as step size, gender, weight, footwear, and height of the person walking on the floor. Greater mass and walking frequency result in larger dynamic forces. Dynamic properties of the floor, including the mode shape, natural frequency, modal mass, and damping, are also critical in determining the vibration response. Every floor vibrates in a unique shape and at a distinctive frequency depending on its stiffness, mass, and boundary conditions. If the stiffness of the floor reduces or its mass increases, the fundamental frequency reduces, which can significantly affect the vibration response of the floor (e.g., resonance effect). Another important parameter for vibration assessment is damping characteristics of the floor, which

indicates the dissipation of energy and movement due to friction and other energy loss mechanisms in the system. Apart from the material type of the floor, damping also depends on the room layout, number and configuration of partition walls and heavy items on the floor, as well as the rigidity of connections. Increasing the number of partition walls increases damping, which results in reduced vibrations.

In addition to the applied dynamic forces and characteristics of the floor, human perception of vibration is also an important factor in quantifying the vibration performance of floors. Humans are more sensitive to floor oscillations of frequencies between 4 Hz to 8 Hz, which is the resonating frequency range of internal organs (Murray et al. 2016). Therefore, vibration limits in design codes are more stringent within this frequency range than other floor frequencies. These limits are also a function of the occupancy type of the building. Vibration requirements for a laboratory or a hospital with sensitive equipment are stricter than those for a residential building.

Based on the fundamental natural frequency (f_n), floors are typically classified into low-frequency floors ($f_n < 9$ Hz) and high-frequency floors ($f_n > 9$ Hz). Acceleration responses of low- and high-frequency floors to the human-induced vibration are very different. The response of low-frequency floors is mainly governed by the resonance phenomenon, which occurs when the walking frequency matches the natural frequency of the floor. A typical walking frequency ranges from 1.5 Hz to 2.2 Hz, and a typical footstep force function can be represented by the Fourier series (Rainer et al. 1988), which is formed from combinations of the static load of a person and its four harmonics. A harmonic is a sinusoidal wave whose maximum amplitude is equal to the dynamic load factor (DLF) times the static load of a person. The frequency of this sinusoidal wave is in an integral multiple of the walking frequency ranging from 1 to 4; with an increase in harmonic number, the DLF decreases, and the harmonic forcing frequency increases. After the fourth

harmonic, the DLF becomes negligible and therefore ignoring subsequent harmonics is a reasonable assumption (Murray et al. 2016). Based on these observations, resonance can only occur on low-frequency floors with a natural frequency from 1.5 Hz (1st harmonic of 1.5 Hz) to 8.8 Hz (4th harmonic of 2.2 Hz). In resonance, the frequency of the applied walking load and the floor system match, amplifying the response until the floor reaches a steady-state acceleration. On the other hand, high-frequency floors (f_n > 9 Hz) do not experience resonance since there is no frequency matching between the vibration source and the structural system. These floors exhibit an impulsive response that does not build over time. It resembles a series of impulse responses to individual footsteps with peaks that die out relatively quickly because of damping.

To further illustrate the differences in the acceleration response of low- and high-frequency floors, two two-way square flat concrete floors were analyzed under walking loads with a frequency of 2.08 Hz using the Abaqus finite element (FE) software (CAE, 2020). Details of the FE modelling procedure will be discussed in Chapter 3. The first floor was a low-frequency floor (f_n = 8.46 Hz) with dimensions of 8 m × 8 m × 175 mm. This floor was excited by the fourth harmonic of the walking frequency and experienced a resonant response, as shown in Figure 1.1. The second floor was 6.5 m by 6.5 m with a thickness of 150 mm and had a natural frequency of 11 Hz, making it a high-frequency floor. The acceleration response of this floor is also shown in Figure 1.1. This floor had an impulsive response as its natural frequency was beyond the fourth harmonic of the walking frequency.

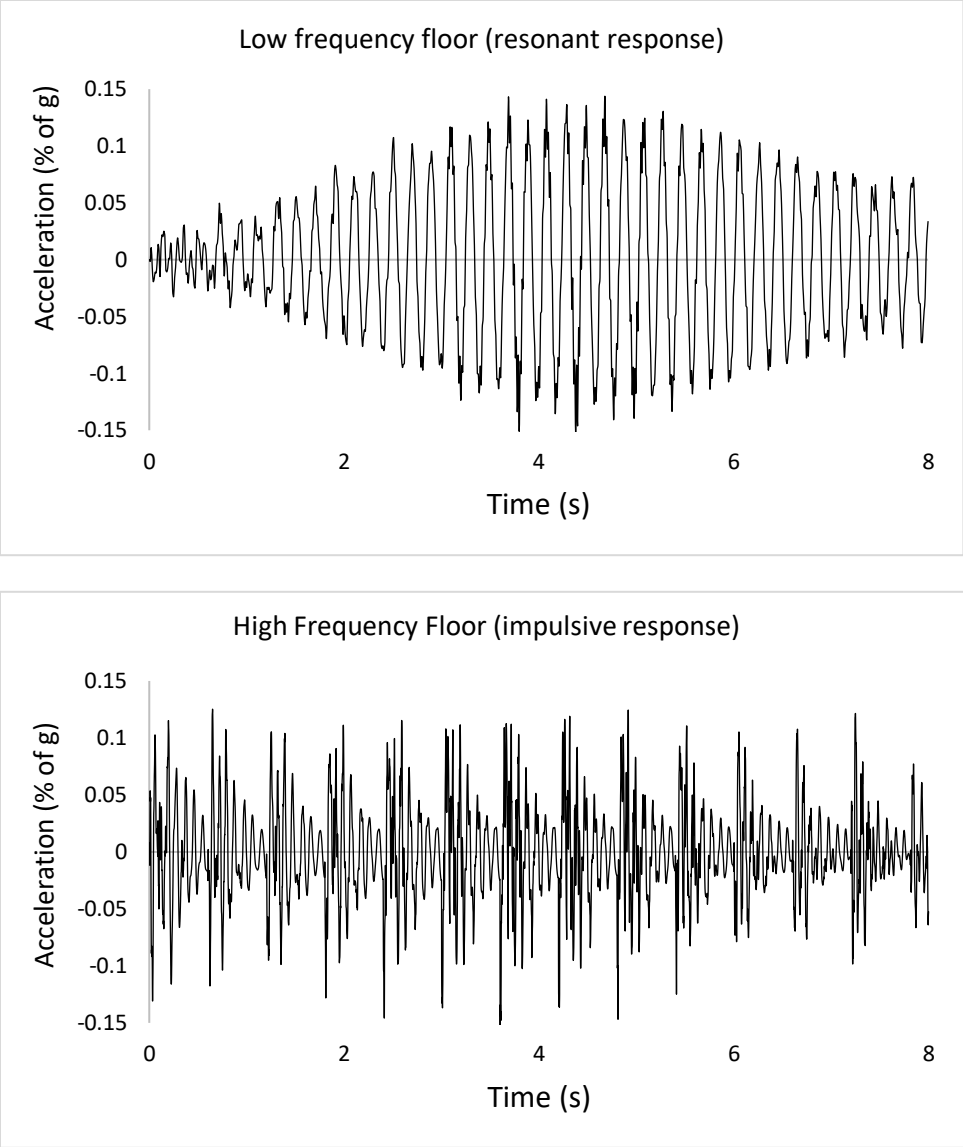

Figure 1.1 Acceleration response comparison of low- and high-frequency floors

In general, there are two types of analysis methods for vibration assessment of floors: 1) simplified methods and 2) FE methods. Simplified analysis methods are computationally efficient making them suitable for design applications. However, the existing simplified analysis methods are mostly calibrated using limited experimental data, restricting their application to specific floor systems and frequencies. Apart from their limited application range, simplified analysis methods generally calculate the acceleration of high-frequency floors in the free vibration phase of the

response after an impulse is applied. However, the peak acceleration caused by walking on stiff floors occurs during the forced vibration phase of the impulse, according to the principles of structural dynamics (Chopra 2011). This discrepancy can considerably impact the accuracy of existing design methods for high-frequency floors. Unlike simplified methods, FE analysis methods can accurately assess the vibration response of any floor system in detail. However, they are not suitable for design purposes because creating the FE model and carrying out the dynamic analysis are time-consuming and require high computational demand and good knowledge of computer modelling and interpretation of FE analysis results.

One type of structure that is highly sensitive to walking-induced vibration is hospitals. Even the slightest amount of vibration on sensitive equipment such as MRIs, CT scanners, etc., can compromise delicate medical procedures. To ensure the safe and smooth operation of medical equipment, there are strict limits for human-induced vibration of hospital floors in design codes. In recent years, there has been a significant interest in building emergency hospitals using the modular construction technique. With the COVID-19 pandemic, the need for building fast-built hospitals has increased significantly. However, there has not been much research conducted on this topic and no design code, or construction guideline is available for building modular healthcare facilities. Considering that hospital design requirements are substantially different from other types of buildings, there is a great need for design and construction guidelines developed explicitly for modular hospitals. Achieving the rigorous floor vibration requirements of hospitals is more challenging for modular buildings than conventional structures as they are lightweight and less restrained, making them more prone to vibration. Work is needed to develop accurate vibration assessment methods that can be used to investigate the vibration response of modular floors and

propose floor designs that are lightweight and suitable for modular construction and yet meet strict vibration requirements of hospitals.

1.2 Research Objectives

The main objectives of this research study can be stated as:

- Evaluate the accuracy, application range and limitations of existing analytical and design methods for assessing vibration response of floors under human walking excitations.
- Develop a simplified rational method based on principles of dynamics that can accurately predict vibration response of both low- and high-frequency floors.
- Investigate the application range of the proposed vibration assessment method on a wide range of floors with different design parameters.
- Develop a schematic design of a modular hospital based on the relevant Canadian standards and previous research conducted on modular construction.
- Using the proposed vibration assessment method, evaluate the suitability of conventional floors for use in modular hospitals and propose floor designs that are lightweight and meet the strict vibration requirements of hospitals.

1.3 Thesis Layout

Chapter 2 provides a detailed literature review on existing analytical and design methods for vibration assessment of floors under human-induced walking load.

Chapter 3 presents the development of the simplified single-degree-of-freedom (SDOF) method for floor vibration assessment. In this chapter, the accuracy of the proposed SDOF method is also

verified against experimental tests and FE analyses. In the end, the performance of the proposed method is evaluated against the SDOF method of AISC.

Chapter 4 provides a comprehensive parametric study to assess the performance and application range of the proposed SDOF method and the AISC-SDOF method in more detail. The effect of a wide range of design parameters, including size, thickness, aspect ratio, support condition and material type, on the vibration response of floors is investigated in this chapter.

Chapter 5 first discusses the importance of considering floor vibration in hospital structures and the advantages and application of modular construction to hospitals. Then, details of a schematic design of a modular hospital that is developed according to the Canadian design and construction practice are presented. Lastly, the newly developed SDOF method is applied to assess the vibration performance of different floor systems designed for modular hospitals.

Chapter 6 provides the summary and conclusions of this research study.

Chapter 2: Literature Review

Considerable efforts have been made to compute the vibration response of structural floors under human walking. Existing methods for vibration assessment can be broadly classified into two categories: 1) Simplified methods and 2) Finite element (FE) analysis methods. With the simplified methods, the modal properties and the peak acceleration of the floor are calculated by approximate expressions mostly calibrated from experimental tests. These methods typically use the maximum vertical deflection of floors calculated from simplified expressions to evaluate the natural frequency and then use an equivalent single-degree-of-freedom (SDOF) system to determine the peak acceleration of the floor. With the FE analysis methods, the structural floor is modelled in detail, and actual walking scenarios are considered enabling accurate evaluation of the complete vibration response of floors. Because of their high computational demand, FE methods are mainly used for complex floor systems or floors with irregularities for which simplified methods are not applicable. Some other methods use FE analysis to evaluate the modal properties of floors, and then the peak acceleration is determined by simplified expressions. In the following sections, the existing analytical methods and commonly used design guidelines for floor vibration are discussed.

2.1 Analytical Methods

One of the early studies that have been the basis for many existing analytical methods is experimental tests conducted by Bachmann et al. (1987). Through measuring the force of a single step under different walking scenarios, they found that the typical range of walking frequency is between 1.5 Hz and 2.5 Hz. It was also shown that the velocity of a person and its stride length during walking solely depend on their walking frequency. These stride lengths and velocities have been used in many FE analyses for determining the distance and time gap between the subsequent

steps. Based on the experimental results of Bachmann et al. (1987), mathematical expressions were also proposed for both vertical and lateral loads due to walking. It was found that lateral loads were almost ten times lesser than vertical loads; therefore, ignoring them is a reasonable assumption for computing the vertical response. Along with other human-induced vibrations such as running, jumping, and dancing, Bachmann et al. (1987) investigated machine-induced vibrations and proposed remedial measures for excessive vibrations.

Rainer et al. (1988) proposed mathematical expressions for determining dynamic forces and peak accelerations due to walking, running, and jumping. The dynamic force was represented by the Fourier series based on force measurements made on an instrumented platform. Several researchers, including Harper et al. (1962), Nilsson (1976, 1980), Ohlsson (1982), and Tuan and Saul (1985), had carried out similar work where they determined the dynamic force of a single step and then simulated walking load by adding two single steps with appropriate time delays. However, Rainer et al. (1988) carried out force measurements under multiple steps instead of a single step to better represent a continuous dynamic force. The experimental program consisted of two footbridge specimens made of precast concrete panels supported on steel trusses. The specimens were simply supported and had a natural frequency of 2.05 Hz and 4.17 Hz; hence they both were considered to be low-frequency structures. Different dynamic load factor (DLF) values and a Fourier series were proposed based on the results of these experiments. The peak acceleration was determined based on the steady-state acceleration of an equivalent SDOF system. The load was represented by multiplying DLF with the static load, and the equivalent mass was taken as half of the mass of the footbridge. The peak acceleration was quite accurately predicted compared to the measured results; the error was less than 5%. However, the expression proposed for peak

acceleration was only applicable to simply supported composite steel decks with low natural frequencies since the equivalent mass used was only suitable for this type of system.

Ohlsson (1998) proposed another simplified method to evaluate the serviceability of cross laminated timber (CLT) floors under walking-induced vibration. The method required calculating three parameters, which were then compared against limiting values given by Eurocode 5 (2004). The three parameters were: 1) the fundamental natural frequency of the floor, 2) the maximum vertical deflection of the floor caused by a unit vertical force at the center of the floor, 3) and the maximum initial vertical velocity of the floor caused by a unit impulse at the center of the floor. These parameters can be computed either by FE analysis or by simplified equivalent beam expressions. A minimum frequency limit of 8 Hz was considered in this study to ensure that the floor does not fall into resonant vibration. Different limiting values under a unit impulse were recommended for maximum vertical deflection and maximum initial velocity to meet serviceability requirements under vibration. This method is limited to high-frequency CLT floors and cannot be applied to low-frequency floors or floors made from other materials.

Kerr (1998) investigated the differences between human-induced vibration on floors and stairs. He expanded the work of Rainer et al. (1988) by measuring more footfall time histories from an extensive set of individuals walking on an instrumented platform. To determine the peak acceleration, the expression proposed by Rainer et al. (1988) was used. Based on the 880 measured footfalls, mathematical expressions were proposed to determine the DLF values as a function of walking frequency.

Mohr (1999) proposed a similar method to that developed by Ohlsson (1988) with two key differences. First, unlike Ohlsson's method, the method proposed by Mohr (1999) was applicable to low-frequency floors and required calculation of the peak acceleration to evaluate the vibration

serviceability. The peak acceleration was calculated assuming a steady-state acceleration response. The second difference between the two methods was with respect to the consideration of the live load. Mohr (1999) included 30% of the live load in the calculation of modal mass, whereas no live load was considered in the Ohlsson's method. To verify the method, experimental tests were conducted on low- and high-frequency CLT and timber cement concrete (TCC) panels which were simply supported on two sides. By comparing the analytical and experimental results, it was concluded that the proposed method underpredicted the peak velocity by 28% on an average.

One of the most comprehensive studies in vibration assessment of floor systems was conducted by Davis (2008). He proposed three different FE analysis methods for low-frequency floors and then evaluated their accuracy against experimental tests carried out on steel-concrete composite floors both on-site and in the laboratory. The key difference between these three analysis methods was in terms of the application of the footstep load. In the first method, individual footsteps were applied at expected locations they would fall considering the spatial variation of walking. Since the method was developed for low-frequency floors, the footstep frequency was selected such that it matched the fundamental natural frequency of the floor to cause resonance. Then, a linear response history analysis was performed to predict the acceleration time history response at the center of the floor. In the second method, a Fourier series with four harmonics was used to represent the walking load. This forcing function was applied at the midspan point for a duration equal to the time required by a person to cross the floor. Similar to the first method, a response history analysis is needed to determine the acceleration time response. In the third method, the frequency response function (FRF) was created by conducting a series of dynamic analyses on the FE model. FRF is the steady-state acceleration versus frequency plot generated by applying a unit sinusoidal load at different frequencies and determining the steady-state accelerations for those

frequencies. The peak acceleration due to walking load was computed by multiplying the peak acceleration obtained from the FRF plot by the dynamic load factor, bodyweight (747.5 N) and partial resonant build-up factor. The peaks of the FRF plot generally occur at the natural frequencies of the floor (fundamental mode, second mode, third mode, etc.) because of the resonance phenomena. Out of all the peaks in the FRF plot, the one at the fundamental frequency gives the highest acceleration due to walking load. In the third method, which forms the basis of the AISC Design code (Murray et al. 2016), out of the four terms of the Fourier series only the one which causes the resonance was selected and applied to the floor in the same way as explained for the second method. When compared to experimental results, the natural frequency predicted by all three methods was within 10% of the experimental values. However, the peak acceleration calculated by the first, second and third methods was overestimated by 47%, 84%, and 71%, respectively, compared to the test results. The first analysis method was the most accurate one as it represented the actual walking scenario more precisely compared to the other two methods. These modelling methods have been developed based on the resonance effect in low-frequency floors, and therefore, they may not be applicable to high-frequency floors which have an impulsive response under human-induced walking.

Recently, Casagrande et al. (2018) proposed two FE modelling methods to assess the response of CLT and TCC floors under human-induced vibration: a simplified method and a comprehensive method. The simplified method was only valid for one-way floors and involved approximating the floor with a beam model supported on two rigid supports. With the comprehensive method, the entire floor was considered in the FE model enabling it to account for the two-way action. To represent actual walking footsteps, several concentrated vertical forces were applied on the floor model with the spatial spacing set according to the standard stride length and with the temporal

spacing equal to the inverse of the walking frequency. Using modal superposition, linear dynamic analysis was carried out to obtain vertical accelerations due to walking at the center of the floor. Compared to the laboratory and on-site experiments, the peak acceleration obtained from the simplified model for one-way floors had about 24% error. In comparison, the error for two-way floors analyzed by the comprehensive method was about 45%. The high level of error for two-way slabs can be attributed to the complex shape of the specimen as compared to the one-way specimen. Both the simplified and comprehensive FE methods were only verified against high-frequency floors made from CLT and TCC. The applicability of these methods to other types of floors has not been investigated.

2.2 Design Guidelines

In North America, the AISC Design Guide 11 entitled *"Vibration of Steel-Framed Structural Systems Due to Human Activity"* (Murray et al. 2016) is the design code typically used to check the serviceability of floors subjected to human-induced vibration. In Europe, design guidelines published by the Steel Construction Institute (SCI) entitled *"Design of Floors for Vibration: A New Approach"* (Smith et al. 2009) and guideline published by ARUP entitled "*A Design Guide for Footfall Induced Vibration of Structures"* (Willford et al. 2006) are widely used for design and assessment of floors under walking vibrations. The design procedures in these guidelines are based on one or more of the following methods: detailed FE methods, simplified methods, and hybrid methods which consist of a combination of FE analyses and simplified expressions. In the following, these design procedures are reviewed with the main focus given to the simplified and hybrid methods as they are more relevant to this study and easier to use for design purposes.

AISC Design Guide 11 (Murray et al. 2016) provides a simplified method and a FE analysis method for calculating the peak acceleration of floors. The simplified method consists of a series

of expressions based on the free vibration and steady-state response of an SDOF system for high- and low-frequency floors, respectively. The free vibration expression for high-frequency floors is based on the Willford et al. (2006) study which will be explained later in this section. The expression of the steady-state acceleration response for low-frequency floors is similar to that proposed by Rainer et al. (1998) as previously discussed. The AISC design expressions for high-frequency floors assume the peak acceleration occurs after applying the impulse load. However, based on dynamic formulations, the peak acceleration under footstep impulse on high-frequency (stiff) floors occurs during the time in which the impulse is being applied on the floor (Chopra (2011). Further, the expressions for high- and low-frequency floors include calibration factors to match computed accelerations with the experimentally measured data. These calibration factors limit the application range of the simplified method to only steel-framed concrete floors with frequencies up to 15 Hz. Another limitation of this method for high- and low-frequency floors is that it is not easy to apply as determining some of the parameters (e.g. effective mass) requires following a complicated procedure. The second method provided in the AISC design guideline is adopted from the study carried out by Davis (2008) and involves using a FE model to determine the natural frequencies and mode shapes of the floor. After modal analysis, the FRF plot is created by conducting a series of dynamic analyses using the FE model. For low-frequency floors, the acceleration is computed by multiplying the maximum acceleration obtained from the FRF plot by the dynamic load factor, average weight of a person and partial resonant build-up factor. Unlike the low-frequency floors, the calculation of acceleration for high-frequency floors is not based on the FE analysis. Despite using the FE analysis for determining modal properties, the acceleration of high-frequency floors is still calculated using the simplified free vibration expression (Willford et al. 2006) and therefore is subjected to the same limitations as those discussed above.

ARUP's Design Guideline proposed by Willford et al. (2006) follows a hybrid analysis approach similar to that used by AISC for high-frequency floors. Willford et al. (2006) collected 880 measured footfalls from experiments carried out by other researchers (Kerr 1998, Rainer 1988, Ohlssen 1982, Galbraith et al. 1970 and Harper 1962) and calculated the mean and design DLF values for each harmonic of footfall force under different walking frequencies. The design DLF is defined as a DLF that has a 25% chance of exceedance. To evaluate the floor vibration, the modal properties are calculated by performing an Eigenvalue analysis using FE software. The peak acceleration for low-frequency floors is estimated using an expression similar to that proposed by Rainer et al. (1988), except that the mass is taken as the modal mass of the floor computed from the FE analysis and that the acceleration is calculated using the design DLF. For high-frequency floors, a set of effective impulse values are proposed for the vibration assessment. To obtain these impulse values, Willford et al. (2006) applied all 880 footfall force-time histories collected from previous tests to floors with different natural frequencies and calculated the peak acceleration. Then, using the free vibration expression of an SDOF spring-mass system, the instantaneous impulse force required to cause this acceleration was determined.

Similar to the AISC method, the method proposed by Willford et al. (2006) neglects the force vibration phase of the impulse for high-frequency floors. It also assumes high-frequency floors are subjected to an instantaneous impulse. An actual footstep impulse, however, is not instantaneous; instead, it occurs for a finite time which raises questions about the accuracy of this method. Furthermore, Willford's method is calibrated based on a broad range of experimental tests. Thus, it has a wider application range compared to the AISC method which is only valid for steel-concrete composite floors with a limited range of frequency.

The SCI's design guideline (Smith et al. 2009) provides two methods for the vibration design of floors: the General Assessment method and the Simplified Assessment method. The General Assessment method uses a hybrid approach which is similar to that presented for the AISC and ARUP design guidelines and consists of a combination of FE analysis and simplified expressions for determining the acceleration due to walking. However, the simplified expressions are different from those used in the other two design guidelines since they are calibrated based on a different set of experimental tests. The Simplified Assessment method is the same as the General Assessment method except that modal properties of the floor are calculated from simplified expressions instead of FE models. There are two key differences between the design procedure of SCI and the previously mentioned design guidelines. Firstly, for low-frequency floors, in addition to the steady-state acceleration expression, SCI also recommends calculating accelerations from the free vibration expression. Secondly, horizontal accelerations are also calculated along with vertical accelerations and compared with different horizontal and vertical vibration limits.

Many researchers assessed the accuracy of the above-mentioned design guidelines against experimental tests. Sladki (1999) compared the measured natural frequencies and peak accelerations for some buildings against predictions of the AISC Design Guide 11 (Allen et al. 1993). He stated that the frequency predictions were accurate, but the predicted accelerations were inaccurate. Hicks (2004) compared experimentally measured and predicted values based on the AISC and SCI design guidelines for eight floors subjected to human-induced vibrations. He reported that the predicted natural frequencies from both design codes correlated well with the measured frequencies. For low-frequency floor specimens, both design codes overestimated accelerations by about 30% and resulted in large coefficients of variation. Hicks (2004) also employed the FE modelling procedure proposed by Willford et al. (2006) to analyze the test

specimens. By comparing the analytical and experimental results, he concluded that the FE analysis method was highly accurate but resulted in a substantially high coefficient of variation (57%). Some analysis cases overestimated the peak acceleration, while others underestimated it. The inconsistency in the predictions was attributed to the large variability in footstep forces. In another study, Davis and Murray (2007) presented comparisons of walking test results with the predictions by the AISC and SCI design guidelines. Five bays were tested; one was built using a composite slab supported by steel beams, and the others were built using a non-composite slab supported by open-web steel joists. The analysis results showed that the AISC procedure overestimated the peak acceleration by 20% on average, and the SCI guide underestimated it by 40%. Both design methods underestimated the natural frequency of the floor specimens.

In addition to the design guidelines discussed above, which are widely used in practice, some research proposed other design procedures for floor vibration as well. Hu et al. (2012) developed a new design method exclusively for high-frequency CLT floors based on fundamentals of dynamics and an experimental study on CLT floors with different construction configurations. Initially, the natural frequency (f) and static deflection (d) of the floor under 1 kN load were determined by simplified expressions for all the specimens. Then, the calculated natural frequency and static deflection values were verified by standard modal tests and static concentrated load tests conducted on the floor specimens. Further, a subjective evaluation was carried out by asking a series of questions from people walking on the floor specimens regarding when they could feel annoying vibrations. Based on this study, a design criterion (see Eq. 2.1) was proposed using the natural floor frequency and the static deflection under 1 kN load. All the floors satisfying this criterion were considered to have an acceptable vibration behaviour. CSA O86-14 (2014) has also implemented this method for the vibration design of high-frequency CLT floors under walking.

$$\frac{f}{d^{0.7}} \geq 13 \qquad (Eq.\,2.1)$$

Casagrande et al. (2018) developed a Uniform Load Distributed (ULD) criterion for the vibration design of timber floors. This criterion was based on the evaluation of the maximum vertical deflection of the floor caused by an instantaneous uniform load and determined by simplified expressions. In order to assess the serviceability of the floor, the maximum deflection was compared against a limiting deflection defined as a fraction of the floor length according to design codes such as Eurocode 5 (2004). In this study, the deflection was used as an indicator of the natural frequency of the floor (i.e., smaller deflection led to higher natural frequency and vice versa). The deflection criterion was imposed to ensure all floors fall under the category of high-frequency floors (f_n > 9 Hz) to avoid the resonance effect. Despite its simplicity, the method did not provide any information about the dynamic behaviour of the floor (e.g., peak acceleration) under vibration. Also, no verification study was conducted by the authors.

2.3 Concluding Remarks

Based on the review of the research literature and design guidelines on vibration assessment of floors, it can be concluded that the existing simplified methods for low- and high-frequency floors are calibrated from experimental data, limiting their application range to specific floor systems and frequencies. Apart from the limited range of applicability, the simplified methods available for high-frequency floors typically calculate the acceleration in the free vibration phase of the response after an impulse is applied. However, according to the principles of structural dynamics, the peak acceleration due to walking on stiff floors occurs during the forced vibration phase of the impulse (Chopra 2011). As shown later in this study, this discrepancy can significantly affect the accuracy of the existing design methods for high-frequency floors. Unlike simplified expressions,

FE analysis methods can accurately assess the vibration response of any floor system in detail. However, they are not suitable for design purposes because creating the FE model and carrying out the dynamic analysis are not only time-consuming but also require high computational demand and good knowledge of FE analysis and interpretation of results.

This study presents simplified SDOF methods for the vibration assessment of low- and high-frequency floors subjected to load actions from human walking. The proposed methods are derived by applying a series of simplifications to detailed FE analysis procedures based on the fundamentals of structural dynamics. Unlike the existing methods, the proposed methods do not include any calibration factor or complex input parameter, making them easy to use, and at the same time applicable to a wide range of floor systems and frequencies. In the following chapters, first, the formulation of the proposed methods for both low- and high-frequency floors is described in detail. Then, the accuracy of the methods is evaluated against experimental tests and FE analyses. The influence of each of the simplifications made in the development of the methods is investigated by comparing the results against those obtained from a series of FE models with different levels of complexity. Finally, the application range of the proposed methods is assessed by performing a comprehensive parametric study that includes different floor systems with a wide range of design parameters and frequencies. Throughout the verification and parametric studies, the performance of the proposed methods is also compared against the simplified method of AISC, which is the common floor vibration design method in North America.

Chapter 3: Proposed Simplified Single-Degree-of-Freedom Method

3.1 FE Modelling Procedure

Before describing the formulation of the proposed single-degree-of-freedom (SDOF) method, the finite element (FE) modelling procedure used for the verification and development of the SDOF method is discussed. The FE model was developed in the Abaqus FE software (CAE, 2020), where the slab and the framing members (joists and girders) were modelled as shell elements. For each slab, a mesh sensitivity analysis was conducted to determine the appropriate size of elements. The element size was selected such that the change in the natural frequency of the floor was less than 0.1 Hz, as recommended by Murray et al. (2016). Slabs whose material properties varied in different directions were modelled using orthotropic shell elements (e.g., steel-concrete composite deck floors). The ones with similar material properties in all directions were analyzed with isotropic elements (e.g., solid concrete slabs). For steel composite deck floors, instead of modelling the steel deck, its stiffness was estimated according to Murray et al. (2016) and included in the model by adjusting the initial elastic modulus of concrete. The slip between the concrete slab and joists and girders was neglected (i.e., complete composite behaviour) since horizontal shear caused by human walking can be easily resisted by commonly used connectors. To be consistent with the construction practice of a typical floor, the connection between the slab, joists, and girders was assumed to be a pinned connection, while fixed end supports were used to represent the connection between girders and columns. In Chapter 4, the influence of having a fixed connection between joists and girders on the vibration behaviour of floors will also be investigated. To investigate the worst-case vibration scenario, only the dead weight of the floor was considered in the FE model (the live load was not included) since the vibration is maximum when a structure is lightly loaded.

The model automatically calculated the mass of the framing members and the slab based on the density defined for each element.

After creating the FE model, an eigenvalue analysis was carried out to determine the modal properties of the floor, including natural frequencies and modal masses. Determination of the fundamental natural frequency was vital for selecting the loading function of the footstep. The loading function was defined based on the footstep force-time histories reported by Davis (2008) from various walking experiments (see Figure 3.1). With low-frequency floors, as mentioned earlier, the maximum response due to resonance occurs when one of the frequencies of the loading function matches the fundamental frequency of the floor. For high-frequency floors, on the other hand, the highest possible stepping frequency (2.2 Hz) was selected to determine the maximum response due to impulsive behaviour. The selected footstep forcing function was applied as concentrated nodal forces on the FE model. To consider the spatial variation in walking, the distance between two footsteps was taken equal to 0.75 m (Bachmann et al. 1987). The temporal variation in walking was taken into account by considering a time lag between subsequent footsteps equal to the inverse of stepping frequency.

According to Murray et al. (2016), damping in structural floors ranges between 1% to 8% of the critical damping. Critical damping is the smallest amount of damping required such that a free vibrating system comes to rest from its initially displaced position without undergoing any oscillation. In this study, the values of damping were obtained from experimental tests. However, values from Table 4.2 of the AISC Design Guide 11 (Murray et al. 2016) can also be used in the absence of experimental data.

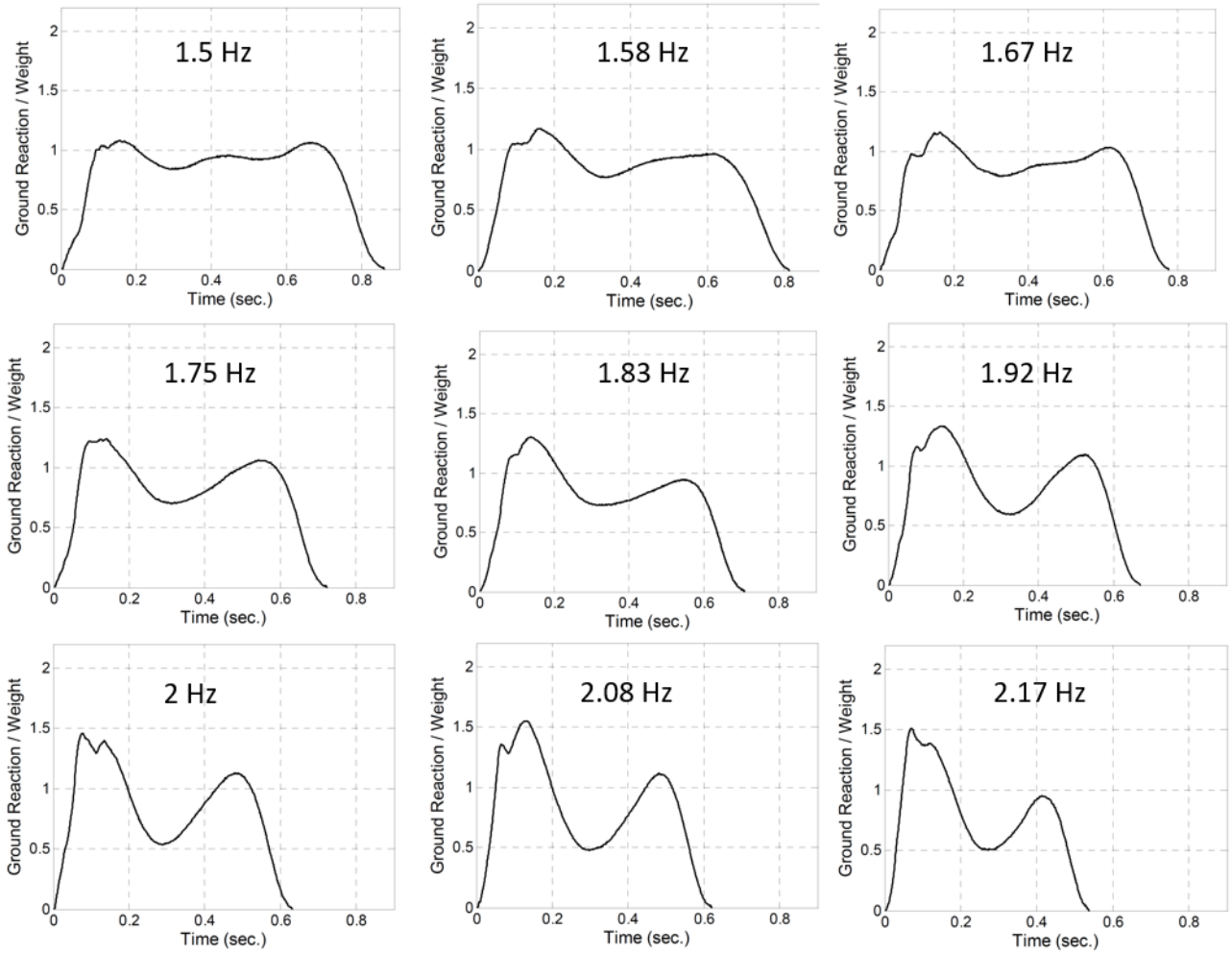

Figure 3.1 Footstep force-time histories for walking frequencies ranging from 1.5 Hz to 2.17 Hz (Davis 2008)

Using the described FE model, modal dynamic analysis was performed to calculate the acceleration response of the floor. The acceleration was evaluated at the center of the floor as the response is highest at this point. For design purposes, the maximum acceleration should be compared to the allowable acceleration limit specified in design codes such as AISC. The allowable acceleration is determined based on the type of floor occupancy (shopping malls, residential, hospitals, etc.) and the fundamental frequency of the floor.

The accuracy of the above-mentioned modelling procedure was verified against the measured response of four floor test specimens subjected to different walking frequencies. The geometry and structural details of the floor specimens are shown in Figure 3.2. The first three specimens were high-frequency floors with frequencies ranging from 10.5 Hz to 15.2 Hz tested by Liu et al. (2015). The last specimen was a low-frequency floor with a frequency of 4.98 Hz tested by Davis (2008). The first specimen was a composite steel deck representing the floor of an intensive care unit in a hospital building. It consisted of a 159 mm thick lightweight concrete slab on a 51 mm thick steel deck. The density and the uniaxial compressive strength of concrete were 1770 kg/m^3 and 20.7 MPa, respectively. The composite slab was supported by five W410x38.8 steel joists at 2.29 m center-to-center spacing and two W610x82 girders located on the perimeter of the slab. The floor was 9.14 m long (girder span) by 8.53 m wide (joist span) and had a total mass of 24,700 kg, which included the superimposed mass as well. The second specimen had an identical structural layout as the first specimen but supported more partition walls which slightly increased its natural frequency. Damping reported for the first and the second specimen from the experimental test was 4.1% of the critical damping.

The third specimen was a concrete floor supported by concrete joists and girders. The floor was 9.14 m (girder span) by 9.75 m (joist span) with an average density of 2,330 kg/m^3 and a concrete compressive strength of 24.1 MPa. The floor was 76.2 mm thick and supported by eleven 152 mm wide by 483 mm deep concrete joists at 975 mm center-to-center spacing and two 559 mm wide by 711 mm deep concrete girders. The total floor mass was 46,600 kg, and damping measured from the experimental test was 2% of the critical damping. The fourth specimen was a 9.1 m x 9.1 m composite slab system with an overall thickness of 222 mm. It was supported by two W360x39 joists and two W530x66 girders, as shown in Figure 3.2. The total mass of the floor was 45,000

kg, and the compressive strength of concrete was 24.1 MPa. Damping was measured as 0.436% of the critical damping from the experiment. Table 3.1 summarizes the main design parameters of each test specimen.

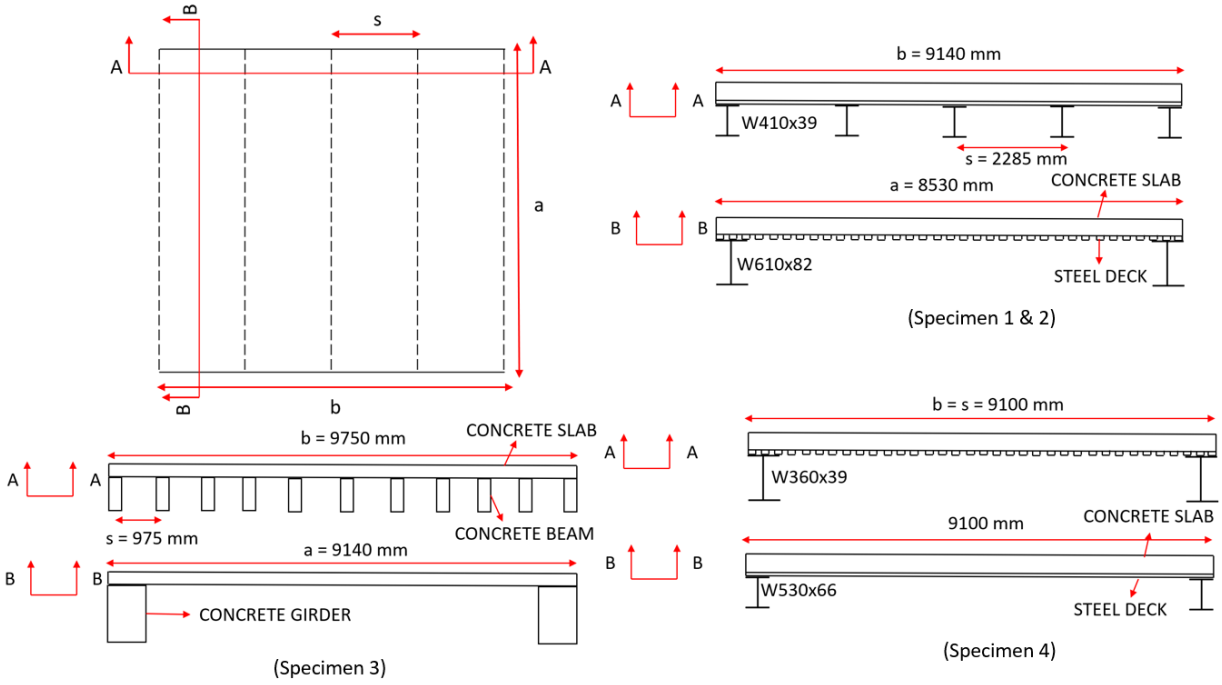

Figure 3.2 Construction details of floor specimens

Table 3.1 Design parameters for test specimens

	Specimen 1	Specimen 2	Specimen 3	Specimen 4
Floor system	Steel-concrete composite	Steel-concrete composite	Solid concrete	Steel-concrete composite
Natural frequency (Hz)	10.5	11.8	15.2	4.98
Dimensions	9.14 m x 8.53 m	9.14 m x 8.53 m	9.14 m x 9.75 m	9.1 m x 9.1 m
Thickness (mm)	210	210	76.2	222
Number of joists	5	5	11	2
Number of girders	2	2	2	2
Total mass (kg)	24700	24700	46600	45000
Damping (%)	4.1	4.1	2	0.436

According to the modelling procedure described above, a FE model was created for each floor system (see Figure 3.3), and dynamic analyses were conducted under different walking frequencies as provided in Table 3.2. Figure 3.4 shows the acceleration time response due to a stepping frequency of 1.67 Hz for specimen 2 which is extracted from Abaqus FE software (CAE, 2020). Table 3.2 also compares the natural frequency and peak acceleration of the floors computed by the FE analysis against those measured from the experiments. The analytical and experimental results for both low- and high-frequency floors correlate well. The mean and standard deviation of the analytical-to-experimental ratio for the natural frequency are 1.002 and 0.055, respectively. Also, the mean and standard deviation of the peak acceleration ratio are 1.02 and 0.19, respectively, demonstrating good accuracy. The differences in the prediction of natural frequencies and peak accelerations can be because of the differences between the analytical model and test specimens in terms of the rigidity of connections and the distribution of mass on the floor (e.g. configuration of partition walls).

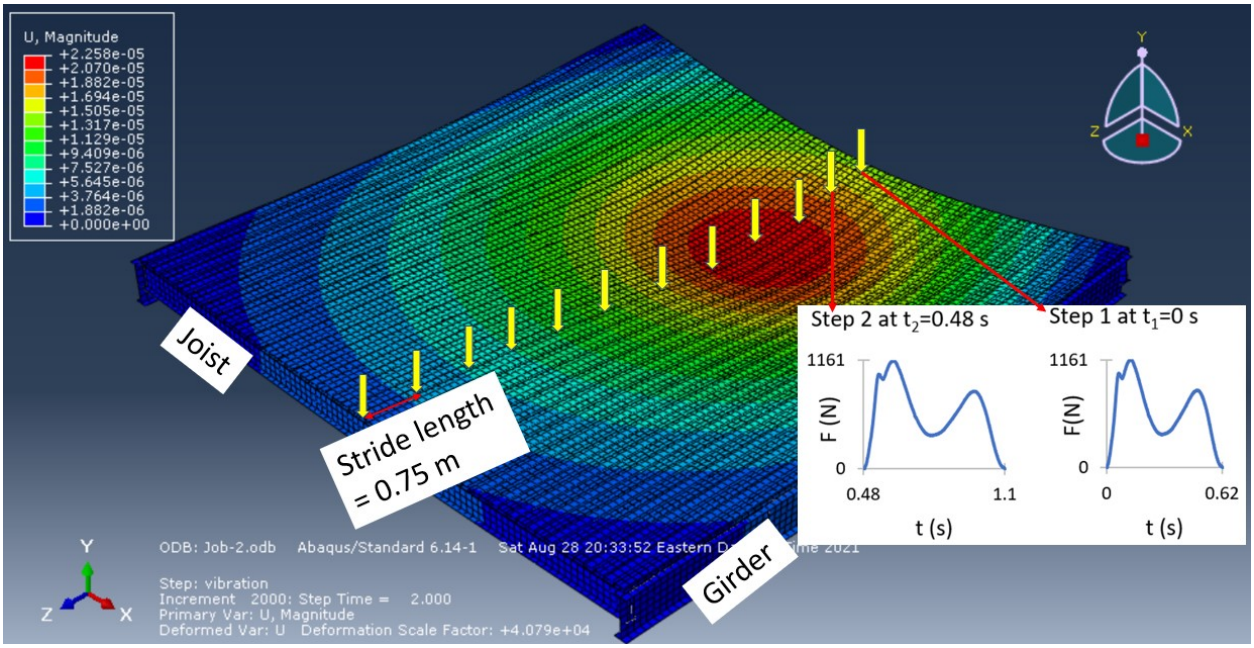

Figure 3.3 FE model for floor specimens 1, 2 and 4

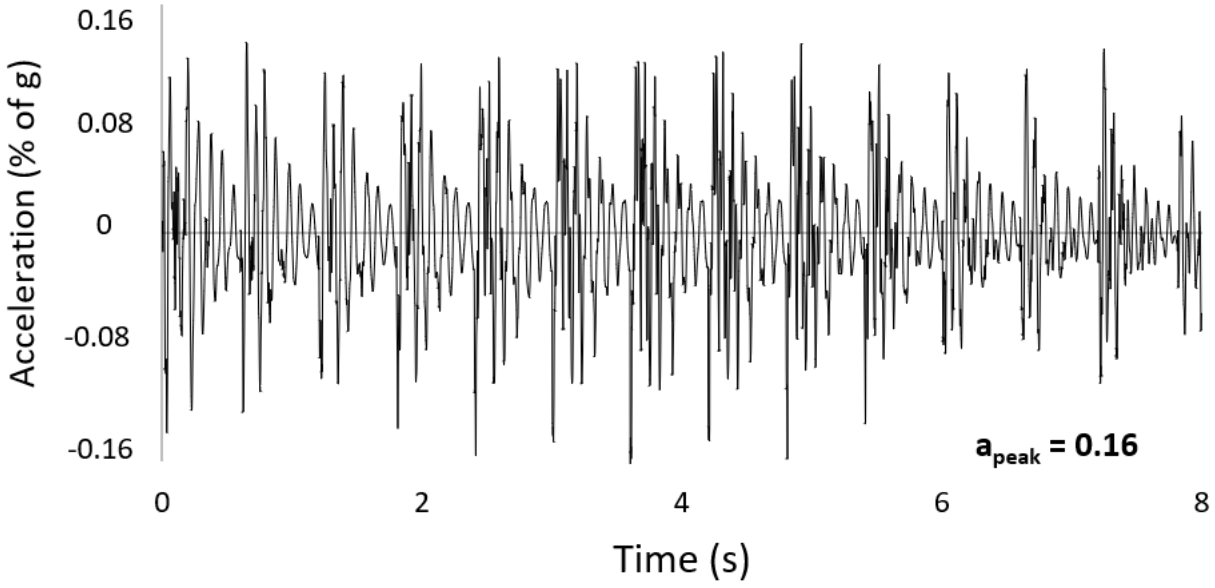

Figure 3.4 Acceleration time response for specimen 2 subjected to 1.67 Hz walking frequency

Table 3.2 Comparison of FE analysis and experimental test results

	Floor type	Walking frequency (Hz)	Experiment		FE analysis		$f_{n\,(FE)}/f_{n\,(exp)}$	$a_{peak\,(FE)}/a_{peak\,(exp)}$
			f_n (Hz)	a_{peak} (% of g)	f_n (Hz)	a_{peak} (% of g)		
Specimen 1	High-freq.	1.67	10.5	0.199	10.04	0.143	0.96	0.72
		2.08		0.454		0.561		1.24
Specimen 2	High-freq.	1.67	11.8	0.162	11.23	0.153	0.95	0.94
		2.00		0.375		0.346		0.92
Specimen 3	High-freq.	2.08	15.2	0.220	15.41	0.275	1.01	1.25
Specimen 4	Low-freq.	1.67	4.98	1.360	5.14	1.465	1.09	1.08
Average							1.003	1.02

3.2 Proposed SDOF Method

The previously discussed FE models are accurate for floor vibration assessment but are complex and time-consuming and therefore not suitable for design purposes. By applying reasonable simplifications to the FE modelling procedure, simple expressions based on equivalent SDOF systems can be developed for the computation of the peak acceleration due to walking load. These expressions are derived by investigating the effect of three simplifications on the analysis results of both high- and low-frequency floors: 1) Investigating the effect of neglecting spatial variation of load, 2) Investigating the effect of simplifying the loading function, and 3) Investigating the effect of reducing a multi-degree-of-freedom (MDOF) floor system into an SDOF system. These simplifications for low- and high-frequency floors are presented in Figures 3.5 and 3.6, respectively. The overall procedure for developing the SDOF analysis method for both low- and high-frequency floors is the same. However, because of the fundamental differences in the response mechanism (resonance response vs. impulse response), the formulation and assumptions

of the proposed method for low- and high-frequency floors have major differences that need to be carefully considered. The following sections provide a detailed description of each simplification and its influence on the vibration assessment.

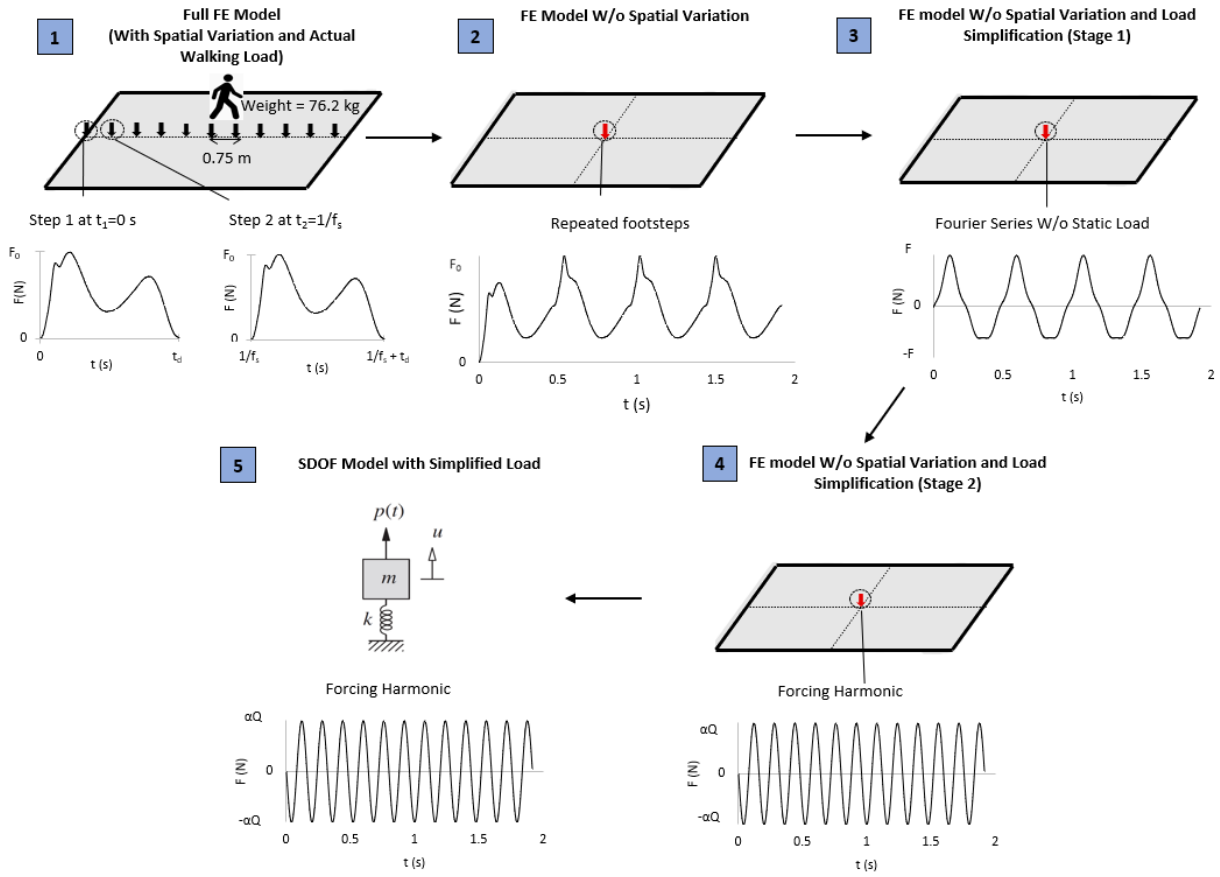

Figure 3.5 Different simplification stages for low-frequency floors

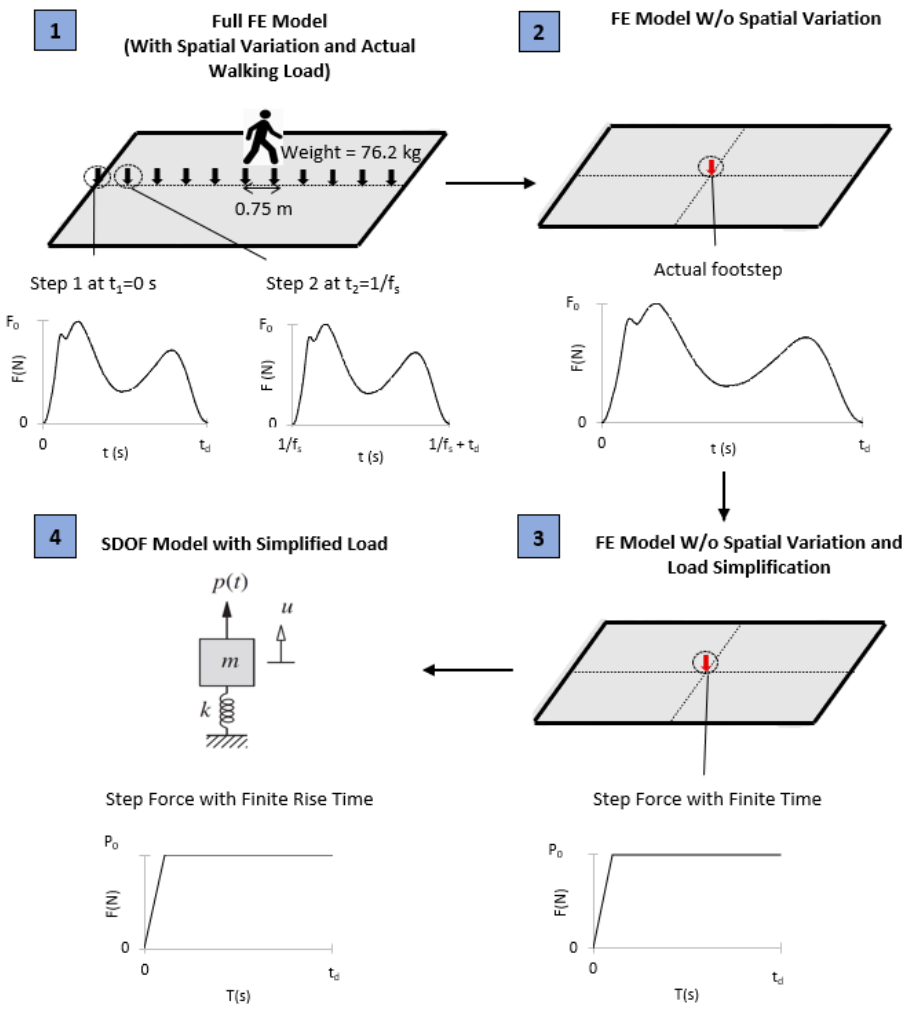

Figure 3.6 Different simplification stages for high-frequency floors

3.2.1 Effect of Spatial Variation of Load

To investigate the effect of spatial variation of load on the peak acceleration, instead of applying footstep load spatially across the floor, the load is applied at the center of the floor. In low-frequency floors, the footstep load is repeatedly applied for a time equivalent to the walking time to cross the floor. Due to resonance, this repetition of load helps build up the acceleration response and amplifies it to reach the steady-state acceleration. On the other hand, the footstep load in high-frequency floors is applied only once to the FE model because of the impulsive nature of the

response. The four floor specimens described before were analyzed again using the same FE models but this time without consideration of the spatial variation of the load. The analysis results are summarized in Table 3.3. On average, ignoring the effect of spatial variation results in a 7% increase in the computed peak acceleration. This slight increase in peak accelerations is expected as the disturbance point, and measuring point coincide at the center resulting in greater accelerations. On the other hand, when the load is varied spatially, the disturbance point varies and coincides only once during the walking event, producing lower peak accelerations. Considering that the change in the peak acceleration is insignificant, it can be concluded that ignoring spatial variation is a reasonable assumption towards simplifying the detailed FE model.

Table 3.3 Comparison of FE analysis results with and without spatial variation (SV) of load

	Floor type	Walking frequency (Hz)	a_{peak} from FE (% of g)		$a_{peak\ (without\ SV)}$ / $a_{peak\ (with\ SV)}$
			with SV	without SV	
Specimen 1	High-freq.	1.67	0.143	0.162	1.13
		2.08	0.561	0.612	1.09
Specimen 2	High-freq.	1.67	0.153	0.17	1.11
		2.00	0.346	0.349	1.01
Specimen 3	High-freq.	2.08	0.275	0.254	0.92
Specimen 4	Low-freq.	1.67	1.465	1.702	1.16
Average					1.07

3.2.2 Loading Function Simplification

To derive simplified acceleration expressions based on SDOF systems, the actual walking load should be simplified into a loading function with a pre-defined shape (triangular, sinusoidal, etc.). In this section, the load simplification process will be discussed first for low-frequency floors and then for high-frequency floors. For low-frequency floors, simplification of the walking load is carried out in two stages, with the level of simplification increasing with each subsequent stage.

In the first stage, the actual footstep force-time history is approximated by a Fourier series loading function (F), as shown in Eq. 3.1, which is applied at the center of the floor for a time equivalent to the walking time required to cross the floor.

$$F(t) = Q + \sum_{i=1}^{i=4} \alpha_i Q sin(2\pi i f_s t - \varphi_i) \qquad (Eq. 3.1)$$

where Q is the bodyweight of a person typically taken as 747.5 N, f_s is the step frequency in Hz, t is the time in seconds, i is the harmonic number, α_i is the dynamic load factor (DLF) of i^{th} harmonic which is equal to the ratio of the dynamic load to the bodyweight, φ_i is the phase lag for i^{th} harmonic in radian which can be taken from the SCI P354 design guideline (Smith et al. 2007) as 0, -π/2, π, and π/2, for the first, second, third and fourth harmonics, respectively. Figure 3.7 shows the DLF versus walking frequency plots for different harmonics obtained from several experiments conducted by different researchers (Willford et al. 2007). As demonstrated, the DLF decreases as harmonics increase and becomes almost insignificant after the fourth harmonic. Therefore, only the first four harmonics are considered in the Fourier series. Figure 3.7 also shows the mean DLF (red line) and the design DLF (blue line) obtained from linear regression analyses. The design DLF is taken higher than the mean DLF to increase the applied loads and provide a margin of safety for the design. However, it should be mentioned that accurate prediction of DLF is challenging as there are many parameters that can affect the walking load. The large scatter in data presented in Figure 3.7, specially for harmonics greater than 1, shows the high variability of DLF. In this study, the mean DLF is used in Eq. 3.1 for calculating the forcing function as this value provides a reasonable and simple estimate of the dynamic effects due to walking. The linear relationship between the mean DLF and walking frequency for each harmonic is provided in Table 3.4.

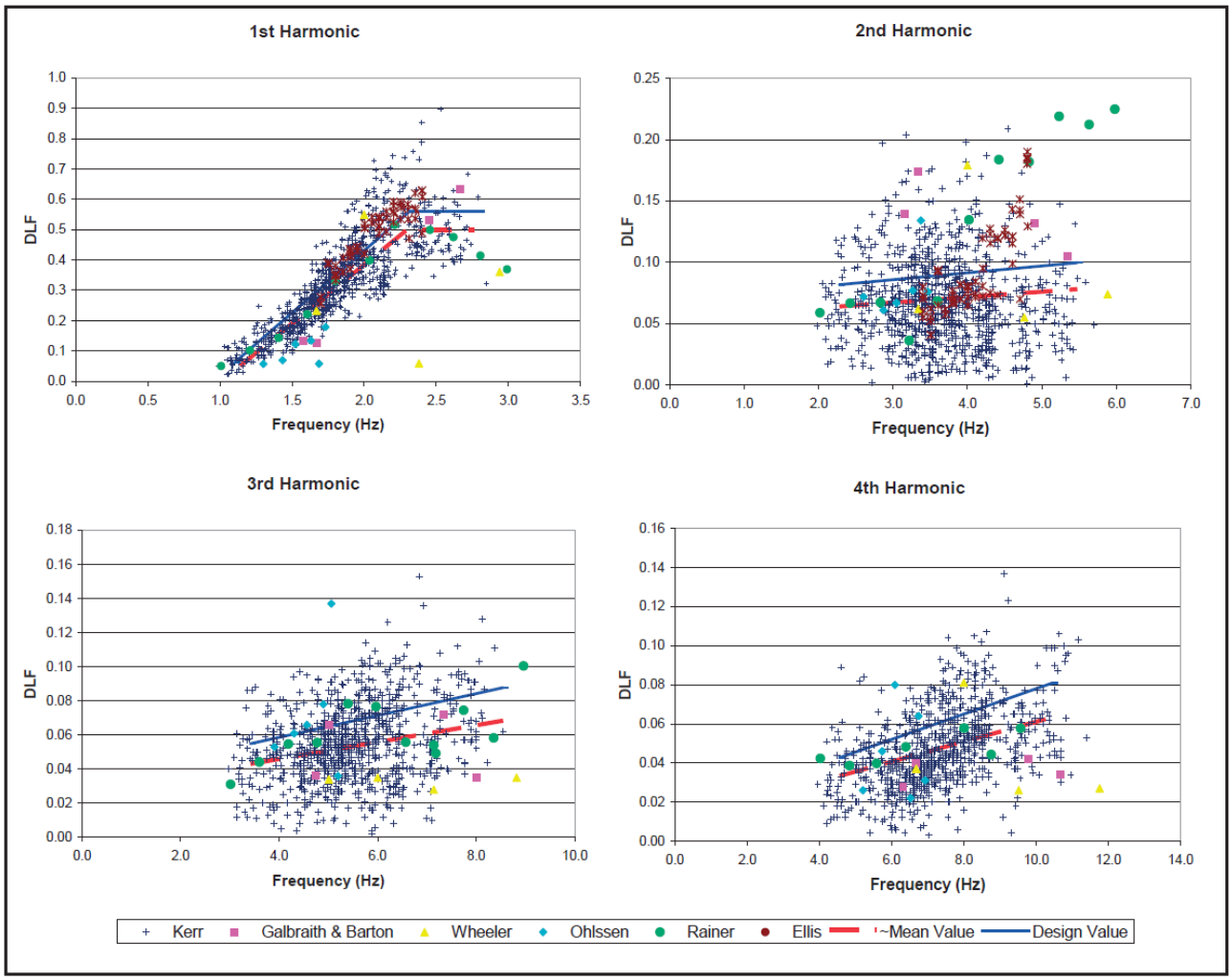

Figure 3.7 Correlation between dynamic load factor (DLF) and walking frequency for different harmonics (Willford et al. 2007)

Table 3.4 Mean dynamic load factor (DLF) values for each harmonic

Harmonic number	DLF
1	$0.45f_s - 0.47$
2	$0.0036(2f_s) + 0.054$
3	$0.0049(3f_s) + 0.020$
4	$0.0051(4f_s) + 0.009$

Comparison of the Fourier series function to the measured footstep force-time history for 2.08 Hz walking frequency presented in Figure 3.8 shows that the Fourier series provides a reasonable approximation of the actual walking load except for the sharp peaks in the case of the actual footsteps. These sharp peaks occur during walking when the toe of the previous foot and the heel of the following foot are both on the ground, and their forcing functions overlap. Similar correlations between the Fourier series and the measured footstep force-time history can be obtained for other walking frequencies as well.

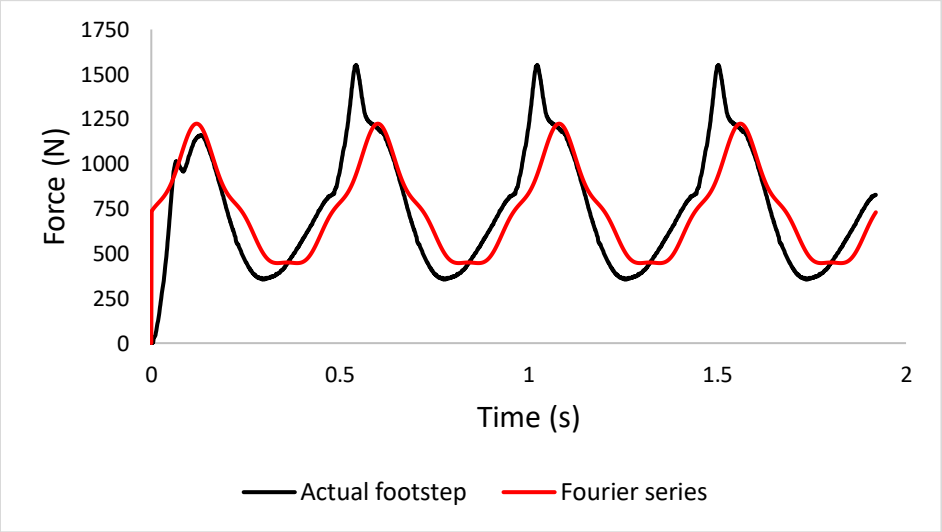

Figure 3.8 Comparison of force time history of test and Fourier series for 2.08 Hz walking frequency

Figure 3.9(a) shows the acceleration response of the low-frequency floor specimen analyzed using the Fourier series (i.e., Stage 1 of load simplification). It can be seen that the peak acceleration occurs in the very initial phase of the response, which is not realistic as resonance in low-frequency floors takes time to build up. It is worth mentioning that the peak acceleration of the experimental test occurred at 4.2 seconds. The initial spike in the computed acceleration is a result of the static component of load in the Fourier series. To avoid this initial spike in the response and allow the

resonance to build up, the static load component needs to be ignored from the Fourier series, which results in Eq. 3.2. Using this equation in the FE model to define the walking load results in the acceleration response shown in Figure 3.9(b), which is much smoother than the response shown in Figure 3.9(a). The peak acceleration in Figure 3.9(b), however, is about 30% less than that obtained from the FE model without consideration of the load simplification. This reduction in the peak acceleration is expected as the peaks of the actual footstep forcing response are not considered by the Fourier series (see Figure 3.9), and the contribution of the static load to the acceleration is neglected in the load simplification. In the following sections, it will be shown that this reduction in the peak acceleration will be compensated once the MDOF-to-SDOF simplification is applied.

$$F(t) = \sum_{i=1}^{i=4} \alpha_i Q sin(2\pi i f_s t - \varphi_i) \qquad (Eq.\ 3.2)$$

As mentioned earlier, the Fourier series is formed from the combination of four harmonics (four sine waves) where the frequency of one of these harmonics matches with the fundamental frequency of the floor, which results in the resonance behaviour of the floor; this harmonic is known as forcing harmonic frequency (f_s). In stage 2 of the load simplification, only the forcing harmonic frequency is used for the analysis instead of considering all the four components of the Fourier series. Determining the forcing harmonic frequency requires a trial-and-error procedure. First, the forcing harmonic frequency is assumed as the natural frequency of the floor (f_n) divided by the smallest integral value of harmonic number (i=1). If the resultant frequency value is between 1.5 Hz and 2.2 Hz, as shown in Eq. 3.3, then this frequency is the forcing harmonic frequency; otherwise, the harmonic number is further increased, and the above procedure is repeated till the assumed frequency for the forcing harmonic satisfies Eq. 3.3.

$$1.5\ Hz \leq f_s = \frac{f_n}{i} \leq 2.2\ Hz\ ;\ 1 \leq i \leq 4 \qquad (Eq.\ 3.3)$$

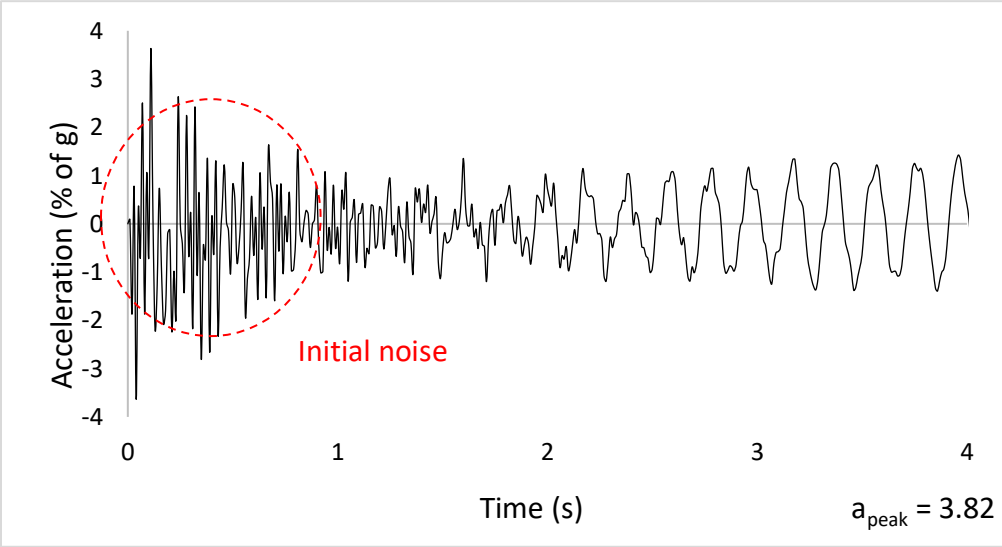

(a)

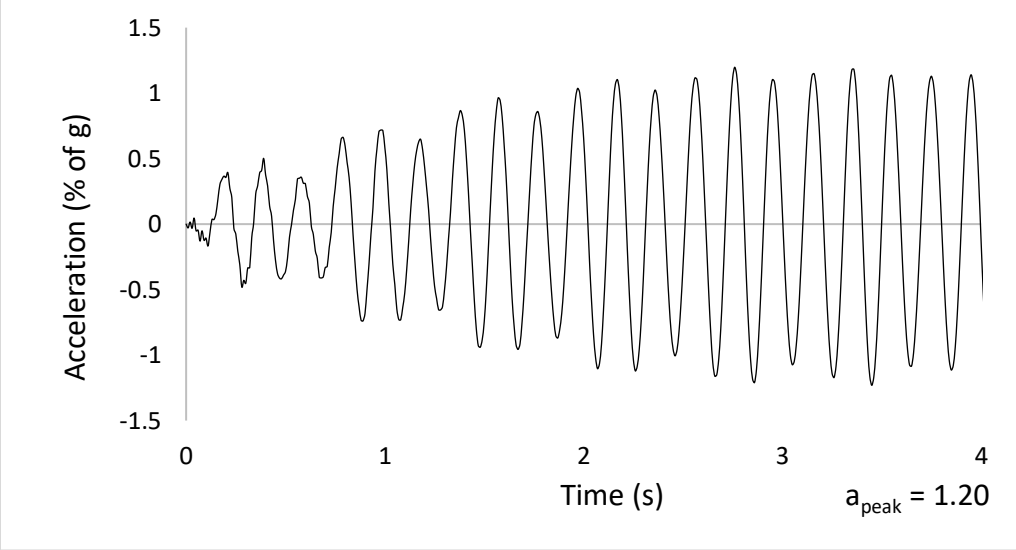

(b)

Figure 3.9 Comparison of acceleration time histories for stage 1 of load simplification with static load (a) and without static load (b) for the low frequency floor (specimen 4)

The smallest harmonic number is selected because it results in the largest DLF and consequently higher accelerations. After determining the smallest harmonic number that satisfies Eq. 3.3, the

DLF is found from Table 3.4, and the force-time history of the forcing harmonic frequency (f_s) is derived from Eq. 3.4 which represents only one term of the Fourier series.

$$F(t) = \alpha_i Q sin(2\pi i f_s t) \qquad (Eq. 3.4)$$

Analyzing the FE model of specimen 4 using Eq. 3.4 as the loading function (stage 2 of load simplification) results in a peak acceleration of 1.18% g, which is only about 2% less than the peak acceleration obtained from the previous analysis performed using Eq. 3.2 (stage 1 of load simplification). Therefore, it can be concluded that the contribution of all the remaining three harmonics of the Fourier series is insignificant and ignoring them is a reasonable assumption towards simplifying the walking load.

For high-frequency floors which have impulsive behaviour, only one load simplification is considered in determining the peak acceleration. In this simplification, the actual footstep impulse is replaced by a loading function with a simplified shape applied once at the center of the floor. According to fundamentals of dynamics, if the pulse duration (t_d) is greater than half of the natural period of the floor ($0.5T_n$), which is always the case for high-frequency floors under walking loads, then the peak acceleration is only influenced by the initial slope of the loading function (Chopra 2011). Therefore, the desired simplified loading function should be such that it matches the initial slope of the actual loading impulse. To determine the appropriate shape for the forcing function, the FE model was analyzed under different forcing function shapes (linear, triangular, half-sine, etc.), and the peak acceleration values were compared against those obtained from the actual footstep force-time history load. It was found that a simple ramp and hold function can provide a good approximation of the peak acceleration if the initial slope of the step force is matched with the actual walking impulse, as shown in Figure 3.10. Based on this ramp and hold forcing function, simplified footstep impulses are derived for different walking frequencies and presented in Table

3.5. In these simplified footstep impulses, the force linearly increases from zero to the initial maximum load of p_o in a rise time of t_r (i.e., ramp), and then the force remains constant till the impulse time of t_d (i.e., hold). The simplified loading function can be represented by Eq. 3.5.

$$p(t) = \begin{cases} p_o\left(\frac{t}{t_r}\right) & t \le t_r \\ p_0 & t_r \le t \le t_d \end{cases} \qquad (Eq.\,3.5)$$

Table 3.6 provides the FE analysis results with and without load simplification for floor specimens. Using the simplified load function on average increases the peak acceleration of high-frequency floors only by about 3% which demonstrates that the proposed load simplification is acceptable.

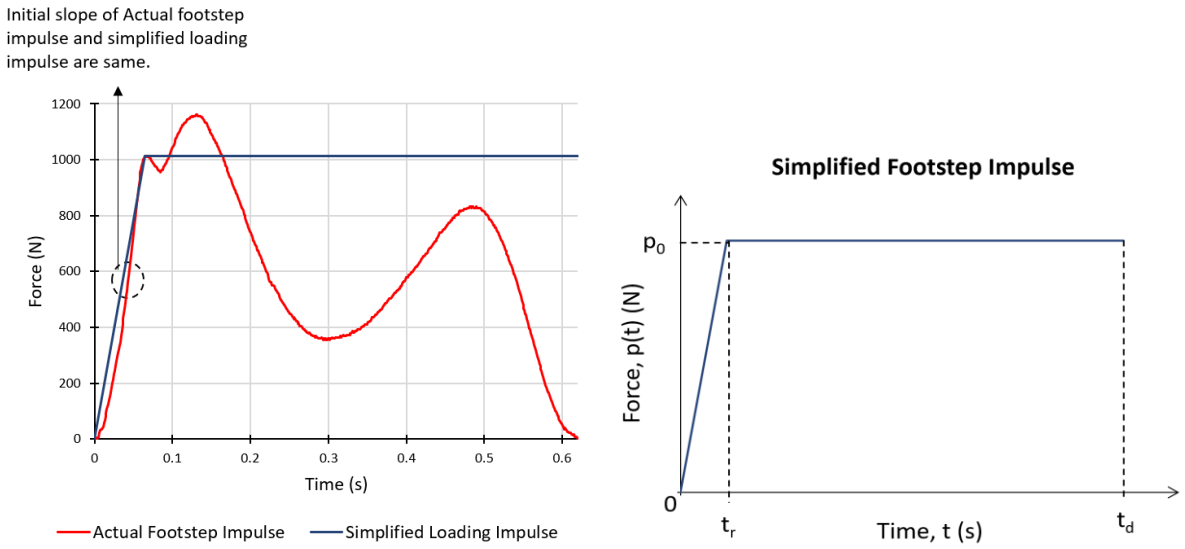

(a) (b)

Figure 3.10 (a) Comparison of actual footstep and simplified ramp and hold loading impulse; (b) Parameters of ramp and hold loading function

Table 3.5 Parameters of simplified footstep impulse for different walking frequencies

Frequency - f_s (Hz)	Initial maximum load - p_0 (N)	Rise time - t_r (s)	Impulse time - t_d (s)
1.50	752	0.095	0.860
1.58	774	0.088	0.813
1.67	729	0.085	0.775
1.75	894	0.090	0.723
1.83	850	0.085	0.709
1.92	841	0.070	0.670
2.00	1094	0.077	0.631
2.08	1014	0.065	0.621
2.17	1237	0.072	0.572

Table 3.6 Comparison of FE analysis results with and without load function simplification (LFS)

	Floor type	Walking frequency (Hz)	a_{peak} of FE (% of g)*		$a_{peak\ (with\ LFS)}$ /$a_{peak\ (w/o\ LFS)}$
			without LFS	with LFS	
Specimen 1	High-freq.	1.67	0.162	0.178	1.10
		2.08	0.612	0.674	1.10
Specimen 2	High-freq.	1.67	0.170	0.154	0.91
		2.00	0.349	0.352	1.01
Specimen 3	High-freq.	2.08	0.254	0.262	1.03
Specimen 4	Low-freq.	1.67	1.702	1.180	0.69
Average					0.97

* All analyses are performed without consideration of the spatial variation of walking load.

3.2.3 Degree-of-Freedom Simplification

In this last simplification step, the MDOF floor system is converted into an equivalent SDOF spring-mass system by using appropriate transformation factors. The degree-of-freedom simplification is performed to derive a single expression for the peak acceleration based on the fundamentals of dynamics. The transformation factors can be divided into two types: 1) the mass transformation factor which converts the total mass of the floor to a mass of the generalized SDOF

system, and 2) the load transformation factor which converts the load applied on the floor to an equivalent load applied on the generalized SDOF system. These transformation factors are thoroughly explained in this section.

According to Biggs (1964), an SDOF system is selected such that the deflection of the equivalent mass is equal to the deflection of the floor center. To derive transformation factors, first, a deflection shape for the floor is assumed. Since vibration is a dynamic response, the actual deflected shape is a combination of several mode shapes. However, the mass participation factor of the fundamental mode shape is the highest; therefore, taking the fundamental mode shape as the assumed deflected shape is a reasonable approximation. The mass transformation factor (K_m) is defined as the ratio of the equivalent mass of the SDOF system (M_e) to the total mass of the floor (M_t) as expressed in Eq. 3.6.

$$K_m = \frac{M_e}{M_t} \qquad (Eq. 3.6)$$

The equivalent mass of the SDOF system (M_e) can be determined by solving the integral presented in Eq. 3.7.

$$M_e = \int_0^A m(x,y)\varphi^2(x,y)dxdy \qquad (Eq. 3.7)$$

In this equation, $\varphi(x,y)$ is the fundamental mode shape at point (x,y) of the floor, $m(x,y)$ is the floor mass at the same point, and A is the total area of the floor. Through a comprehensive parametric study, the sensitivity of K_m to different floor design parameters was investigated. The parametric study involved conducting eigenvalue analyses on a large number of floors with a wide range of design parameters using the Abaqus FE software (CAE, 2020) to determine the fundamental mode shape and mass values of the floors. Once $\varphi(x,y)$ and $m(x,y)$ values are determined, K_m values were

calculated for each floor using Eqs. 3.7 and 3.8. It was observed that the value of K_m only depends on the support condition and the aspect ratio (λ) of the floor, as shown in Table 3.7.

Table 3.7 Mass transformation factor (K_m) values for floors with different support conditions and aspect ratios (λ)

Supported on four sides		
Aspect ratio (λ)	K_m (simply supported)	K_m (fixed supported)
1.0	0.2504	0.1654
1.2		0.1656
1.4		0.1663
1.6		0.1672
1.8		0.1683
2.0		0.1695
2.5		0.1726
3.0		0.1754
Supported on two sides		
	K_m (simply supported)	K_m (fixed supported)
All aspect ratios	0.49	0.39

A similar set of equations can be presented for the load transformation factor (K_l). As expressed in Eq. 3.8, K_l is defined as the ratio of the equivalent load applied on the SDOF system (P_e) to the total load applied on the floor (P_t) (Biggs, 1964). P_e can be determined by solving the integral presented in Eq. 3.9 where $p(x,y)$ is the load at point (x,y) of the floor, $\varphi(x,y)$ is the shape value at the same point, and A is the total area of the floor. Since the total load is applied at the center of the floor where the deflected shape $\varphi(x,y)$ is one, solving this integral results in an equivalent SDOF load (P_e) equal to the total load applied on the floor (P_t). Therefore, the value of the load transformation factor is 1 for all floors regardless of their geometry and structural details.

$$K_l = \frac{P_e}{P_t} \qquad (Eq. 3.8)$$

$$P_e = \int_0^A p(x,y)\varphi^2(x,y)dxdy \qquad (Eq. 3.9)$$

According to Murray et al. (2016), the fundamental natural frequency (f_n) of the floor can be estimated from Eq. 3.10, in which g is the acceleration due to gravity equal to 9.81 m/s^2 and Δ is the deflection at the floor center.

$$f_n = 0.18\sqrt{\frac{g}{\Delta}} \qquad (Eq.3.10)$$

The deflection at the floor center (Δ) can be calculated from Eqs. 3.11 and 3.12 for one-way and two-way floors, respectively, as suggested by Timoshenko et al. (1989).

$$\Delta_{one\ way} = \frac{5wL^4}{384\ EI} \qquad (Eq.3.11)$$

$$\Delta_{two\ way} = \frac{\xi w a^3}{D} \qquad (Eq.3.12)$$

$$D = \frac{Eh^3}{12(1-\nu^2)} \qquad (Eq.3.13)$$

where w is the dead load of the floor, L is the span of the floor, E is the elastic modulus, and I is the effective moment of inertia of the floor. In Eq. 3.12, D is the flexural rigidity of the floor in N-m, and ξ is a numerical factor estimated from Eq. 3.13 and Table 3.8, respectively, and a is the shorter length of the floor. In Eq. 3.13, h is the thickness of the floor, and ν is the Poisson's ratio. In Table 3.8, ξ is expressed in terms of the floor aspect ratio (λ), which is the ratio of the larger length by the shorter length of the floor.

Table 3.9 compares the natural frequency computed from the above equations against that obtained from the FE analysis for the four floor specimens. It can be seen that, on average, the calculated natural frequencies are within 3% of the FE results, which shows a good correlation.

Table 3.8 Numerical factor (ξ) values for different aspect ratios (λ)

Aspect ratio (λ)	Numerical factor (ξ)
1.0	0.00406
1.1	0.00485
1.2	0.00564
1.3	0.00638
1.4	0.00705
1.5	0.00772
1.6	0.00830
1.7	0.00883
1.8	0.00931
1.9	0.00974
2.0	0.01013
3.0	0.01223

Table 3.9 Comparison of results of FE analysis and proposed SDOF system

	Floor type	Walking frequency (Hz)	FE analysis*		SDOF system*		$f_{n\,(SDOF)}/f_{n\,(FE)}$	$a_{peak\,(SDOF)}/a_{peak\,(FE)}$
			f_n (Hz)	a_{peak} (% of g)	f_n (Hz)	a_{peak} (% of g)		
Specimen 1	High-freq.	1.67	10.04	0.178	9.82	0.183	0.98	1.03
		2.08		0.674		0.728		1.08
Specimen 2	High-freq.	1.67	11.23	0.154	12.55	0.200	1.12	1.30
		2.00		0.352		0.331		0.94
Specimen 3	High-freq.	2.08	15.41	0.262	14.73	0.187	0.96	0.71
Specimen 4	Low-freq.	1.67	5.14	1.180	5.45	1.309	1.06	1.11
Average							1.03	1.03
Coefficient of variation							0.06	0.17

* All analyses include load simplification.

Finally, the stiffness (k) of the spring of the SDOF system can be calculated from Eq. 3.14, in which ω_n is the angular frequency determined from Eq. 3.15.

$$k = M_e\omega_n^2 \qquad (Eq.3.14)$$

$$\omega_n = (2\pi f_n) \qquad (Eq.3.15)$$

Once the mass and load transformation factors, the natural frequency, and the stiffness of the floor are determined, the MDOF floor system can be converted into an SDOF spring-mass system. By applying the simplified loading functions described in Section 3.2.2 to the SDOF spring-mass system and using fundamentals of dynamics, expressions for the calculation of peak acceleration can be derived. Since the simplified loading functions are different for low- and high-frequency floors, expressions for the peak acceleration are also different. For low-frequency floor systems, as described earlier, the simplified forcing function is represented by Eq. 3.4 in which the frequency of the forcing function matches the fundamental frequency of the floor to simulate the resonance effect. The resonance amplifies the acceleration time response before the steady-state peak acceleration is reached. By imposing this forcing function to the SDOF spring-mass system, Eq. 3.16 for the peak acceleration (a_{peak}) of low-frequency floors can be derived, where β is the damping ratio.

$$a_{peak} = \frac{\alpha_i Q}{2\beta M_e} \qquad (Eq.3.16)$$

For high-frequency floors, the simplified loading function is represented by Eq. 3.5. The application of this simplified loading function on the equivalent SDOF spring-mass system results in the deflection time history of $u(t)$ that can be calculated by Duhamel's integral as expressed in Eq. 3.17. The peak acceleration in high-frequency floors occurs in the very initial phase of the

impulse load, and therefore, the effect of damping can be ignored in the calculation of peak acceleration.

$$u(t) = \begin{cases} \frac{1}{M_e \omega_n} \int_0^{t_r} p(t) sin(\omega_n (t - T)) dT & t \le t_r \\ \frac{1}{M_e \omega_n} \int_{t_r}^{t_d} p(t) sin(\omega_n (t - T)) dT & t_r \le t \le t_d \end{cases} \qquad (Eq. 3.17)$$

By solving the integrals and double differentiation of *u(t),* the acceleration time response can be determined as:

$$a(t) = \begin{cases} \frac{p_0}{M_e \omega_n t_r} [\sin(\omega_n t)] & t \le t_r \\ \frac{p_0}{M_e \omega_n t_r} [\sin(\omega_n t) - \sin(\omega_n (t - t_r))] & t_r \le t \le t_d \end{cases} \qquad (Eq. 3.18)$$

Knowing the acceleration time response, the peak acceleration can be expressed as:

$$a_{peak} = max \begin{cases} \frac{p_0}{M_e \omega_n t_r} & t \le t_r \\ \frac{p_0}{M_e \omega_n t_r} [\sin(\omega_n t_1) - sin(\omega_n (t_1 - t_r))] & t_r \le t \le t_d \end{cases} \qquad (Eq. 3.19)$$

where t_1 can be determined from Eq. 3.20 in which n is the smallest integer that results in the t_1 value that is higher than t_r and less than t_d.

$$t_r \le t_1 = \frac{n}{2f_n} + \frac{t_r}{2} \le t_d \qquad (Eq. 3.20)$$

Table 3.9 compares the peak acceleration calculated by the FE analysis and the proposed SDOF model for the four experimentally tested floor specimens described before. The peak acceleration calculated by the SDOF model for the low-frequency floor was 11% more than the value obtained from FE analysis. For the high-frequency floors, on average, the peak acceleration was within 2% of the FE analysis results. The coefficient of variation of the peak acceleration results was

relatively higher than that for the calculated natural frequency values (0.17 vs. 0.06), which was expected as the calculation of the peak acceleration is more complicated than the natural frequency. Considering the extent of simplification made in the analysis procedure and the complexity involved in the response of floors under vibration, the peak accelerations estimated by the proposed SDOF model are reasonably accurate. In the next chapter, the performance of the SDOF model will be evaluated in more detail.

The step-by-step procedure for using the proposed SDOF method to estimate the peak acceleration of low- and high-frequency floors is presented in Figure 3.11. The simplified expression for the peak acceleration of low-frequency floors is derived from the steady-state acceleration response, and therefore it is only valid for resonating step frequency (not any other step frequency). This resonating frequency is responsible for the overall maximum peak acceleration across the range of stepping frequency; therefore, the proposed expression can capture the peak acceleration for a given floor. In high-frequency floors, on the other hand, the peak acceleration expression is valid for any given stepping frequency. Since these floors exhibit an impulsive type of behaviour, their acceleration response intensifies as the stepping frequency increases. Therefore, for computing the overall maximum peak acceleration, the highest stepping frequency (2.2 Hz) should be selected.

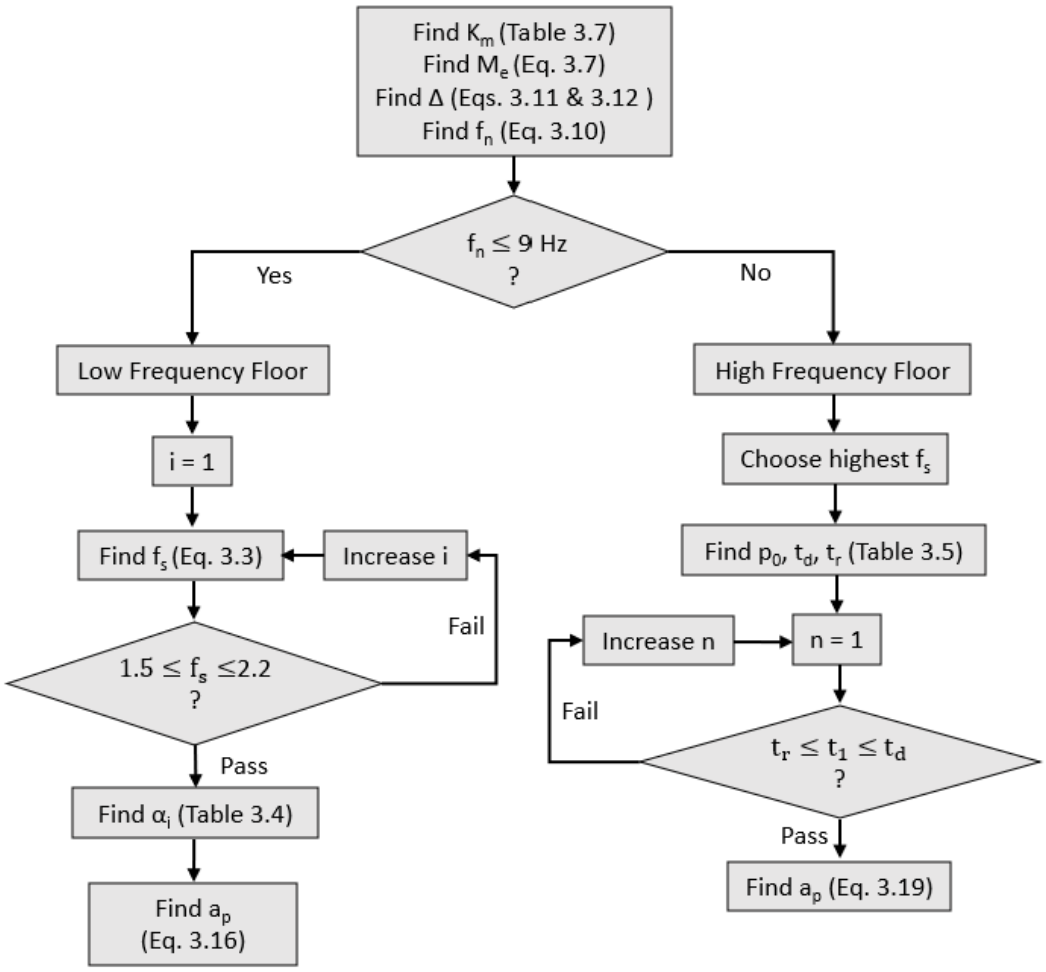

Figure 3.11 Algorithm of the proposed SDOF method for the calculation of peak acceleration

3.3 Comparison of the Newly Developed SDOF Method to the SDOF Method of AISC

The AISC Design Guide 11 (Murray et al. 2016) provides two methods for the computation of peak acceleration which both are widely used for the vibration design and assessment of floors across North America. The first method is a simplified method developed based on an equivalent SDOF system making it suitable for design purposes, while the second method is more comprehensive and requires FE analyses. This section first provides a brief overview of the SDOF method of AISC and then compares the performance of the AISC-SDOF method and the proposed SDOF method by analyzing the floor specimens described in Section 3.1.

3.3.1 Low-Frequency Floors

In AISC, the peak acceleration for low-frequency floors is calculated from Eq. 3.21 derived based on the steady-state resonance acceleration response of an equivalent SDOF system originally proposed by Rainer et al. (1988). In this equation, the peak acceleration is expressed as a function of DLF (α) determined from Eq. 3.22, the weight of an average person (Q) usually taken as 747.5 N, damping ratio (β), the effective mass of the floor (M), and a reduction factor (R).

$$a_{peak} = \frac{P}{2\beta M} = \frac{R\alpha Q}{2\beta M/2} \qquad (Eq\ 3.21)$$

$$\alpha = 0.83e^{-0.35f_n} \qquad (Eq\ 3.22)$$

By comparing Eq. 3.21 of AISC to Eq. 3.16 proposed in this study, it can be seen that although the basis of both methods is the same (the steady-state acceleration response of an SDOF system), there are significant differences between them. Firstly, AISC assumes that the equivalent SDOF mass of the system equals half of the floor's effective mass (M), which results in a mass transformation factor (K_m) of 0.5. The calculation of M is complicated, which makes the design process of AISC tedious compared to the proposed method. Also, assuming a constant value for K_m, proposed based on experiments conducted on one-way simply supported footbridges, raises questions about the accuracy and the application range of the AISC method. As shown in Table 3.7, the value of K_m can range from 0.16 to 0.49 depending on the end support condition and the floor aspect ratio. It can be seen that the assumption made in AISC is only accurate for simply supported floors supported on two sides for which the K_m value is 0.49. The SDOF method proposed in this study takes into account the effect of end support condition and the floor aspect ratio in the calculation of K_m. The second difference between the two methods is that the DLF used in the SDOF method of AISC was obtained based on only the experiments conducted by Rainer et

al. (1988). However, the DLF used in the proposed method was adopted from Willford et al. (2006), which was determined based on 880 measured footfalls from the experiments conducted by several researchers, including Rainer et al. (1988). Using DLF from a more extensive set of experimental tests improves the application range and accuracy of the proposed method. Furthermore, the AISC method reduces the peak acceleration by a factor of two ($R=0.5$) to consider the fact that the walker and potentially annoyed person are not simultaneously at the same location on the floor. This factor is not considered in the proposed SDOF method since the experimental tests used for the verification studies were conducted such that both the point of disturbance and observation are at the same location. To have a consistent comparison between the two methods, the reduction factor was not considered for the AISC method in the analyses performed in this study.

3.3.2 High-Frequency Floors

AISC provides Eq. 3.23 for the peak acceleration of high-frequency floors in which R_m is the higher mode effect taken as 2.0 and I_{eff} is the effective impulse calculated from Eq. 3.24.

$$a_{peak} = \frac{2\pi f_n R_m I_{eff}}{M/2} g \qquad (Eq. 3.23)$$

$$I_{eff} = \left(\frac{f_s^{1.43}}{f_n^{1.30}}\right)\left(\frac{Q}{17.8}\right) \qquad (Eq. 3.24)$$

Eq. 3.24 was derived by analyzing floors with different natural frequencies under several force-time histories of footfalls and computing their peak accelerations. These peak accelerations were then equated to an expression that determines the peak acceleration in the free vibration phase of an SDOF system subjected to an instantaneous impulse. Compared to the proposed SDOF expression (Eq. 3.19), the AISC expression has several major limitations. Firstly, an actual footstep

impulse is not instantaneous; instead, it occurs for a finite time; therefore, the assumption of instantaneous impulse made in the AISC method may affect the accuracy of the results. Secondly, as mentioned earlier, peak acceleration under impulse loading occurs during the forced vibration phase of the response (Chopra 2011). In contrast, in AISC, the peak acceleration is determined after applying the impulse in the free vibration phase. In the proposed SDOF model, the forced vibration phase of the response is considered in the derivation of the formulation. Thirdly, similar to the low-frequency floors, the AISC's expression for high-frequency floors is only valid for a floor system that is simply supported on two sides as K_m is assumed as 0.5. In the case of the proposed SDOF method, the support condition and the aspect ratio of the floor are considered in the calculation of K_m. Fourthly, the I_{eff} factor used in the AISC expression is calibrated based on analysis of a limited number of floors with frequencies ranging from 9 Hz to 15 Hz. However, the peak acceleration expression of the proposed SDOF method is derived by applying reasonable simplifications to the actual footstep impulse, as shown in Figure 3.10 and Table 3.5, without requiring any calibrations. As it will be shown in Chapter 4, which includes a thorough parametric study, the proposed SDOF method has a broader application range compared to the AISC method. Another difference between the two methods is that the AISC expression considers the effect of higher modes on the peak acceleration through a higher mode factor (R_m). In the proposed SDOF method, no such parameter is considered since detailed FE analyses of floors showed that the mass participation factor of the fundamental mode is typically high enough to neglect the rest of the modes for the calculation of the peak acceleration. Thus, to convert the MDOF floor to an SDOF system, only the deflected shape of the fundamental mode is considered in the derivation of the formulation. As it will be shown in the verification and parametric studies, this assumption did not have a noticeable effect on the results.

Table 3.10 compares the peak acceleration calculated by the SDOF method of AISC and the proposed SDOF method for the four floor specimens described before. It can be seen that for the high-frequency floors, the AISC method is conservative, resulting in peak accelerations that are about 2.5 times the experimentally reported values. For the low-frequency floor, the AISC method is even more conservative, overestimating the peak acceleration by a factor of 3. It should be noted that to be consistent with the experimental tests the peak acceleration of the low-frequency floor is calculated by neglecting the reduction factor of 2.0 described above. Considering the reduction factor results in the peak acceleration ratio of 1.53. Table 3.10 also shows that the proposed SDOF method predicted the peak acceleration of both low- and high-frequency floors with good accuracy.

Table 3.10 Comparison of the peak acceleration calculated by the new SDOF method and the AISC SDOF method with the experimental results

	Floor type	Walking frequency (Hz)	a_{peak} (% of g)			$a_{peak\ (New\ SDOF)}/a_{peak\ (Test)}$	$a_{peak\ (AISC\ SDOF)}/a_{peak\ (Test)}$
			Test	New SDOF	AISC SDOF		
Specimen 1	High-freq.	1.67	0.199	0.183	0.468	0.92	2.35
		2.08	0.454	0.728	1.040	1.60	2.29
Specimen 2	High-freq.	1.67	0.162	0.200	0.473	1.23	2.92
		2.00	0.375	0.331	0.953	0.88	2.54
Specimen 3	High-freq.	2.08	0.220	0.187	0.500	0.85	2.27
Specimen 4	Low-freq.	1.67	1.360	1.309	4.156	0.96	3.06
Average						1.07	2.62

Chapter 4: Evaluate the Application Range of the Proposed Simplified Methods

To further verify the accuracy of the proposed single-degree-of-freedom (SDOF) method for vibration assessment and evaluate its application range, a comprehensive parametric study was conducted by modelling and analyzing 26 floors. As shown in Table 4.1, the floors were varied in terms of five key design parameters: thickness, size, aspect ratio, support condition and material type. In this table, the shorter length, longer length, and overall thickness of the floor are represented by *a*, *b*, and *t*, respectively. In order to have a consistent comparison, the density and grade of concrete used for all floors were taken as 2400 kg/m^3 and 25 MPa, respectively, except for the lightweight concrete floor in which the density and grade of concrete were chosen as 1800 kg/m^3 and 35 MPa. The damping was assumed as 3%, which was evaluated from AISC Design Guide 11 (Murray et al. 2016) for a typical floor. All 26 cases presented in Table 4.1 were solid concrete floors that were simply supported on their four edges except the ones that fall under the "material type" and "support condition" categories. Figure 4.1 shows the structural details of different floor systems considered in this parametric study.

The peak acceleration is the most critical parameter for the vibration assessment of a floor subjected to walking. As discussed earlier, the full finite element (FE) model with spatial variation and actual walking load gives the most accurate peak acceleration value; hence this value was used as a reference peak acceleration to evaluate the accuracy of the new SDOF method. In addition to the FE and proposed SDOF methods, the peak acceleration was computed using the SDOF method of AISC (Murray et al. 2016) to examine the accuracy and application range of this commonly used design guideline as well.

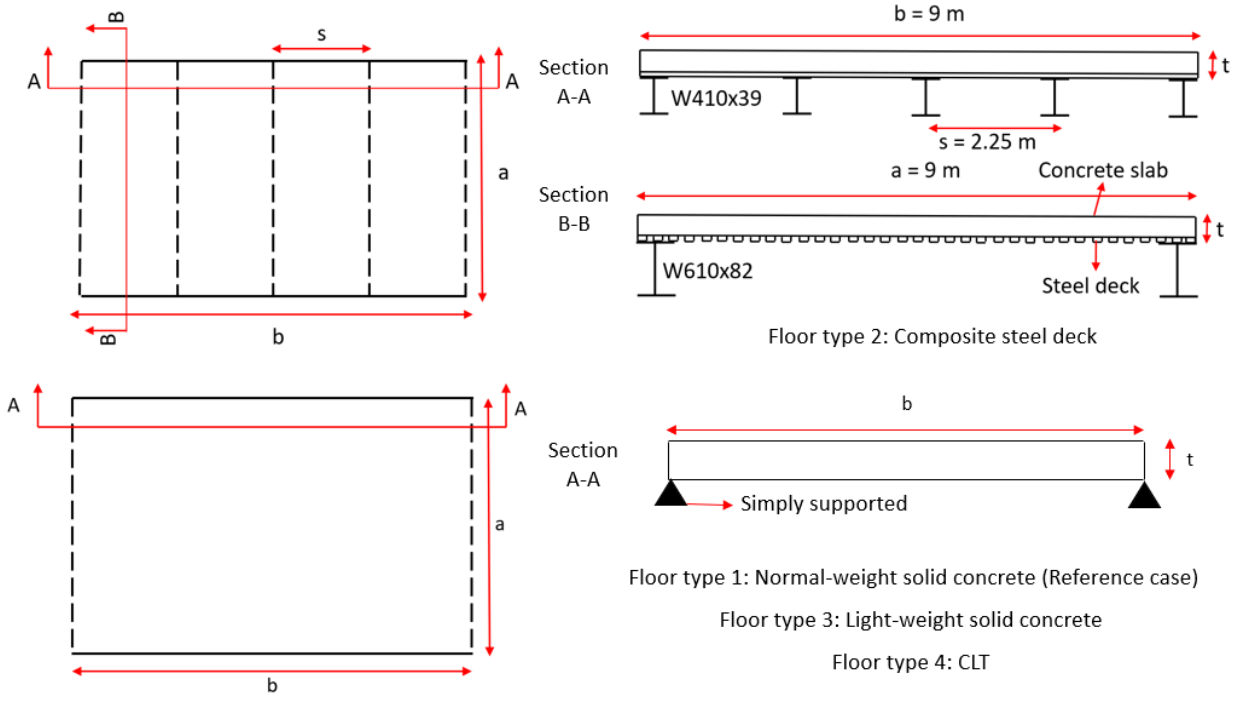

Figure 4.1 Structural details of floor types used in parametric study

Since the assumptions and formulation used for the peak acceleration expression of low- and high-frequency floors are different, an adequate number of floors with different frequencies were considered in the parametric study so that accuracy of each SDOF method can be discussed separately for low- and high-frequency floors. For high-frequency floors, the SDOF method of AISC is only recommended for floors with a natural frequency of less than 15 Hz; therefore, floors with higher natural frequencies were not considered in this parametric study. However, at the end of this chapter, additional cases will be added to the parametric study to further evaluate the application range of the proposed SDOF method for highly stiff floors (15 Hz < f_n < 60 Hz). These high frequencies can occur in the case of small size lightweight floors typically used in modular construction. Most of the floors discussed in this parametric study meet the CSA A23.3:19, CSA S16:19, and CSA O86:14 code strength and serviceability requirements; however, in order to cover

a wide range of design parameters some floor cases had to be selected that do not fully satisfy the code requirements. These floor cases, which are underlined in Table 4.1, are provided only for the evaluation of different vibration assessment methods and should not be used for design applications.

To evaluate the maximum response of low-frequency floors, as mentioned in Section 1.1, the walking frequency should be selected such that one of its harmonics matches with the fundamental frequency of the floor to cause resonance. For high-frequency floors, however, the highest frequency (2.2 Hz) within the typical range of walking frequency should be selected in order to maximize the response due to impulsive behaviour. The selected walking frequency (f_s) for analysis of each floor case is shown in Table 4.1. The table also shows the ratio of peak acceleration computed by the AISC and proposed SDOF methods to that obtained from the full FE analysis. A ratio of one indicates that the SDOF method predicted the peak acceleration with perfect accuracy. If the ratio is less than one, the SDOF method underpredicted the peak acceleration, and if it is greater than one, the results are overpredicted.

Table 4.1 Comparison of the natural frequency and peak acceleration computed by the proposed SDOF method and AISC's SDOF method with FE results for 26 floor cases

Case no.	Floor type	Design parameter	a (m)	b (m)	t (mm)	f_s (Hz)	FEA		SDOF			a_{peak} (new SDOF) /a_{peak} (FEA)		a_{peak} (AISC) /a_{peak} (FEA)	
							f_n (Hz)	a_{peak} (m/s^2)	f_n (Hz)	a_{peak} (m/s^2) New method	a_{peak} (m/s^2) AISC method				
1	High-freq.	Size	5.5	5.5	150	2.2	15.30	0.064	12.55	0.068	0.182	1.06		2.84	
2			6	6	150	2.2	12.88	0.105	10.56	0.097	0.161	0.92		1.53	
3			6.5	6.5	150	2.2	10.98	0.131	11.86	0.126	0.144	0.96		1.10	
4	Low-freq.		8	8	175	2.08 (4th)	8.46	0.103	9.14	0.096	0.056	0.93		0.54	
5			9	9	175	1.67 (4th)	6.70	0.060	5.49	0.063	0.080	1.05		1.34	
6			10	10	175	1.83 (3rd)	5.43	0.062	5.97	0.055	0.102	0.89		1.64	
Average												Low-freq.	High-freq.	Low-freq.	High-freq.
												0.96	0.98	1.17	1.82
7	High-freq.	Thickness	6	6	125	2.2	10.76	0.180	11.62	0.167	0.203	0.93		1.13	
8			6	6	150	2.2	12.88	0.105	10.56	0.097	0.161	0.92		1.53	
9			6	6	175	2.2	14.98	0.047	12.28	0.050	0.132	1.06		2.81	
10	Low-freq.		9	9	145	1.83 (3rd)	5.48	0.091	6.03	0.084	0.152	0.92		1.68	
11			9	9	175	1.67 (4th)	6.70	0.060	5.50	0.063	0.080	1.05		1.34	
12			9	9	200	1.83 (4th)	7.41	0.054	8.00	0.062	0.056	1.15		1.04	
Average												Low-freq.	High-freq.	Low-freq.	High-freq.
												1.04	0.97	1.35	1.82

Table 4.1 Comparison of the natural frequency and peak acceleration computed by the proposed SDOF method and AISC's SDOF method with FE results for 26 floor cases - Continued

Case no.	Floor type	Design parameter		a (m)	b (m)	t (mm)	f_s (Hz)	FEA		SDOF			$a_{peak\ (new\ SDOF)}$ /$a_{peak\ (FEA)}$		$a_{peak\ (AISC)}$ /$a_{peak\ (FEA)}$	
								f_n (Hz)	a_{peak} (m/s^2)	f_n (Hz)	a_{peak} (m/s^2) New method	a_{peak} (m/s^2) AISC method				
13	High-freq.	Aspect ratio	1	6	6	150	2.2	12.88	0.105	14.17	0.093	0.161	0.89		1.53	
14			1.4	6	8.4	150	2.2	9.75	0.102	8.99	0.095	0.125	0.93		1.23	
15			2	6	12	150	2.2	9.20	0.100	9.94	0.093	0.092	0.93		0.92	
16	Low-freq.		1	9	9	190	1.83 (4^{th})	7.41	0.072	8.00	0.062	0.056	0.86		0.78	
17			1.4	9	12.6	190	1.83 (3^{rd})	5.50	0.056	4.51	0.045	0.082	0.80		1.46	
18			2	9	18	190	1.51 (3^{rd})	4.54	0.031	3.72	0.029	0.080	0.94		2.58	
Average													Low-freq.	High-freq.	Low-freq.	High-freq.
													0.87	0.92	1.61	1.22
19	High-freq.	Support condition	Pin	6	6	110	2.2	9.48	0.212	9.10	0.205	0.240	0.97		1.13	
20			Fix	6	6	110	2.2	14.92	0.120	13.40	0.091	0.200	0.76		1.67	
21	Low-freq.		Pin	10	10	150	1.55 (3^{rd})	4.66	0.058	5.35	0.059	0.104	1.02		1.80	
22			Fix	10	10	150	2.17 (4^{th})	8.55	0.112	7.96	0.110	0.162	0.98		1.44	
Average													Pin	Fix	Pin	Fix
													0.99	0.87	1.47	1.56

Table 4.1 Comparison of the natural frequency and peak acceleration computed by the proposed SDOF method and AISC's SDOF method with FE results for 26 floor cases - Continued

Case no.	Floor type	Design parameter		a (m)	b (m)	t (mm)	f_s (Hz)	FEA		SDOF			$a_{peak\ (new\ SDOF)}$ /$a_{peak\ (FEA)}$		$a_{peak\ (AISC)}$ /$a_{peak\ (FEA)}$	
								f_n (Hz)	a_{peak} (m/s^2)	f_n (Hz)	a_{peak} (m/s^2)					
											New method	AISC method				
23	High-freq.	Floor type	Specimen 1	3	3	100	2.2	14.9	0.180	14.12	0.135	0.226	0.75		1.26	
24			Specimen 2	9	9	210	2.2	10.04	0.561	10.70	0.728	0.692	1.30		1.23	
25			Specimen 3	3.5	3.5	75	2.2	13.72	0.150	13.40	0.182	0.397	1.21		2.65	
26			Specimen 4	4	4	125	2.2	14.43	0.260	14.95	0.234	0.644	0.90		2.48	
Average													Spec. 1 & 2	Spec. 2 & 4	Spec. 1 & 2	Spec. 2 & 4
													1.02	1.05	1.24	2.56

To better understand the results, the peak acceleration ratio is plotted against the floor frequency as well as variations in each design parameter (size, thickness, aspect ratio, etc.) in Figures 4.2 to 4.7 for all 26 floor cases. From Figure 4.2 it can be seen that the proposed SDOF method computed the peak acceleration of floors with various frequencies ranging from 4.5 Hz to 15 Hz with good accuracy. However, the AISC method generally overestimated the peak acceleration for both the low- and high-frequency floors. For the low-frequency floors with f_n less than 6.5 Hz, the accuracy deteriorated with the decrease in floor frequency. On the other hand, for high-frequency floors with f_n greater than 13 Hz, the accuracy deteriorated with increase in the frequency of the floor. The results show that the peak accelerations predicted by AISC did not correlate well with the FE analysis results, particularly for floors with frequencies less than 6.5 Hz or higher than 13 Hz.

The reason for the overestimation of the results for the low-frequency floors is the dynamic load factor (DLF) used in the AISC method. Figure 4.3 compares DLF values used by the SDOF and FEA methods of AISC as well as those implemented in the proposed SDOF method. In this igure, the blue curve represents the DLF implemented in the proposed SDOF method which was proposed by Willford et al. (2007) based on a vast set of experimental tests. The red curve represents the DLF used in the AISC-SDOF method, which was obtained based on a small set of experiments conducted by Rainer et al. (1988). It is believed that the larger number of test data used by Willford et al. (2007) compared to Rainer et al. (1988) resulted in more accurate DLF values. It can be seen from Figure 4.3 that as the harmonic forcing frequency (which equals to the natural floor frequency for the case of resonance) decreases below 8 Hz, the DLF of the AISC-SDOF method significantly increases and deviates from the DLF of the proposed SDOF method. Since the peak acceleration is directly proportional to the DLF, higher values of DLF results in the overestimation of the peak acceleration by the AISC-SDOF method. For harmonic forcing

frequencies larger than 8 Hz, however, the DLF of the AISC-SDOF method becomes smaller than that used for the proposed SDOF method, which leads to underestimation of the results. Figure 4.3 also shows the DLF values used in the FE analysis method of AISC (the grey curve), which correlate well with the values of the proposed SDOF method since both methods use the values reported from Willford et al. (2007). For high-frequency floors, AISC considers the vibration problem to be very rare as resonance does not take place. The peak acceleration expression of AISC was calibrated against FE analyses and experimental tests mainly conducted on floors with natural frequencies less than 13 Hz. Thus, as shown in Figure 4.2, the accuracy of the AISC method quickly deteriorates as the floor frequency increases beyond 13 Hz.

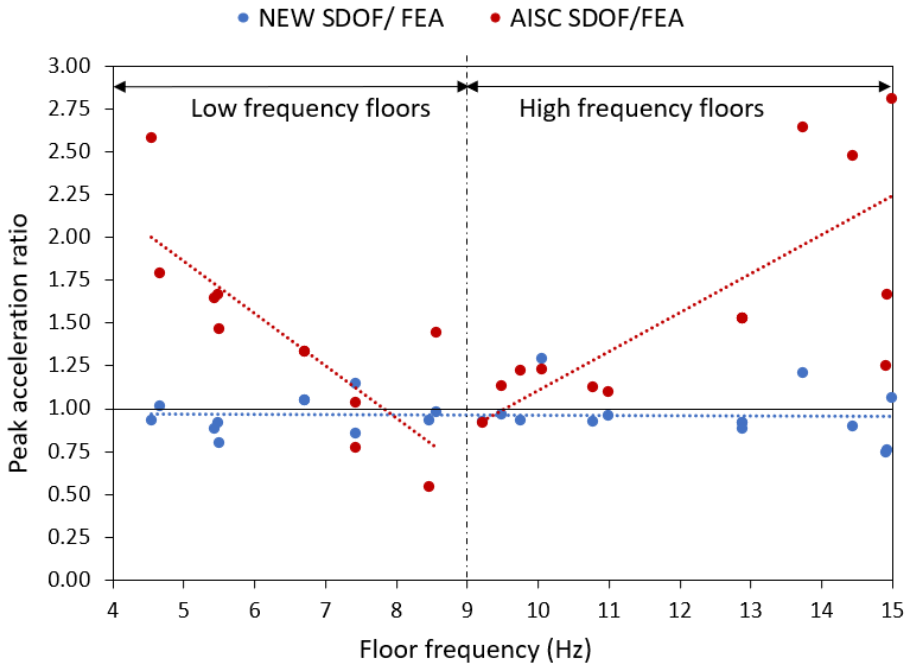

Figure 4.2 Correlation between peak acceleration ratio and floor frequency for new SDOF method and AISC-SDOF method for 26 floor specimens

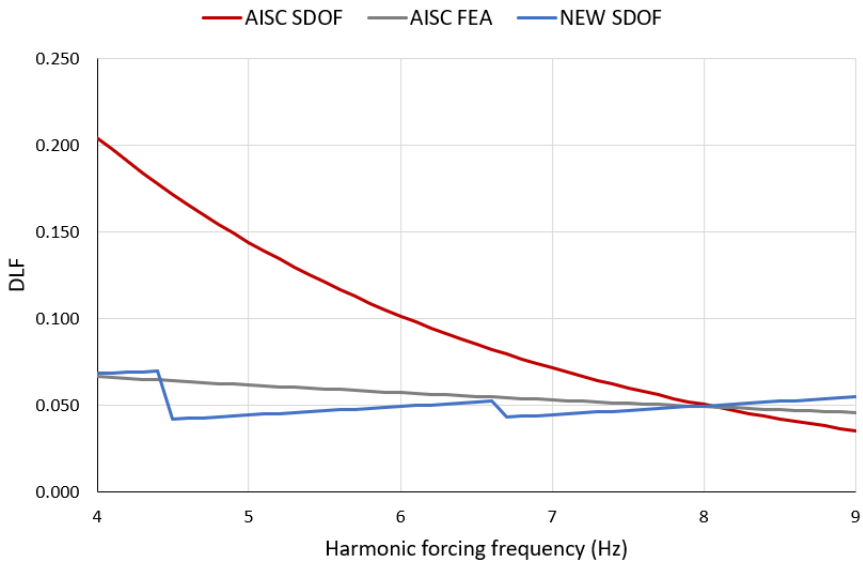

Figure 4.3 Comparison of the DLF used for AISC-SDOF, AISC-FEA, and proposed SDOF method

Figure 4.4 shows the effect of floor size on the performance of the AISC and proposed SDOF methods. Apart from the floor size, the rest of the design parameters were kept the same for low- and high-frequency floors to have a consistent comparison. It can be seen that the proposed method was able to accurately predict the peak acceleration of square floors of different dimensions ranging from 5.5 m to 10 m. The average peak acceleration ratio for all six floors was 0.97, which demonstrates an excellent correlation between the results of the proposed model and the FE method. The AISC method, however, did not perform well for low-frequency floors larger than 9 m x 9 m and high-frequency floors smaller than 6 m x 6 m.

Figure 4.5 evaluates the accuracy of the AISC and proposed SDOF methods for floors with different thickness values. The only design parameter that was changed for low- and high-frequency floor cases presented in this figure was the floor thickness. It can be seen that the proposed SDOF method predicted the peak acceleration with excellent accuracy for floors with thicknesses varying from 125 mm to 200 mm resulting in a mean ratio of 1.01. The AISC method

significantly overestimated the results for both low- and high-frequency floors with thicknesses less than 175 mm and more than 150 mm, respectively. The peak acceleration predictions of AISC were more accurate for low-frequency floors with larger thicknesses and high-frequency floors with smaller thicknesses.

Figure 4.6 shows the variation of peak acceleration in terms of the aspect ratio of the floor. The aspect ratio was changed from 1 to 2 while keeping all the other design parameters of the floor the same. Again, the peak accelerations computed by the proposed SDOF method and the FE analysis correlated quite well, resulting in a mean ratio of 0.89. The AISC method underpredicted the peak acceleration for the low-frequency floor with the square shape and started to overpredict the results as the aspect ratio increased. In the case of high-frequency floors, the AISC method overpredicted the peak acceleration of the square floor, but the predictions improved as the aspect ratio increased.

To investigate the effect of support conditions on the performance of the AISC and proposed SDOF methods, a total of four floors were defined (two low-frequency and two high-frequency floors) in which only the support condition of the floors was changed from pinned to fixed. The other design parameters were chosen such that upon changing the support condition, the floor type (low-frequency or high-frequency) remained the same. It is worth noting that although the majority of the floors in practice are designed assuming pinned support conditions, there is always some level of fixity at the support that can influence the natural frequency and consequently the vibration performance of the floor. As shown in Figure 4.7, the accuracy of the proposed SDOF method remained consistent as the support condition changed for both the low- and high-frequency floors resulting in a mean peak acceleration ratio of 0.93. The AISC method, however, overestimated the results of three out of four cases and only calculated the peak acceleration of the high-frequency floor with pinned support condition with good accuracy.

The results presented in Figures 4.4 to 4.7 confirms the conclusion made from Figure 4.2 that the performance of the SDOF method of AISC is highly sensitive to the natural frequency of the floor. As the design parameters of the floor change, its natural frequency changes which directly affects the accuracy of the AISC method. If the natural frequency of the floor falls below 6.5 Hz or becomes more than 13 Hz, the AISC method typically cannot predict the peak acceleration well. For example, as the size or aspect ratio of a high-frequency floor reduces (Figures 4.4 and 4.6) or its thickness increases (Figure 4.5), the floor becomes stiffer and therefore, its natural frequency increases resulting in less accurate predictions from AISC. A similar trend is observed for the effect of the support condition. As shown in Figure 4.7, changing the support condition of a high-frequency floor from pinned to fixed support increases the stiffness and frequency of the floor, which again negatively affects the accuracy of the AISC method.

The last design parameter that was considered is the material type of the floor. The vibration performance of floors with four different material types was investigated: normal weight solid concrete floor, lightweight solid concrete floor, composite steel deck floor, and cross-laminated timber (CLT) floor. The structural and geometric details of these floor systems are shown in Figure 4.1. To be consistent in the comparison, all four floors were designed as one-way high-frequency slabs since most non-conventional floors (e.g., CLT floors) are lightweight floors with high natural frequencies. The first floor system was a normal weight solid concrete floor with a thickness of 100 mm supported on its two edges. The floor was 3 m long by 3 m wide and had a total mass of 2,160 kg. The second floor was a lightweight solid concrete floor with dimensions of 3.5 m by 3.5 m and a thickness of 75 mm. The density and grade of concrete used for this floor were 1800 kg/m^3 and 35 MPa, respectively, and the total mass was 1,655 kg. The third floor was a composite steel deck which consisted of a 159 mm thick concrete slab on a 51 mm thick steel deck. The floor was

9 m by 9 m and had a total mass of 32,700 kg. Five W410x38.8 steel joists supported the composite deck at 2.25 m center-to-center spacing, and two W610x82 girders supported the joists. The fourth floor was made from cross-laminated timber (CLT) with dimensions of 4 m by 4 m and a thickness of 125 mm. The stress grade of CLT was "E_1" and density was 500 kg/m^3 resulting in a total floor mass of 1000 kg.

Figure 4.8 shows the computed peak acceleration ratios for each floor system. It can be seen that the proposed SDOF method provided accurate results for all four floors regardless of their material type. The AISC method, however, only predicted the peak acceleration of the normal weight solid concrete and composite steel deck floors well and significantly overestimated the results for the lightweight solid concrete and CLT floors. This overestimation is perhaps due to the fact that the empirical expressions used in the AISC method are not calibrated for floors made from such materials.

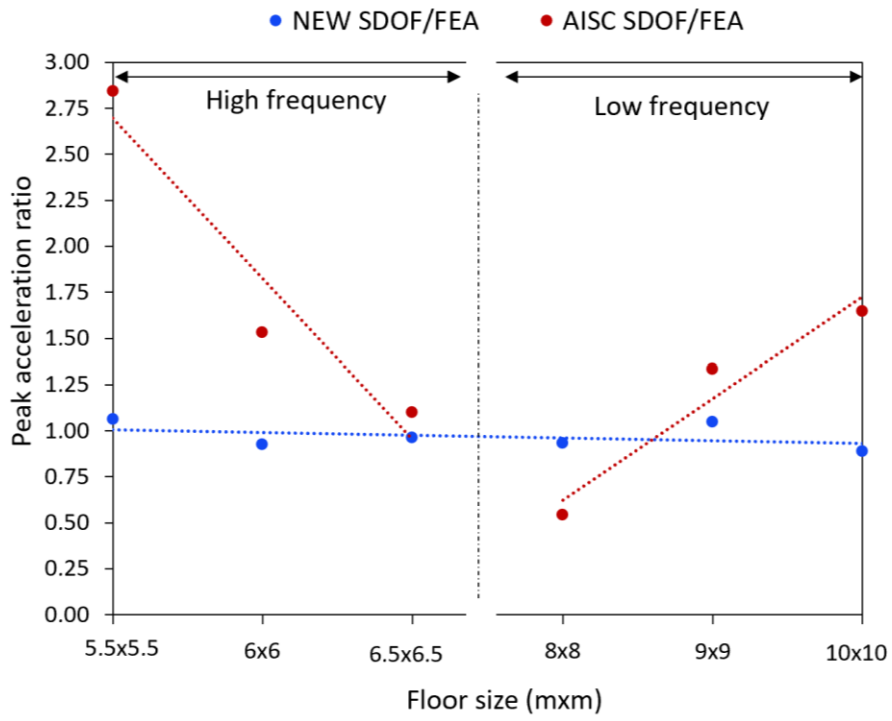

Figure 4.4 Variation of peak acceleration ratio in terms of floor size

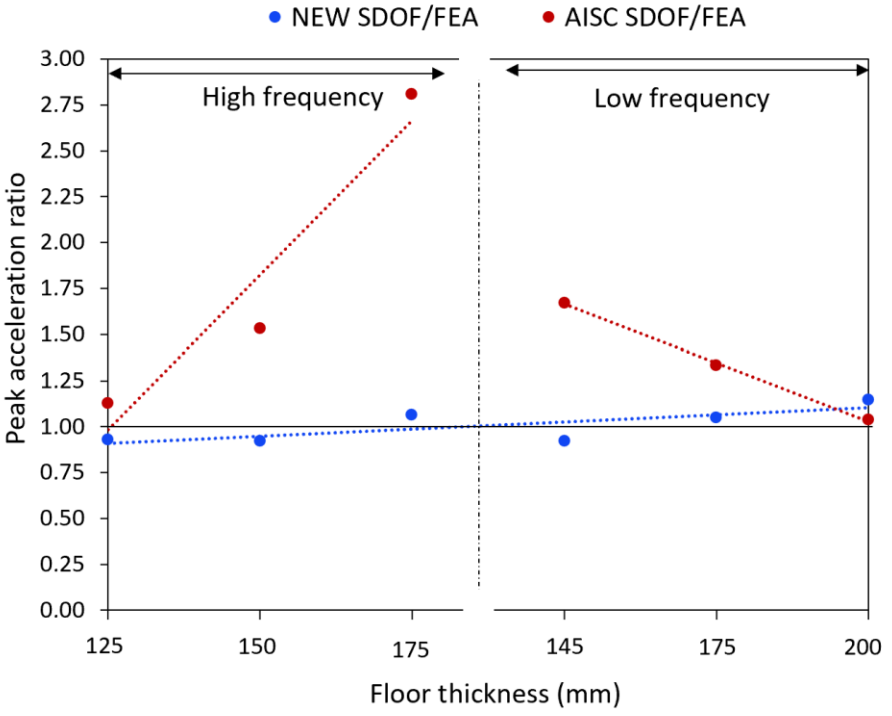

Figure 4.5 Variation of peak acceleration ratio in terms of floor thickness

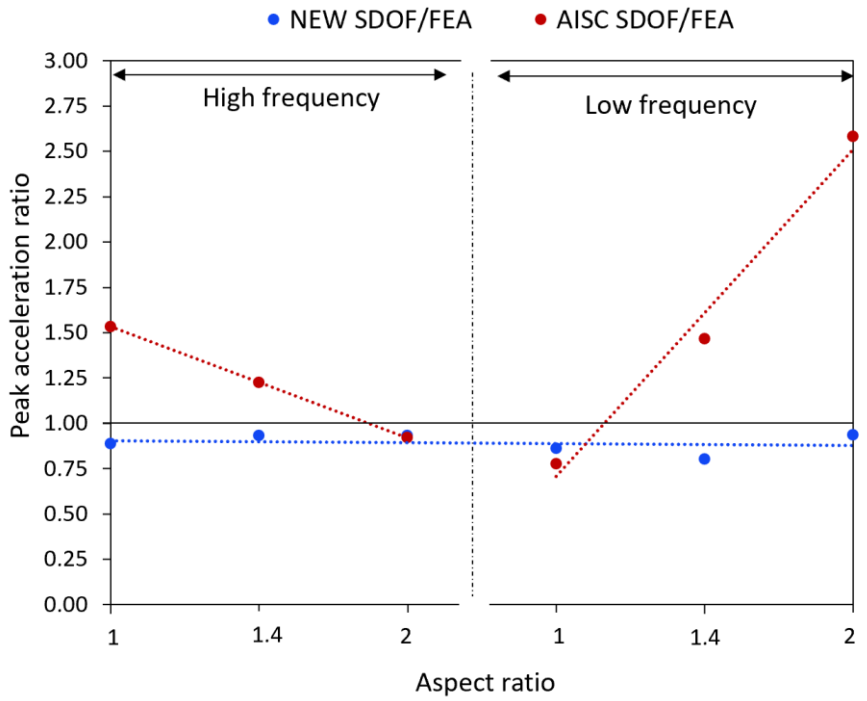

Figure 4.6 Variation of peak acceleration ratio in terms of floor aspect ratio

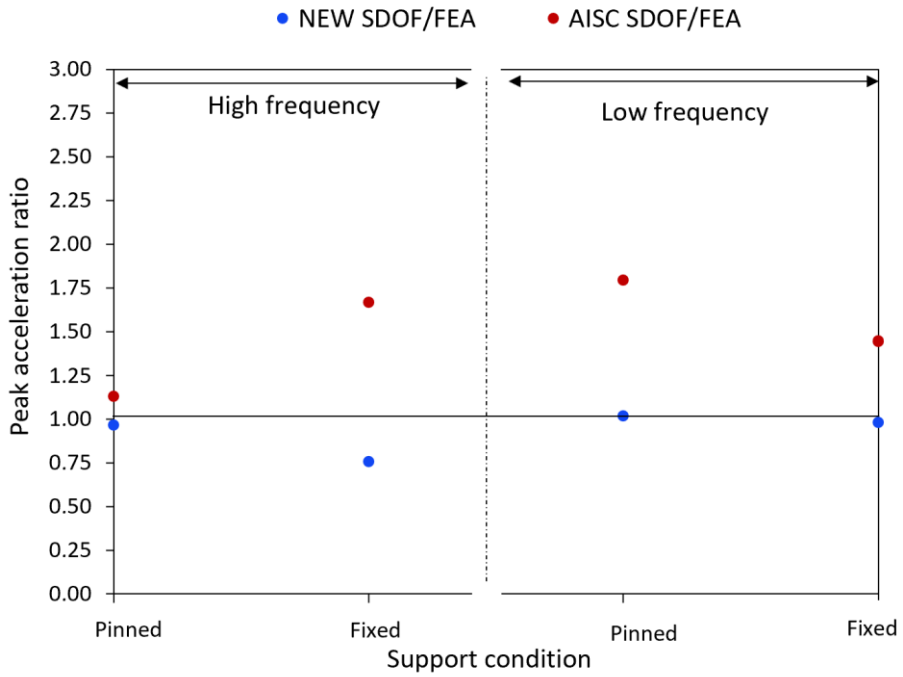

Figure 4.7 Variation of peak acceleration ratio for different support conditions

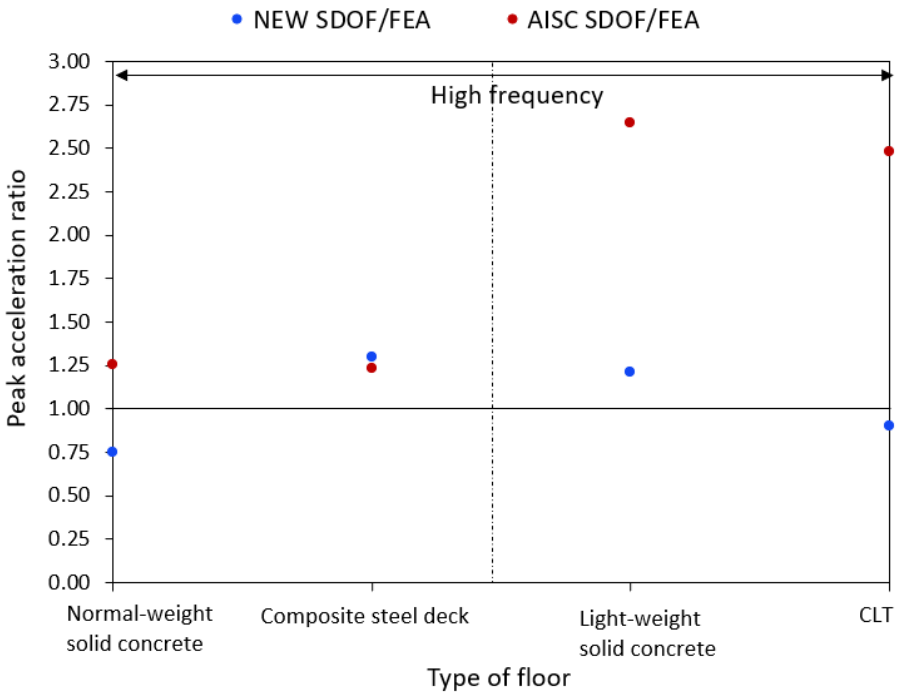

Figure 4.8 Variation of peak acceleration ratio for floors with different material types

The 26 floor cases discussed above all had frequencies less than 15 Hz and therefore were within the recommended application range of the AISC method. Unlike the AISC method, no calibration was involved in the development of the proposed SDOF method, and therefore, it is expected that this method would be applicable to floors with frequencies even greater than 15 Hz. Floors with such high natural frequencies are typically used in modular construction where prefabricated floors have relatively small dimensions (equal to the module size) and need to be lightweight for ease of transportation. In order to evaluate the performance of the proposed method for such floors, an additional 41 cases were considered in the parametric study resulting in a total of 67 floor cases. Most of the additional floors were highly stiff floors with natural frequencies ranging between 15 Hz and 60 Hz. All the additional cases were plain concrete floors with the same material and damping properties as those discussed above for the first 26 cases. The structural details and the predicted peak accelerations for these additional floors are presented in Table 4.2. The table also

includes the peak acceleration values predicted by the AISC and proposed SDOF methods. It should be noted that the SDOF method of AISC is not recommended for floors with frequencies beyond 15 Hz. The analyses provided here are to just evaluate the extent of overestimation or underestimation of results in case if an engineer uses the AISC method for such highly stiff floors.

Figure 4.9 shows the variation of the peak acceleration ratio in terms of the floor vibration for all 67 cases investigated in this parametric study, including the new cases with frequencies higher than 15 Hz. Table 4.3 also provides the mean and standard deviation of the results for three different ranges of frequencies: low-frequency floors (f_n < 9 Hz), high-frequency floors (9 Hz < f_n < 15 Hz), and very high-frequency floors (f_n > 15 Hz). From Figure 4.9 and Table 4.3, it can be concluded that the proposed SDOF method was able to accurately capture the peak acceleration of all analysis cases ranging from flexible floors with frequencies as low as 4 Hz to extremely stiff floors with frequencies up to 60 Hz. The mean and standard deviation of the peak acceleration ratio for all 67 cases were 0.97 and 0.17, respectively, which demonstrate an excellent correlation between the proposed SDOF method and the FE analysis results throughout the entire range of floor frequencies considered. The wide application range of the proposed method is attributed to its rational basis and the fact that no calibration was involved in the derivation of its formulation.

The results presented in Figure 4.9 show that the SDOF method of AISC overestimated the peak acceleration of almost all low- and high-frequency floors. For a few low-frequency floors with natural frequencies close to 9 Hz, the ASIC method underestimated the peak acceleration. The mean and standard deviation of the AISC-to-FEA peak acceleration ratios for the low-frequency floors were 1.50 and 0.54, respectively. For high-frequency floors, these values were 1.55 and 0.59, respectively. The level of overestimation of the peak acceleration tends to increase as the natural frequency reduces for the low-frequency floors and increases for the high-frequency floors.

Beyond the 15 Hz, the AISC method overestimated the peak acceleration by more than two times which was expected as the method is not calibrated for floors with such high frequencies.

Table 4.3 summarizes the results for all 67 floors investigated in the parametric study and presents them in terms of different ranges of natural frequencies. From Table 4.3 and Figure 4.9 it can be concluded that in general, the SDOF method of AISC performed better for low-frequency floors than for high-frequency floors, which is expected as the main focus of AISC is on the response amplification due to the resonance effect in low-frequency floors. Furthermore, the basis of the AISC method for low-frequency floors aligns better with the principles of dynamics compared to the expressions used for high-frequency floors. Neglecting the fact that the peak acceleration occurs during the forced vibration phase of the impulse and also assuming that the actual footstep as an instantaneous impulse significantly affect the accuracy of the AISC method for high-frequency floors. Additionally, the expression of effective impulse used in the formulation of high-frequency floors is highly calibrated and has no physical significance. It is worth noting that in addition to the SDOF methods, AISC also has FE analysis methods for both low- and high-frequency floors, the FE analysis method works well for low-frequency floors as the modal properties and peak acceleration both are evaluated from a detailed computer model. On the other hand, for high-frequency floors only the modal properties are evaluated from FE analysis, not the peak acceleration. Peak acceleration is determined from the same calibrated expression as done in the AISC's SDOF method which works reasonably well only for floors with frequencies from 9 Hz to 15 Hz. Also, the FE analysis methods are very time consuming and may not be suitable for engineering design applications.

Table 4.2 Comparison of the natural frequency and peak acceleration computed by the proposed SDOF method and AISC's SDOF method with FE results for additional 41 floor cases

Case no.	Floor type	One-way/ Two-way	a (m)	b (m)	t (mm)	f_s (Hz)	FEA		SDOF			$a_{peak\ (new\ SDOF)}/a_{peak\ (FEA)}$	$a_{peak\ (AISC)}/a_{peak\ (FEA)}$
							f_n (Hz)	a_{peak} (m/s^2)	f_n (Hz)	a_{peak} (m/s^2)			
										New method	AISC method		
1	Low-freq.	One-way	9.7	9.7	250	2 (2^{nd})	4.08	0.040	4.25	0.038	0.082	0.95	2.06
2		Two-way	9.7	9.7	125	2.08 (2^{nd})	4.16	0.147	4.64	0.106	0.232	0.72	1.58
3		One-way	9.7	9.7	255	2.08 (2^{nd})	4.16	0.037	4.52	0.032	0.078	0.86	2.10
4		Two-way	7	9.8	90	2.08 (2^{nd})	4.16	0.338	4.53	0.239	0.454	0.71	1.34
5		Two-way	9.7	9.7	150	1.67 (3^{rd})	4.9	0.085	4.3	0.056	0.152	0.66	1.78
6		One-way	9.7	9.7	300	1.67 (3^{rd})	4.9	0.022	5.32	0.017	0.050	0.77	2.28
7		Two-way	6	12	90	1.67 (3^{rd})	4.9	0.184	4.73	0.139	0.236	0.76	1.28
8		Two-way	7	9.8	130	2.08 (3^{rd})	6.25	0.110	6.78	0.110	0.146	1.00	1.32
9		Two-way	6	12	115	2.08 (3^{rd})	6.25	0.155	6.45	0.119	0.116	0.77	0.74
10		Two-way	7	9.8	135	1.67 (4^{th})	6.51	0.068	6.89	0.096	0.128	1.41	1.88
11		Two-way	9.7	9.7	200	1.67 (4^{th})	6.52	0.037	7.26	0.042	0.080	1.14	2.16
12		Two-way	9.7	9.7	225	1.83 (4^{th})	7.32	0.029	7.85	0.041	0.054	1.41	1.86
13		Two-way	9.7	9.7	250	2 (4^{th})	8.12	0.062	7.64	0.040	0.038	0.65	0.62
14		Two-way	9.7	9.7	260	2.08 (4^{th})	8.34	0.031	8.54	0.039	0.056	1.26	1.80
15		Two-way	6	12	155	2.08 (4^{th})	8.34	0.088	8.03	0.095	0.042	1.08	0.48
16	High-freq.	Two-way	5	5	125	1.67	15.46	0.063	17.21	0.064	0.150	1.02	2.41
17		Two-way	5	5	125	2.08	15.46	0.105	17.21	0.085	0.260	0.81	2.51
18		Two-way	4.9	9.8	200	2.08	16.27	0.035	14.56	0.029	0.062	0.83	1.77
19		One-way	3	3	100	1.67	17.2	0.144	16.3	0.150	0.433	1.04	3.01

Table 4.2 Comparison of the natural frequency and peak acceleration computed by the proposed SDOF method and AISC's SDOF method with FE results for additional 41 floor cases - Continued

Case no.	Floor type	One-way/ Two-way	a (m)	b (m)	t (mm)	f_s (Hz)	FEA		SDOF			$a_{peak\ (new\ SDOF)}/a_{peak\ (FEA)}$	$a_{peak\ (AISC)}/a_{peak\ (FEA)}$
							f_n (Hz)	a_{peak} (m/s^2)	f_n (Hz)	a_{peak} (m/s^2)			
										New method	AISC method		
20	High-freq.	One-way	3	3	100	2.08	17.2	0.180	16.3	0.135	0.594	0.75	3.30
21		Two-way	5	5	150	1.67	18.48	0.063	17.21	0.064	0.150	1.02	2.41
22		Two-way	5	5	150	2.08	18.48	0.090	17.21	0.071	0.210	0.79	2.32
23		Two-way	3	4.5	100	2.08	18.8	0.150	19.98	0.182	0.397	1.21	2.65
24		Two-way	5	5	175	2.08	21.48	0.080	19.76	0.083	0.175	1.04	2.19
25		One-way	3	3	125	1.67	21.5	0.068	19.79	0.052	0.324	0.76	4.76
26		One-way	3	3	125	2.08	21.5	0.180	19.79	0.165	0.445	0.92	2.47
27		Two-way	5	5	200	2.08	24.46	0.070	25.34	0.078	0.147	1.08	2.04
28		One-way	3	3	150	1.67	25.7	0.062	27.2	0.036	0.256	0.69	4.92
29		One-way	3	3	150	2.08	25.7	0.120	27.2	0.104	0.350	0.87	2.93
30		Two-way	3	3	150	1.67	25.7	0.047	24.2	0.054	0.312	1.15	6.64
31		Two-way	3	3	150	2.08	25.7	0.093	24.2	0.096	0.429	1.03	4.61
32		Two-way	3	4.5	125	1.67	29.2	0.080	32.32	0.091	0.286	1.14	3.58
33		Two-way	3	4.5	125	2.08	29.2	0.100	32.32	0.084	0.392	0.84	3.92
34		Two-way	3	6	150	2.08	30.33	0.048	32.72	0.050	0.182	1.04	3.79
35		Two-way	3.6	4.5	125	2.08	33.8	0.660	34.23	0.77	2.49	1.17	3.77
36		Two-way	3	4.5	150	1.67	34.8	0.040	35.6	0.032	0.226	0.80	5.65
37		Two-way	3	4.5	150	2.08	34.8	0.070	35.6	0.085	0.310	1.23	4.49
38		Two-way	3	3	125	1.67	42.28	0.070	45.7	0.092	0.395	1.31	5.64
39		Two-way	3	3	125	2.08	42.28	0.107	45.7	0.124	0.543	1.16	5.07

Table 4.2 Comparison of the natural frequency and peak acceleration computed by the proposed SDOF method and AISC's SDOF method with FE results for additional 41 floor cases - Continued

Case no.	Floor type	One-way/ Two-way	a (m)	b (m)	t (mm)	f_s (Hz)	FEA		SDOF			$a_{peak\ (new\ SDOF)}/a_{peak\ (FEA)}$	$a_{peak\ (AISC)}/a_{peak\ (FEA)}$
							f_n (Hz)	a_{peak} (m/s^2)	f_n (Hz)	a_{peak} (m/s^2)			
										New method	AISC method		
40	High-freq.	Two-way	3.6	4.5	150	2.08	53.7	0.24	50.72	0.24	1.15	1.00	4.79
41		Two-way	3.6	4.5	175	2.08	59,8	0.23	56.72	0.25	1.5	1.09	6.52

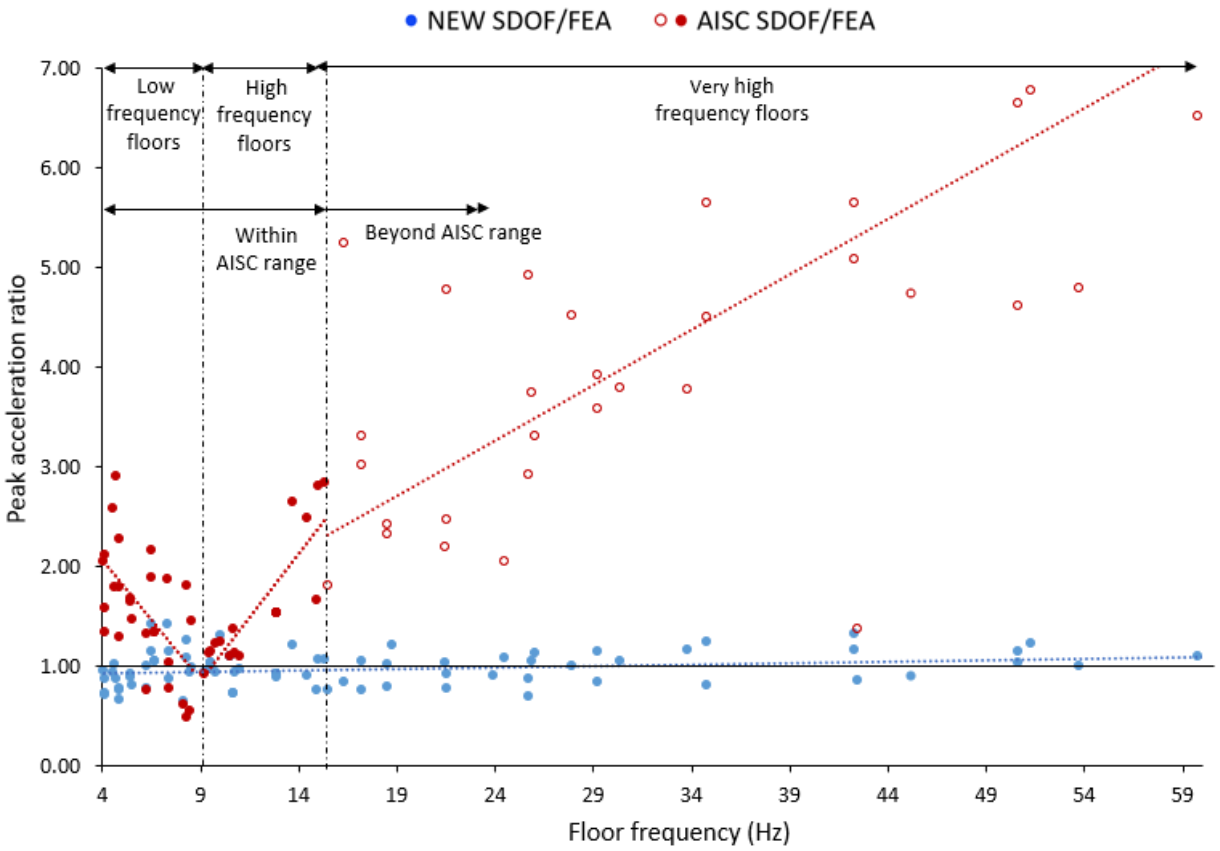

Figure 4.9 Correlation between peak acceleration ratio and floor frequency for new SDOF method and AISC SDOF method for all 67 case studies

Table 4.3 The mean and standard deviation of acceleration ratios for all 67 case studies categorized in terms of floor frequency

Floor frequency	Number of data points	$a_{peak\ (AISC\ SDOF)} / a_{peak\ (FEA)}$		$a_{peak\ (New\ SDOF)} / a_{peak\ (FEA)}$	
		Mean	Standard deviation	Mean	Standard deviation
4 Hz < f_n < 9 Hz	26	1.50	0.54	0.95	0.20
9 Hz < f_n < 15 Hz	15	1.55	0.59	0.97	0.14
15 Hz < f_n < 60 Hz	26	4.16	2.10	0.99	0.16
4 Hz < f_n < 60 Hz	67	2.40	2.07	0.97	0.17

Chapter 5: Application of the Proposed SDOF Methods for Vibration Analysis of Floors of Modular Hospitals

5.1 Background

In hospitals, even the slightest amount of vibration on sensitive equipment such as MRIs, CT scanners, or operating microscopes can have a significant impact on the operation of diagnostic equipment, including the potential of putting patients at risk during delicate procedures when the high precision operation of the medical equipment is paramount for successful outcomes. Primary sources of vibration include mechanical and occupant walking. Vibrations from mechanical equipment can be controlled by isolating the equipment from the floor by dampers, while vibration caused by human walking requires careful consideration in the design of the floor. There are strict limits for human-induced vibration of hospital floors in design codes. For instance, in CSA Z8000 (2018), which is the standard for planning, design and construction of health care facilitates, the limit for peak acceleration due to human-induced vibration for an inpatient hospital room is ten times more stringent than the limit specified for an office or residential building. Therefore, it becomes even more critical in the case of hospitals to accurately assess the floor vibration as the vibration limits are stringent and crucial for the operation of hospitals.

The application of modular construction for building hospitals has attracted increasing attention in recent years, specially since the global pandemic. Modular floors typically have high natural frequencies since they are lightweight and have relatively small dimensions for ease of transportation and construction. As shown in the previous chapters, the single-degree-of-freedom (SDOF) method of AISC significantly overestimates the vibration response of floors with high

natural frequencies. Considering the strict floor vibration requirements for hospitals, the overestimation of the vibration response by the AISC-SDOF method can pose considerable challenges in the design process and limit the available design options for engineers.

This chapter shows that by using a more accurate design method, like the one proposed in this study, engineers can have more flexibility in the design of modular floors for hospitals. The chapter first presents various methods for building emergency hospitals which is then followed by an overview of the existing studies conducted on modular construction. A modular hospital design is proposed based on the Canadian health care facilities design code (CSA Z8000) as well as applicable Canadian structural design codes (CSA A23.3, CSA S16, etc.). Considerations are also given to transportation requirements and patient capacity in the design process. To the best of the authors' knowledge, this is the first systematic modular hospital design that is developed based on safety and serviceability requirements and construction practice in Canada. Several conventional and modern floor systems are presented for the proposed modular hospital. The vibration response of these floors is evaluated against the stringent vibration requirements of CSA Z8000 using different analysis methods, including the SDOF method proposed in Chapter 3. Based on the analysis results, a set of floor designs that are lightweight, suitable for modular construction, and meet the floor vibration requirements of hospitals are proposed.

5.2 Emergency Hospitals

To address the hospital bed shortage and healthcare infrastructure saturation during the COVID-19 pandemic, the construction of fast-built hospitals has become one of the main priorities of governments. China, for example, built several temporary hospitals across the country, including an impressive 1,600-bed hospital in the city of Wuhan in a matter of days. Even before the global pandemic, the construction of fast-built hospitals was an important topic for emergency response

following the natural crisis, diseases, and wars. For many years, the only options for building an emergency hospital were either using temporary tents or transforming other types of existing structures such as schools or stadiums into hospitals. In recent years, the development of the modular construction technique has revolutionized the design and construction of emergency hospitals. With this novel construction technique, building components (modules) are prefabricated off-site and assembled on-site, leading to a significant reduction in the construction time and improvement in flexibility. During a crisis such as a global pandemic where many hospital beds are needed in a short period of time, conventional construction is not a feasible solution as it requires significant time and effort for planning, design and construction. In the following, a brief overview of different types of emergency hospitals is provided, with the main focus being on modular hospitals.

Owens et al. (2005) studied the challenges faced while using a deployable rapid shelter hospital made by the United States during a major earthquake in Bam, Iran. This shelter hospital was a tent-like structure with essential medical supplies, surgical equipment, and a highly skilled medical crew. Apart from the issues associated with the medical, water and electricity supplies, a significant challenge was operating and maneuvering patients as these tent structures were very tight in space. Overall, this type of field hospital deployment was a great success. Canada also used these rapidly deployable tent-type shelters, which were bigger in size, to extend the capacity of existing hospitals during the COVID-19 outbreak.

Ansary et al. (2010) investigated the use of other types of structures such as schools, cultural facilities, and community halls as emergency shelters following natural catastrophes, diseases, and wars. These shelters can be integrated with a temporary hospital to give immediate and adequate medical care and offer necessary living circumstances for patients. For example, following a

typhoid outbreak in 1910 in Montreal, the city authority turned the Northern Power Company's plant into an emergency medical center in under a week to treat affected patients. Also, during the 1918 Spanish influenza pandemic, 38% of inpatient beds were installed in existing structures such as homes, hotels, industries, and education institutions.

Chen et al. (2020) proposed layout designs for converting large public venues (gymnasiums, warehouses, stadiums, etc.) to temporary shelter hospitals like the Fangcang shelter hospital during the COVID-19 outbreak in China. These facilities provided medical treatment, illness monitoring, food, accommodation, and social activities to patients who were separated from their families and communities. The main factors considered in the development of design layouts were: 1) quick and cost-effective transformation of the existing structure into an emergency hospital, 2) provide large areas for medical care, triage and periodic monitoring, and 3) ensure proper isolation between different areas. Many other countries like India, the United States, and European countries used these large public venues as emergency hospitals to combat the surge of patients during the COVID-19 pandemic.

Chen et al. (2021) studied the design and construction of the Wuhan's hospital built for treating COVID-19 patients. The tight timeline was the biggest challenge for the construction of this 79,000 m^2 hospital. It typically takes 3 to 5 years for such a construction to be completed. However, with the use of modular construction technique, this hospital was built in a record-breaking time of only two weeks. The hospital layout consisted of three patient wards, an Intensive Care Unit (ICU), a dispatching center, a sewage treatment plant, an oxygen station, and a fire station. The architectural layout was designed such that the risk of transmission of COVID-19 was minimal. The hospital was divided into three zones based on the intensity of contamination (clean, semi-contaminated and contaminated areas). Negative pressure isolation areas were kept in every ward

to restrict airborne cross-infection. A layer of High-density polyethylene (HDPE) anti-seepage membrane was laid below the hospital area, which acted as a blanket to ensure thermal and physical isolations for protecting the soil and groundwater.

The hospital was mostly built based on two standard types of light steel-framed modules with dimensions of 6 m x 3 m x 2.9 m and 6 m x 2 m x 2.9 m. These modules were the basic units that were combined horizontally or stacked vertically to create different areas of the hospital. The only area that was not built by these standard modules was the medical technology center which required a height of 4.3 m and a large open space. A conventional steel frame structure was chosen for this area. The connections between beams and columns of the modules were made of cold-formed steel welding. The walls and roof were made of composite panels consisting of two steel plates filled with glass fibre insulation cotton in between them. The roof panel also included waterproof and thermal insulation and drainage systems. The floor of the modules was made of a light steel truss that supported a wooden floor. In some of the lightweight areas, a hardened floor from pre-existing parking lot on the site was used as a foundation, while for the rest of the hospital a raft foundation was constructed. The use of building information model (BIM) technology and unmanned aerial vehicles (UAVs) in the design played a vital role in significantly reducing the project completion time.

Several design concepts were proposed for building modular hospitals from shipping containers. Ratti et al. (2021) developed the Connected Units for Respiratory Ailments (CURA), an emergency hospital design made from modifying shipping containers to combat the surge of COVID-19 patients in Italy. The size of these modules was 6.10 m x 2.55 m x 2.60 m which was the size of a standard shipping container. These modules could be used as a self-standing system or to expand an existing hospital. Each module was pre-installed with all the medical facilities and

equipment necessary to treat critical patients. Inflatable tunnels were used to connect multiple modules. Each module was kept under negative pressure with a HEPA filter to limit the spread of infection. Petrova et al. (2021) proposed a similar type of modular design for a vaccination clinic in the United States. Li et al. (2021) developed a free-standing modular hospital with an innovative design that was built adjacent to an existing cancer center in the Netherlands. This was a 5-story building in which 256 modules were stacked vertically and expanded horizontally.

In conclusion, several solutions have been developed for building emergency hospitals which include tents and temporary shelters, transforming existing structures, and modular buildings such as prefabricated modules and shipping containers. Among these solutions, modular buildings seem to be the most appropriate one since they are structurally sound and can be highly customized according to the safety and serviceability requirements (vibration, isolation, fire safety, acoustics, etc.) of hospitals specified in design codes. In the following section, a brief overview of the research studies carried out on modular buildings is provided.

5.3 Modular Construction

Modular construction is becoming increasingly more popular as off-site prefabrication of buildings results in faster construction with better quality and less waste. The process of conventional construction generally needs to be carried out in sequential steps. For example, Heating, ventilation, and air conditioning (HVAC) units can be installed only once the roof is built, or the interior finishing can only start after the construction of the ceiling and walls is completed. The sequential process of conventional construction leads to longer completion time, higher cost, more complex construction with more limit on flexibility, and requiring a large number of skilled workers. However, different stages of the construction can be performed simultaneously in modular construction, which can considerably reduce the time and complexity of the project.

Installing a modular structure on-site can take as little as a few hours. Most of the construction processes of modular buildings are carried out under controlled plant conditions, which improve the quality and life span of the building and reduce the required construction material. Betram et al. (2019) studied modular buildings in the real estate industry and found that using the modular construction technique accelerated project timelines by 20% to 50% resulting in an estimated 20% cost saving in construction projects. There was also an overall reduction of 5% to 10% in the building material compared to the conventional construction technique. Advantages like less material waste, increased building life span, and better energy performance make modular buildings more environmentally sustainable. Due to these advantages, modular construction has been used for a wide variety of building types such as military accommodations, residential buildings, hotels, and, more recently healthcare facilities.

Because of its unique advantages, the modular construction technique has been the subject of several research studies in recent years. Lacey et al. (2018) carried out a comprehensive literature review on the design and construction of modular buildings and their performance under various loading conditions. In the following, a brief review of the existing studies on different aspects of modular buildings is provided.

5.3.1 Structural system of modular buildings

Depending on the building material, modular buildings can be categorized as steel modules (Lawson et al. 2008), precast concrete modules (Gunawardena 2016), and timber frame modules (Lawson et al. 2014). Steel modules can be further classified as Modular Steel Building (MSB) modules (Annan 2008), light steel framed modules (Lawson et al. 2008), and shipping container modules (Giriunas 2012). Each type of module has its own range of applications based on its advantages and disadvantages. MSB modules are suitable for high-rise buildings, hotels, and

residential apartments but are prone to corrosion. Light steel framed modules are lightweight and only ideal for low-rise buildings. Steel shipping container modules are easy to transport; however, additional reinforcement is often required to strengthen their wall openings. These modules are mainly used for military operations and post-disaster emergency shelters. Precast concrete modules are typically used for prisons and secure accommodations. Their advantages include good thermal performance, fire resistance, and acoustic insulation. However, these modules are difficult to transport and assemble because of their heavy weight. Timber frame modules are generally used in 1- to 2-storey buildings. Timber is a sustainable material and easy to fabricate; however, it has low durability and fire resistance which can be detrimental for structures.

Steel modules, which are more popular than the other types of modules, are typically classified as either column supported modules or continuously supported modules. The column supported modules have perimeter beams that span between corner or intermediate columns (Annan 2008, Fathieh 2013, Gunawardena 2016), while the continuously supported modules are supported by load bearing walls (Gorgolewski et al. 2001, Lawson et al. 2005). The column supported modules are suitable for medium and high-rise construction applications and are more common than the continuously supported modules.

Some modular buildings are hybrid structures rather than being entirely stand-alone modular. In these buildings, modular units are supported and arranged around a conventional structural system, such as a concrete core or a steel frame, for lateral stability (Lawson et al. 2008, Lawson et al. 2010). Gunawardena et al. (2016) proposed a new modular design for a ten-storey building in which the traditional core structure is replaced with strategically positioned rigid modules to provide stability against seismic loads. For the ease of transportation and assembly, the weight of modules is a critical factor that needs to be considered in the design and fabrication process.

Recently, some researchers explored the application of lightweight composite materials such as fibre reinforced polymer sandwich panels to floor, roof, and wall components of modular buildings (Manalo et al. 2017). This area of research is still nascent and requires further studies.

5.3.2 Connections in modular buildings

The effectiveness of modular structures to sustain applied loads is dependent on the connection of frame components and modules. Despite the necessity for a comprehensive understanding, there have been only a few investigations on the connections in modular buildings (Park et al. 2016). As shown in Figure 5.1, connections can be classified into three categories: intra-module connections, inter-module connections, and the connection between modules and the foundation.

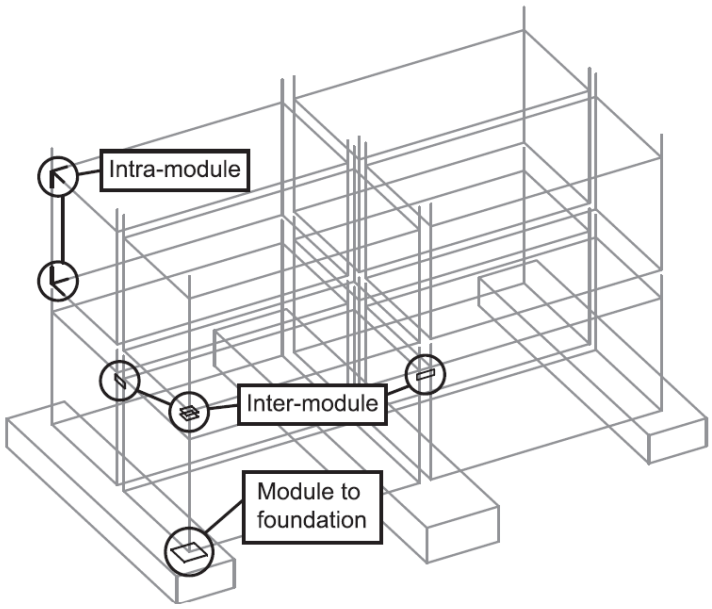

Figure 5.1 Different types of connection in modular buildings (Lacey et al. 2018)

Connections within a module (e.g. beam-to-column and joist-to-girder connections) are called intra-module connections, which can be either welded or bolted connections. Single web plates (Hong et al. 2011), double angle cleats (Styles et al. 2016), and bolted endplates (Ha et al. 2016) are examples of bolted connections between columns and beams. An example of welded intra-

module connection was provided by Annan et al. (2009), who examined welding of secondary beams of modular floors directly to the main perimeter beams. Using bolted connections allows disassembling of the module if needed, but the moment capacity of these connections is relatively low compared to welded connections.

Connections between adjacent modules are known as inter-module connections. Bolted connections are more favoured compared to on-site welding as they require less skilled labour and also provide more flexibility by allowing dismantling and rearranging of the modules. Examples of inter-module connections are horizontal connections between hollow columns using tie plates (Gorgolewski 2001), vertical connections between HSS columns with bolted end plates (Lawson et al. 2014), and pre-tensioned connections of columns (Chen et al. 2017).

In situ or precast concrete footings, drilled concrete piles, steel piles, or a mix of these may be used as foundations for modular buildings. If not properly restrained to a suitable foundation, low-rise modular structures located in areas with significant lateral loads may be susceptible to overturning and sliding failures. Chains, cables, keeper plates, or welding are widely used to connect modules together to improve the lateral stability. As an alternative to the usual cast-in or post-fixed steel bearing plate, Park et al. (2016) designed an embedded column-to-foundation connection for modular buildings that improved the ductility of columns.

5.3.4 Hazards and their Effects on modular buildings

Several researchers have investigated the performance of modular structures under different types of hazards. Gunawardena et al. (2013) and Styles et al. (2016) studied the effect of wind loading on mid-rise modular buildings. Fathieh and Mercan (2016) performed nonlinear static push-over and dynamic analyses to assess the torsional behaviour of modular buildings with steel braced

frames under earthquake loads. Harrison (2003) studied the response of blast resistant modular buildings for the petroleum and chemical processing industries. Recently, Lawson (2017) investigated the progressive collapse resistance of a three-storey structure built from container modules by simulating column removal scenarios using computer models and experimental tests. Some studies focused on the fire resistance of modular structures. Gallagher (2013) studied different fire incidents in modular homes and found that the use of combustible materials and the presence of a space between modules can intensify the spread of fire. Ngo et al. (2016) carried out a numerical study on the fire performance of modular buildings with glass fibre reinforced polymer (GFRP) facades. Transport and handling are other important factors that need to be considered in the design of modular buildings. Deflection criteria are typically used to determine the number and position of lift points for module components. Limited studies are available in the research literature in this regard. For example, Smith et al. (2007) evaluated the response of timber frame modules under transport and handling loads and discussed possible damage modes.

5.4 Concluding Remarks

Significant work has been done on the design and performance assessment of modular buildings. However, there has not been much research on applying this novel construction technique to hospital structures. There are no design standards or construction guidelines for building modular healthcare facilities. The modular hospitals recently used for the COVID-19 response were mostly designed and built in a similar fashion as other types of modular structures such as residential buildings and hotels with some special modifications to accommodate the functionality of a hospital. Considering that design requirements for hospitals are substantially different than other types of buildings, there is a great need for design and construction guidelines specifically developed for modular hospitals.

One of the important serviceability design requirements in hospitals for the safe operation of sensitive medical equipment and patient comfort is to limit the human-induced vibration of floors. Strict floor vibration limits are set by design codes for healthcare facilities. Achieving these rigorous requirements in modular structures is more difficult compared to conventional structures as they are lightweight and less restrained, which generally leads to higher deflections and vibrations in modular structures. Although there has been research on floor vibration response of hospitals built by conventional construction techniques (e.g., Liu et al. 2015), there is no study dedicated to the floor vibration assessment of modular hospitals or any other type of modular structure. The existing floor vibration design procedures, including the widely used AISC Design Guide 11 (Murray et al. 2016), are primarily developed for conventional structures with relatively heavy floor systems and may not be applicable to modular buildings. These design guidelines are calibrated based on limited experimental data and cannot accurately predict the vibration response of modern lightweight floor systems, which are commonly used for modular buildings. Furthermore, the primary focus of existing design codes is on the vibration behaviour of long-span floors with low frequencies where resonance amplifies the response. For example, the SDOF design method of AISC is only applicable to floors with frequencies less than 15 Hz, which is well below the natural frequency of a typical modular floor. Because of their lightweight and small dimensions, modular floors tend to have much higher stiffness and natural frequency compared to conventional floors. The analysis results presented in the previous chapters show that the AISC method tends to be overly conservative for high-frequency floors even within its application range which makes it nearly impossible to meet the stringent floor vibration limits for modular hospitals.

5.5 Proposed Modular Hospital Design

As discussed above, there is no systematic design procedure for modular hospitals that is suitable for Canadian design and construction practice. In this section, a modular hospital design is proposed based on the relevant Canadian standards, including the Canadian healthcare facilities code (CSA Z8000 2018), Canadian structural codes (CSA A23.3, CSA S16, etc.), and transportation requirements specified by the Highway Traffic Act of Ontario (2020). It should be noted that the main focus of the proposed design is on the hospital layout and design of modules that can be easily adapted in different layout configurations to meet the various functional requirements of hospitals. There are many other aspects to the design of hospitals that are beyond the scope of this study and not considered here.

According to the Highway Traffic Act of Ontario (2020), the maximum allowable module width is restricted to 3.6 m based on the maximum width of a standard trailer. The maximum module height is restricted to 3.2 m as determined from the minimum clearance of 2.75 m required according to CSA Z8000 (2018) and an additional 0.45 m space for ductwork and service utilities. The maximum module length is restricted to 4.5 m such that a maximum number of modules can be accommodated on a standard trailer to improve transportation efficiency. Based on these dimensions, two standard module types are defined (see Figure 5.2); the larger module is 4.5 m x 3.6 m x 3.2 m, while the smaller one is 4.5 m x 1.8 m x 3.2 m. As shown in Figures 5.3 and 5.4, these standard modules are the basic building units that can be combined horizontally in both planar directions to make different sections of a hospital ward, including patient rooms, reception area, nursing stations, corridors, etc. For example, a typical patient room is made by combining two large modules (bed area) and a small module (attached washroom) as shown in Figure 5.3, a nursing station is built by assembling ten large modules, and small modules are used for the

corridor. Using two different module sizes allowed efficient use of the space without making the design and construction complicated. The smaller modules are suitable for washrooms, corridors, and the entrance area, while larger modules are needed for patient rooms, laboratory, ICUs, and other large areas.

The proposed layout of the hospital ward, including all rooms and corridors, are designed in accordance with the key space requirements of CSA Z8000 (2018). For instance, in an airborne infection isolation room (AIIR), the minimum bed area, anteroom area and washroom area should be 26 m^2, 7.5 m^2 and 7.5 m^2, respectively. As shown in Figure 5.4, the proposed bed area, anteroom area and washroom area are 32.4 m^2, 8.1 m^2 and 8.1 m^2, respectively, satisfying the minimum space requirements. Similarly, minimum corridor sizes, minimum nursing area per inpatient room, minimum triage area, etc. are considered while designing the hospital layout. The architectural layout of the hospital is designed such that the risk of contamination is minimal. As can be seen in Figure 5.4, the AIIRs, which are the most infectious areas, are kept sufficiently safe from the rest of the hospital as they have a negative pressure anteroom at their entrance to prevent air from escaping into the corridors and other areas when the staff enter or exit, limiting the possibility of airborne infection transmission. The waste disposal and service rooms are kept at the backside of the hospital so that service repairs and waste disposals do not hinder the treatment and management of patients. The nursing station and PPE rooms are placed at the center of the hospital ward so that staff and PPE are easily accessible to all patient rooms. The hospital layout is designed such that the traffic flow and contact of people are minimum to improve the work efficiency and reduce the possibility of virus transmission. Corridors adjacent to the patient rooms and nursing station are set as a one-way path to reduce the risk of infection. A typical hospital ward is designed to

accommodate 25 patients. As shown in Figure 5.6, the patient capacity can be further increased by combining multiple hospital wards.

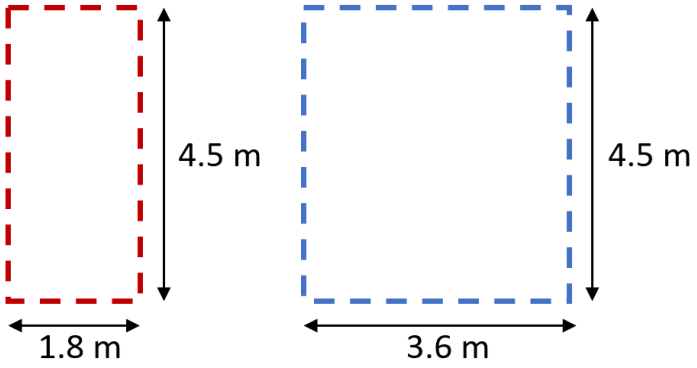

Figure 5.2 Small module (left) and large module (right)

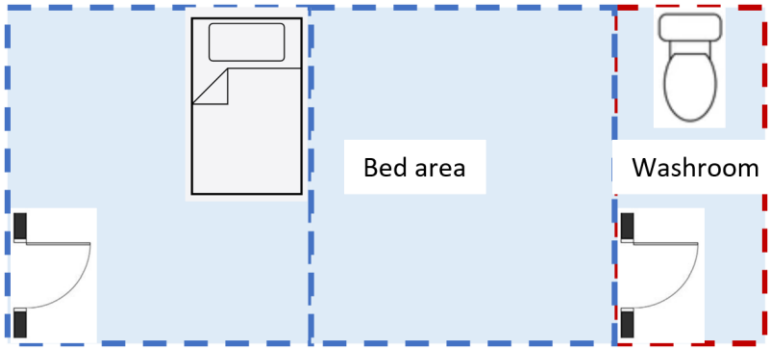

Figure 5.3 Layout of a single modular patient room

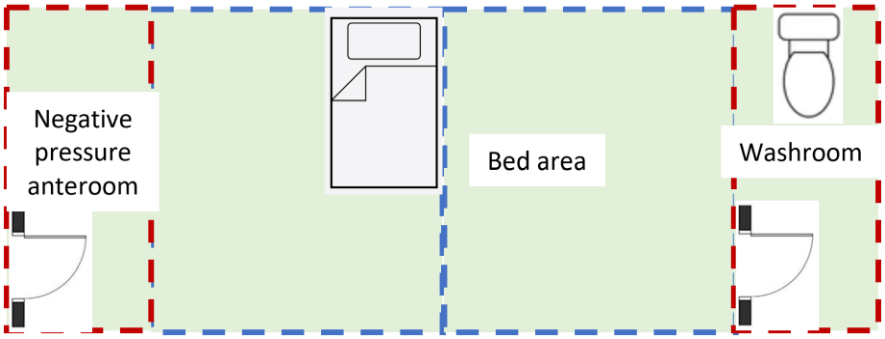

Figure 5.4 Layout of a modular airborne infection isolation room (AIIR)

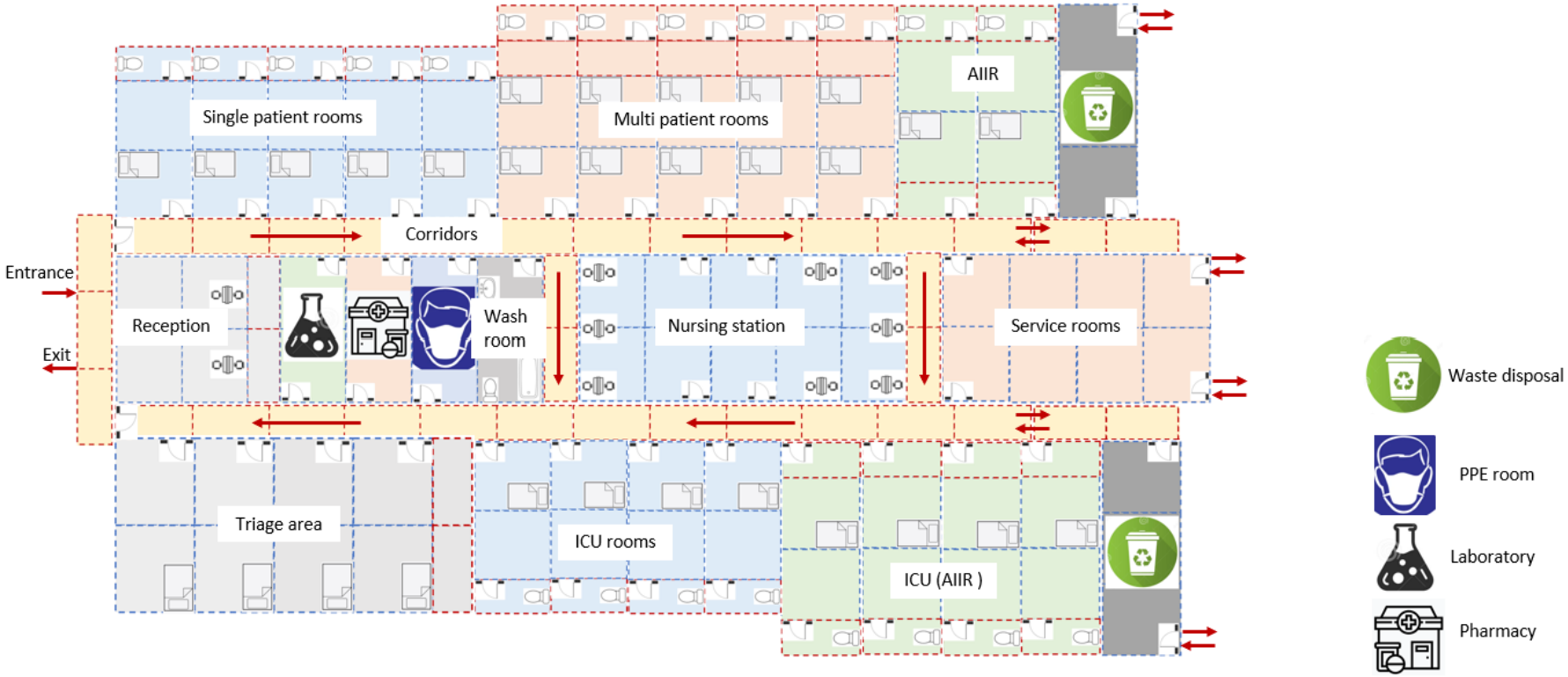

Figure 5.5 Typical modular hospital ward with 25 beds

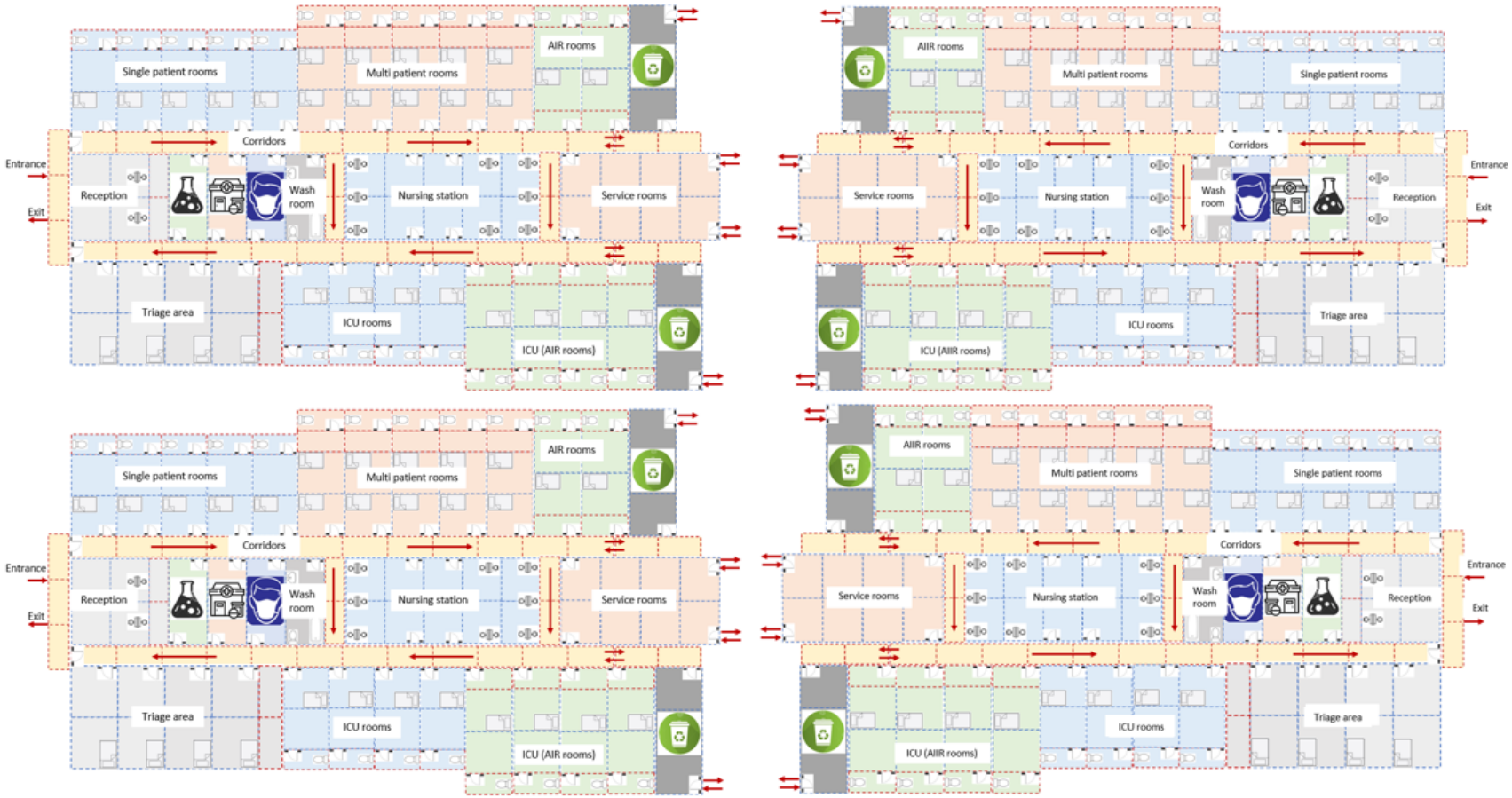

Figure 5.6 Four modular hospital wards with a total patient capacity of 100

Structural steel sections are selected for framing members (columns and beams) of the module units. For simplicity, the design of these members is carried out according to the dimensions and requirements of the larger module. These member sizes are also adopted in the smaller module as they would simplify the modular design and provide a conservative design for the smaller module. The columns and beams are designed according to the strength requirements of CSA S16 (2019). Only the gravity loads were considered in the design and lateral loads were ignored as the main focus of this study is on the design of the modular floor, which is generally governed by the gravity loads. Application of the proposed design to actual field deployment requires consideration of lateral loads to ensure stability against wind and seismic loads.

According to CSA Z8000 (2018), the general office area has the highest floor live load (3.6 kN/m^2) in a hospital. To simplify and standardize the design, this live load is considered for all floor areas. The live load of the roof is also taken as 1.5 kN/m^2 as specified in CSA Z8000 (2018). To determine the section size for beams and columns, the module was analyzed under gravity loads using the ETABS (CSI 2018) computer software. The W150x37 steel section was found to be suitable for both columns and beams, as shown in Figure 5.7. In the model, the connection between beams and columns was assumed to be a moment connection which is commonly used in practice for the intra-modular connections, as discussed earlier. The design of the ceiling and walls was not included in this study. One design option that can be considered for these members is to use sandwich panels proposed by Summers (2008), which consists of two steel panels with an infill material between them for acoustic and thermal insulation.

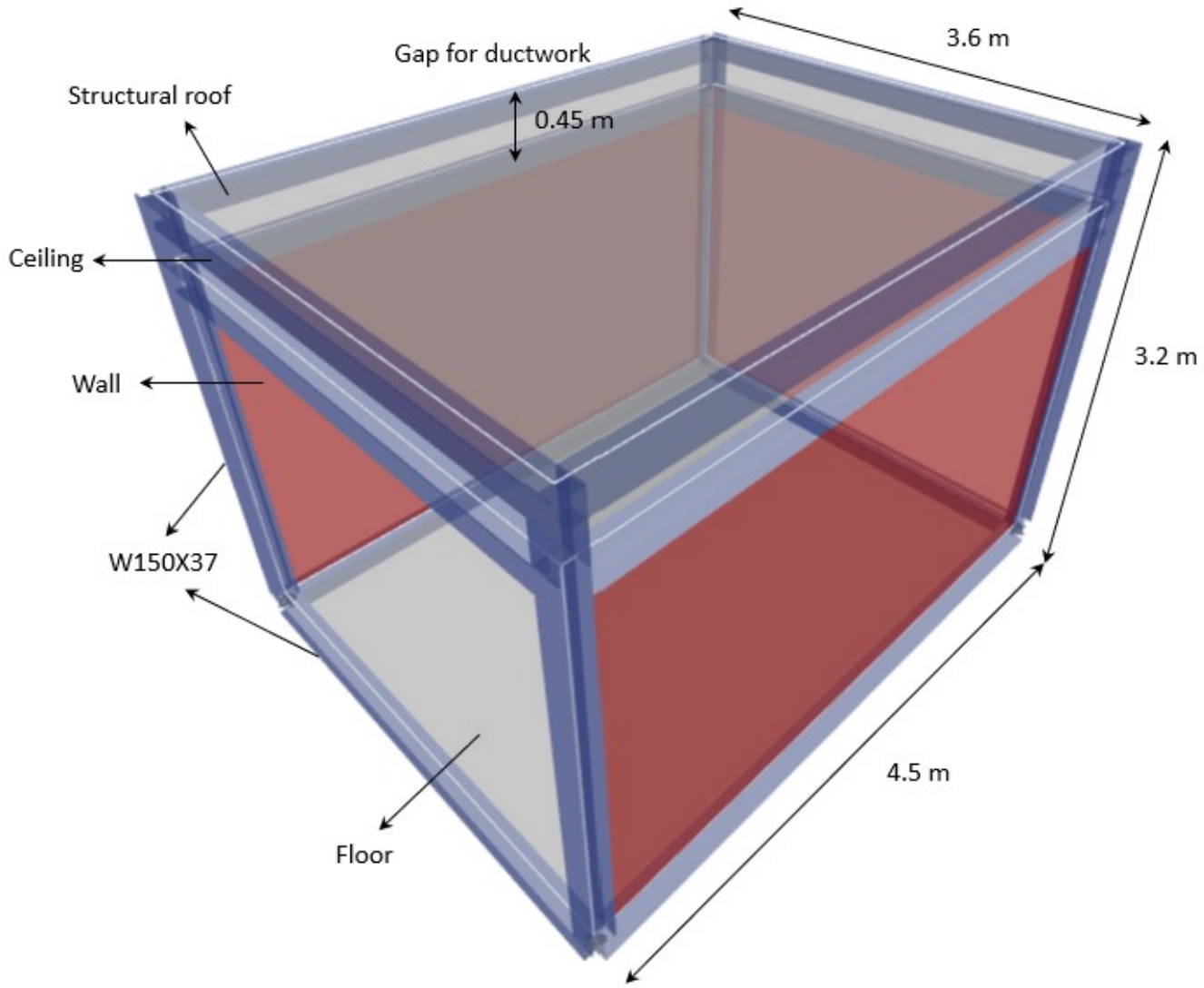

Figure 5.77 Dimensions and details of the large module unit

5.6 Proposed Floor Designs for Modular Hospitals

As shown in Table 5.1, a total of 12 floor designs were considered for the proposed modular hospital. A wide range of floor systems was evaluated, including solid concrete floors (normal and high strength concrete), hollow core concrete floors, a cross laminated timber (CLT) floor, a timber concrete composite (TCC) floor, steel-concrete composite floors, and an innovative glass fiber reinforced polymer (GFRP) floor. The density and cylindrical compressive strength of normal

strength concrete floors were 2400 kg/m^3 and 25 MPa, respectively. For the lightweight high strength concrete floors, the density and compressive strength were 1800 kg/m^3 and 60 MPa. The CLT floor had a density and stress grade of 500 kg/m^3 and "E_1", respectively. The damping was determined to be about 3% for all floors based on the recommendations of the AISC Design Guide 11 (Murray et al. 2016). All 12 floors were designed such that they met the strength and serviceability requirements (except the floor vibration requirement) of the applicable Canadian design codes under the gravity loads. The main focus of the study is on the vibration response of the floors under walking loads and whether they meet the stringent peak acceleration requirements for hospitals specified in the AISC design guideline.

The study was conducted in three phases. In the first phase, four types of floors were designed with structural details similar to those used in conventional construction. The first floor was a two-way 125 mm thick solid slab made from normal strength concrete. The second one was a two-way CLT floor with a thickness of 105 mm. The third floor was a one-way 150 mm thick hollow core concrete floor, and the last one was a one-way steel-concrete composite floor that consisted of a 100 mm thick concrete slab supported on a 40 mm thick steel deck. All four floors were supported by twelve W150x37 joists and two W150x37 girders. Figure 5.8 shows the structural details and dimensions of the floors. The floors were designed such that they satisfied all the strength and serviceability requirements of the Canadian concrete and steel design codes (CSA A23.3 2019 and CSA S16 2019).

The vibration response of the floors was calculated using three different methods: the finite element (FE) analysis method, the SDOF method proposed in Chapter 3, and the SDOF method of AISC. The modelling and analysis procedures were similar to those described in the previous chapters. Table 5.2 presents the peak acceleration values obtained from each analysis method. The

AISC method overestimated the peak acceleration by a factor of 3 to 4 compared to the FE method. This overestimation was expected as AISC is generally a conservative method for high-frequency floors and more importantly, the natural frequency of the floors is well beyond the recommended application range of AISC (f_n <15 Hz). The peak acceleration values computed by the proposed SDOF method are reasonably close to the FE analysis results demonstrating that the proposed method is accurate for such high-frequency floors. Table 5.2 also presents the peak acceleration limits specified by the AISC design guideline for residential and office buildings as well as hospitals. It can be seen that the limits for hospitals are ten times more stringent than those for residential and office buildings. Comparing the peak acceleration limits against the calculated values shows that none of the floors met the vibration requirement for hospitals. However, based on the analysis results of the proposed SDOF and FE methods, all floors met the vibration limits for residential and office buildings. It is worth noting that because of the conservatism of AISC, only one out of four floors met the limits for residential and office buildings according to this method.

In the second phase of the study, the section size of joists and girders, as well as the floor thickness were increased to satisfy the vibration requirements of hospitals. By increasing section sizes and the floor thickness, the stiffness and consequently the natural frequency of the floor increases, which leads to reduced vibration levels and an increase in vibration limits. The section size of girders and joists was increased from W150x37 to W310x107 and W150x37, respectively. To be consistent with Phase 1, the number of joists and girders did not change. The thickness of the solid concrete floor was increased from 125 mm to 150 mm; the CLT floor was replaced with a TCC floor which consisted of a 25 mm thick concrete layer on top of a 245 mm thick CLT; the thickness of the hollow core concrete floor was increased from 150 mm to 200 mm; and the thickness of the

steel-concrete composite floor was increased from 140 mm to 226 mm (a 150 mm thick concrete slab supported on a 76 mm thick steel deck).

The peak acceleration values computed by different analysis methods, as well as the peak acceleration limits obtained from AISC, are shown in Table 5.2. It can be seen that similar to Phase 1, the analysis results of the proposed SDOF method and FE method agreed well, while the SDOF method of AISC significantly overestimated the peak acceleration values as the natural frequency of the floors was far more than the application range of AISC. Unlike Phase 1, all floors passed the peak acceleration limit for hospitals according to the results of the proposed SDOF and FE methods. However, there is a significant increase in the self-weight of the floors compared to Phase 1, which raises questions about the applicability of the floors to modular construction. The weight of the TCC and hollow core floors was approximately 25% less than the other two floors, making them better options for module construction.

Modular construction requires lightweight floors as prefabricated components are transported and lifted from the plant and assembled at the site. In the third phase of the study, the floors were designed using lightweight high-performance materials to reduce their self-weight and make them more suitable for modular construction. For the concrete floors (the solid slab, the hollow core floor, and the steel-concrete composite floor), the normal strength concrete was replaced with lightweight high strength concrete, and the structural steel joists were changed to light gauge steel joists. The light gauge steel is a cold-formed steel that can be made in the form of thin “C” or “Z” sections and has the same material properties as the structural steel. In the proposed floor designs, C-shaped light gauge sections with dimensions of 356 mm x 89 mm x 3 mm (C356x13.8) were used as joists to transfer loads from the floor to girders. It is worth noting that girders and columns of modules are still made from the structural steel sections since light gauge thin sections are prone

to buckling and have poor fire resistance, hence not suitable to transfer heavy loads. The use of lightweight high strength concrete enabled reducing the thickness of the steel-concrete composite floor from 226 mm to 186 mm (a 110 mm thick concrete slab and a 76 mm thick steel deck).

In addition to the above-mentioned floor systems, a high-performance floor made from fibre-reinforced polymer (FRP) layers was also designed according to the loads and layout of the proposed modular hospital. FRP is widely used in the aerospace industry because of its high stiffness-to-weight ratio and long durability compared to conventional construction materials such as steel and concrete. In recent years, the use of FRP floors has become quite prominent in the construction of bridge decks. One such floor deck system, which is known as *"ASSET"* and proposed by Knippers et al. (2006), was adapted and applied to the proposed modular hospital design to enhance the vibration performance of the floor. As shown in Figure 5.8, the proposed floor design was 220 mm deep and consisted of 12 mm thick glass FRP (GFRP) elements. The floor was supported by twelve light gauge steel C356x13.8 joists and two structural steel W310x107 girders. The density, elastic modulus, and Poisson's ratio of the floor were 1685 kg/m^3, 52 GPa, and 0.3, respectively.

From Table 5.2, it can be seen that similar to the previous two phases, the SDOF method of AISC largely overestimated the peak acceleration values as the natural frequency of the floors was well beyond the application range of AISC. On the other hand, the peak acceleration results of the proposed SDOF method and the FE method correlated very well. According to the results of these two analyses methods, all four floors defined in Phase 3 passed the peak acceleration limit for hospitals. However, as compared to Phase 2, the self-weight of the floors has been significantly reduced, making these floors more suitable for modular buildings. The average self-weight of the conventional floors was reduced by 37% compared to Phase 2, with the hollow core concrete floor

being the lightest one among the conventional floors with a self-weight of 4539 kg. The weight of the GFRP floor was 2586 kg which was 43% less than the hollow core floor while providing the same vibration performance. All floor systems met the strength and serviceability requirements of the applicable Canadian design codes.

From the above study, it can be concluded that in order to satisfy the vibration requirements of hospitals for conventional floors, the section size of joists and girders and the floor thickness need to be significantly increased, making the floor too heavy for modular construction. However, by using high-performance lightweight materials, similar vibration performance can be achieved while greatly reducing the floor weight. Three conventional floor designs made from lightweight high strength concrete were proposed that had relatively low self-weight and met the peak acceleration limit specified by AISC for hospitals. It was also shown that by using a GFRP floor system with a novel cross-section shape, the self-weight can be reduced by about half making this floor system the most suitable option for modular hospitals. Overall, the peak acceleration determined by the proposed SDOF method correlated reasonably well with the FE method, resulting in a mean ratio of 1.05 and a standard deviation of 0.11. The proposed SDOF method was able to accurately predict the peak acceleration of floors with natural frequencies up to 80 Hz, which is well beyond the application range of AISC (f_n < 15 Hz). Using the AISC method for such high-frequency floors results in serious overestimation of the peak acceleration, making it almost impossible to meet the design criteria defined in the code.

Table 5.1 Design parameters for modular hospital floors

Study phase	Case no.	Floor system	Floor type	Natural frequency (Hz)	Floor slab thickness (mm)	Girders	Joists	Total mass (kg)
First phase	1	Solid concrete slab	Two-way	33.8	125	2-W150x37	12-W150x37	6490
	2	CLT	Two-way	27.9	105	2-W150x37	12-W150x37	3396
	3	Hollow core	One-way	25.9	150	2-W150x37	12-W150x37	5500
	4	Steel-concrete composite	One-way	26.0	140	2-W150x37	12-W150x37	5719
Second phase	1	Solid concrete slab	Two-way	53.7	150	2-W310x107	12-W310x45	8360
	2	TCC	Two-way	60.8	270	2-W310x107	12-W310x45	6200
	3	Hollow core	One-way	51.3	200	2-W310x107	12-W310x45	6544
	4	Steel-concrete composite	One-way	45.2	226	2-W310x107	12-W310x45	8605
Third phase	1	Solid concrete slab*	Two-way	62.1	150	2-W310x107	12-C356x13.8+	5427
	2	Hollow core*	One-way	54.8	200	2-W310x107	12-C356x13.8+	4539
	3	Steel-concrete composite*	One-way	57.7	186	2-W310x107	12-C356x13.8+	4798
	4	GFRP	One-way	81.5	220	2-W310x107	12-C356x13.8+	2586

* The floor is made from high strength light-weight concrete.

+ Joists are made from light gauge thin steel sections.

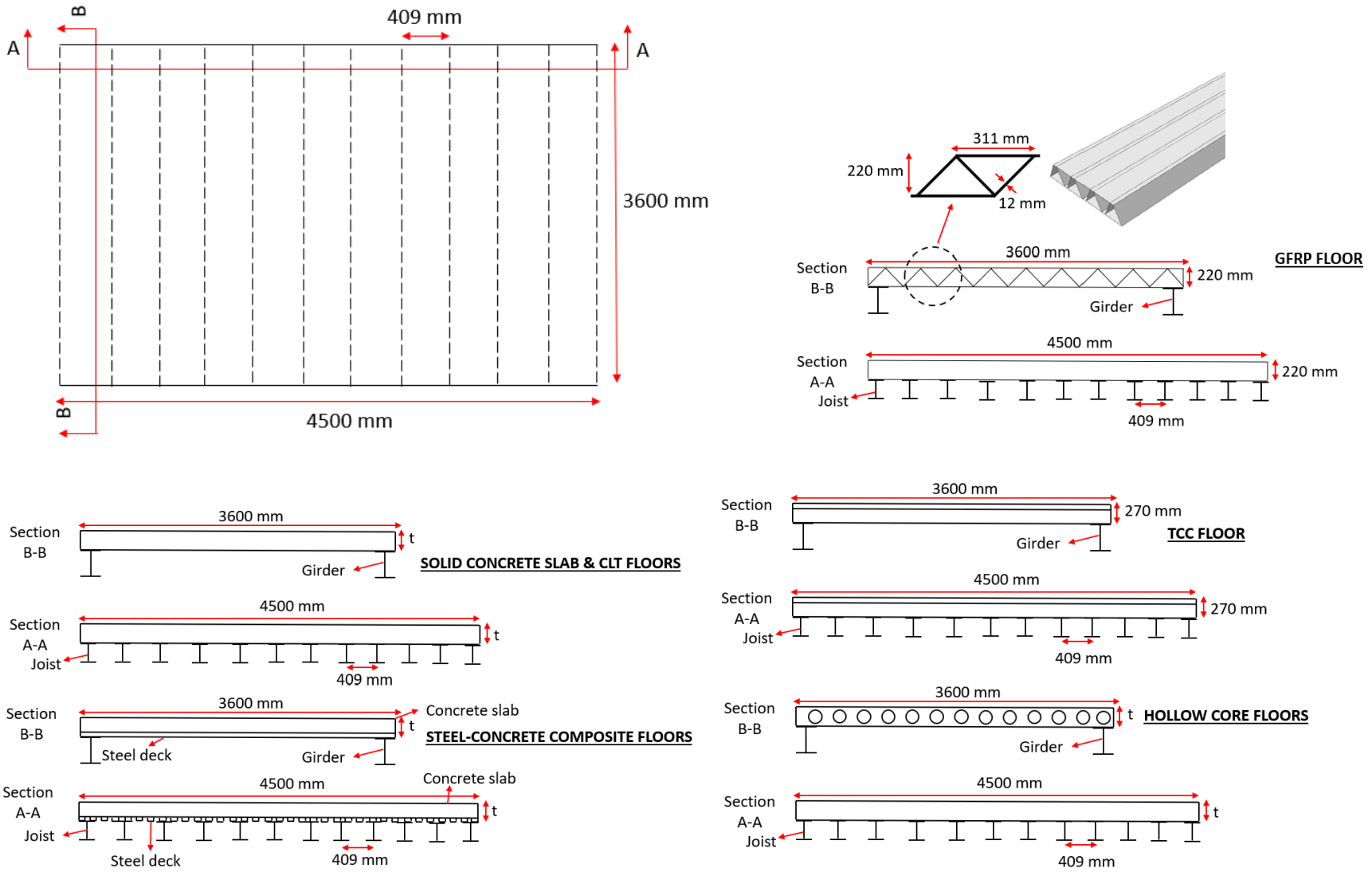

Figure 5.8 Construction details of modular floor systems

Table 5.2 Comparison of the peak accelerations calculated by different analysis methods

Study phase	Case no.	Floor system	Natural frequency (Hz)	Calculated a_{peak} (% of g)			a_{peak} (% of g) design limits		a_{peak} (new SDOF) /a_{peak} (FEA)	a_{peak} (AISC) /a_{peak} (FEA)
				FEA	New SDOF	AISC-SDOF	Residential & office	Hospital		
First phase	1	Solid concrete slab	33.8	0.66	0.77	2.49	2.1	0.21	1.17	3.77
	2	CLT	27.9	1.14	1.13	5.14	1.9	0.19	0.99	4.51
	3	Hollow core	25.9	0.6	0.63	2.24	1.8	0.18	1.05	3.73
	4	Steel-concrete composite	26.0	0.66	0.74	2.18	2.5	0.18	1.12	3.30
Second phase	1	Solid concrete slab	53.7	0.24	0.24	1.15	2.5	0.25	1.00	4.79
	2	TCC	60.8	0.23	0.25	1.50	2.5	0.25	1.09	6.52
	3	Hollow core	51.3	0.22	0.27	1.49	2.5	0.25	1.23	6.77
	4	Steel-concrete composite	45.2	0.25	0.22	1.18	2.5	0.25	0.88	4.72
Third phase	1	Solid concrete slab*+	62.1	0.25	0.29	2.47	2.5	0.25	1.16	9.88
	2	Hollow core*+	54.8	0.26	0.24	2.16	2.5	0.25	0.92	8.31
	3	Steel-concrete composite*+	57.7	0.23	0.21	1.99	2.5	0.25	0.91	8.65
	4	GFRP+	81.5	0.25	0.28	3.29	2.5	0.25	1.12	13.16
Mean									1.05	6.51
Standard deviation									0.11	2.87

* The floor is made from high strength light-weight concrete.

+ Joists are made from light gauge thin steel sections.

Note: the green colour indicates that the peak acceleration of the floor is less than or close to the vibration limit for hospitals, while the red colour shows that the peak acceleration is considerably higher than the design limit.

5.7 Effects of Inter-Module Connections and Exterior Walls on Floor Vibration

In the previous section, the floor vibration assessment and design were carried out for only a single module floor; however, as shown in Figure 5.5, every room in the proposed hospital layout is assembled by combining at least three modules. A series of detailed FE vibration analyses were carried out on the solid high strength concrete floor to see the effect of considering connections between modules (i.e. inter-module connections) on the vibration response of the floor. As shown in Figure 5.9, a FE model of a single inpatient room was created, which consisted of two large modules and a small module. Figure 5.3 demonstrates the configuration of modules in an inpatient room. The FE modelling procedure was the same as that described in Chapter 3. The connection between girders of the adjoining modules was assumed to be a fixed connection to achieve maximum resistance against floor vibration. In practice, it is difficult to achieve a fully fixed connection as there is always some level of rotation in the connection that should be considered in the design. It is worth noting that if pinned connections were assumed between adjoining modules of a room, the vibration response of the floor would be identical to that calculated for a single module.

A series of FE analyses were performed in which locations of the applied walking load (the disturbance point) and the obtained peak acceleration (the receiver point) both varied. It was found that the maximum vibration occurred when the source of vibration and receiver both were at the center of the middle module. Also, the calculated peak acceleration decreased by 23%, and the natural frequency increased by 22% compared to the single modular floor. This trend was expected as combining modules with a fixed connection increases the stiffness of the floor, which results in a higher natural frequency and a lower vibration level.

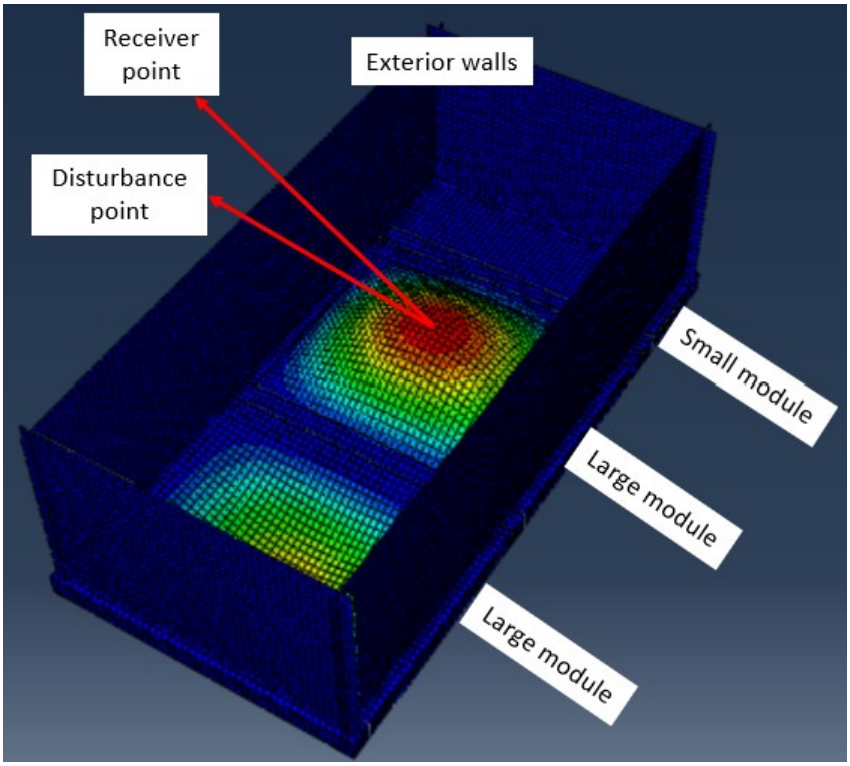

Figure 5.9 FE model of an inpatient room with consideration to inter-module connections and exterior walls

Then on this combined modular floor, four reinforced concrete walls were added on the perimeter of the room, and vibration assessment was conducted using the FE model shown in Figure 5.9. The walls were 100 mm thick and assumed to have a fixed connection with perimeter girders and beams. It was observed that the natural frequency of the floor increased by 12%, and the vibration further decreased by 10%. The addition of the walls to the room made the floor stiffer as a system, which led to reduced peak acceleration and increased natural frequency. Table 5.3 presents the analysis results with and without considering the effects of the fixity of inter-module connections and perimeter walls. Other techniques of floor stiffening that can be used to reduce the vibration level include increasing the moment capacity of the connections between the slab, joists and girders or using pre-tensioned or post-tensioned girders and joists. Future research is needed to quantify the effect of each stiffening method on the vibration response of floors.

Table 5.3 Comparison of analysis results with and without considering inter-module connections and exterior walls

Case no.	FE model	Floor frequency (Hz)	a_{peak} (% of g)
1	A single modular floor without exterior walls	62.1	0.25
2	An inpatient room (3 modules combined) without exterior walls	75.8	0.19
3	An inpatient room (3 modules combined) with exterior walls	85.1	0.17

Chapter 6: Summary, Conclusions and Future Work

6.1 Summary

The primary focus of this study was to develop simplified rational methods for vibration assessment of floors under walking loads that are applicable to a wide range of floor types with various natural frequencies. Initially, a detailed finite element (FE) model for floor vibration assessment was developed in which the actual walking load, including its spatial and temporal variations were simulated, and peak accelerations were evaluated by conducting modal dynamic analyses. Then based on this FE model, simplified single-degree-of-freedom (SDOF) methods were developed for vibration analysis of both low- and high-frequency floors. Derivation of the SDOF methods required applying three simplifications to the detailed FE model: 1) neglecting the effect of spatial variation of the walking load, 2) approximating the actual force-time history with predefined forcing functions, and 3) converting the multi-degree-of-freedom (MDOF) floor system into an equivalent SDOF system. Through a series of analyses, the effect of each simplification on the vibration response of the floor was examined, and they were found to be appropriate. Unlike the existing floor vibration assessment methods, no calibration was involved in the development of the proposed SDOF methods, and the formulation was derived solely based on principles of dynamics. The accuracy of the proposed SDOF methods was verified by analyzing experimental tests of low- and high-frequency floor specimens reported in the literature. Additionally, to assess the application range of the proposed methods, a thorough parametric study was carried out on 67 floors in which standard design parameters such as size, thickness, aspect ratio, support condition and floor system were changed. The performance of the proposed methods

was also compared against the SDOF method of AISC, which is commonly used across North America for the design and evaluation of floors under human-induced vibrations.

To further demonstrate the application and the advantages of the proposed SDOF methods, they were employed for vibration assessment of floors of modular hospitals. Because of their dimensions and lightweight, modular floors typically have natural frequencies well beyond the application range of existing design and analysis procedures. In addition, the floor vibration requirements for healthcare facilities are very stringent, requiring reliable analysis methods that can accurately predict the peak acceleration due to walking. To carry out this part of the research, first a schematic design of a modular hospital was proposed based on the relevant Canadian standards; the main focus of the proposed design was on the hospital layout and structural details of modules, particularly the floors. In a three-phase study, a total of 12 floor designs were considered for the proposed modular hospital. The first phase included four floor designs with structural details similar to those used in conventional construction. In the second phase, the section sizes of the floors of Phase 1 were increased to satisfy the vibration requirements of hospitals. In the third phase, high-performance lightweight materials were used to reduce the self-weight of the floors, making them suitable for modular construction. The vibration response of each floor was evaluated using the FE analysis method, the proposed SDOF method, and the AISC-SDOF method. At the end, the effects of considering inter-module connections and exterior walls on the floor vibration response were also investigated.

6.2 Conclusions

Based on the results of this research study, the following conclusions can be drawn:

- Comparison of the analysis results of different FE models showed that considering the spatial variation of the walking load does not have much influence on the peak acceleration of the floor.

- The analysis results confirmed that the Fourier series can simulate the force-time history of walking on low-frequency floors reasonably well. It was also found that the force-time history of walking load for high-frequency floors can be represented with a simple ramp and hold function developed by matching the initial slope of the forcing function with the actual walking impulse.

- The proposed SDOF method accurately captured the peak acceleration of all analysis cases ranging from flexible floors with frequencies as low as 4 Hz to extremely stiff floors with frequencies up to 60 Hz. The mean and standard deviation of the peak acceleration ratio for all 67 floor cases were 0.97 and 0.17, respectively, which demonstrate an excellent correlation between the proposed SDOF method and the FE analysis results throughout the entire range of floor frequencies. The broad application range of the proposed method is mainly because of its rational basis and development of the formulation without using any calibration factor.

- The analysis results showed that the SDOF method of AISC overestimated the peak acceleration of almost all low- and high-frequency floors. The level of overestimation of the peak acceleration increased as the natural frequency of the floors reduced. The AISC-SDOF method performed reasonably well for floors with natural frequencies between 6.5 Hz and 13 Hz.

- In general, the SDOF method of AISC performed better for low-frequency floors than for high-frequency floors, which is expected as the main focus of AISC is on the response amplification due to the resonance effect in low-frequency floors.
- In terms of the floor type, the AISC-SDOF method only predicted the peak acceleration of the normal weight concrete solid floor and the composite steel deck floor well while significantly overestimating the results for the lightweight concrete solid floor and the CLT floor. This overestimation is attributed to the empirical expressions used in the AISC method, which are not calibrated for floors made from such materials.
- The analysis results on modular floors showed that typical floor designs used in conventional construction do not meet the strict vibration limits for hospitals when applied to modular construction.
- Increasing the thickness and section size of joists and girders of conventional floors in order to meet the vibration requirements of hospitals led to a significant increase in the floor weight, making it not suitable for modular construction. The timber concrete composite (TCC) floor and hollow core floor performed better as their weight was about 25% less than that for the solid concrete floor and steel-concrete composite floor.
- By replacing the structural steel joists and normal strength concrete with light gauge steel joists and high strength lightweight concrete, the average floor weight was reduced by 37%, yet the vibration levels remained unchanged and below the code limits. Also, using the glass fibre reinforced polymer (GFRP) floor with a truss-shaped cross-section further reduced the floor weight by 43% while still meeting the vibration limits of hospitals. All

these floor designs were deemed appropriate for modular hospitals because of their lightweight and adequate vibration performance.

- By using fixed inter-module connections and considering exterior walls in the FE model, the stiffness of the floor increased, which resulted in higher natural frequencies and reduced vibration levels. The reduction in the peak acceleration by using fixed inter-module connections was 23%, while this reduction for considering exterior walls in the model was 10%. Considering these factors and other floor stiffening methods in the vibration assessment provide engineers with more flexibility in the design of modular floors while meeting the strict vibration requirements for hospitals.

- From the parametric and verification studies it is confirmed that the proposed SDOF method provides more accurate results compared to AISC's SDOF method over a wide range of frequencies, especially for high-frequency floors. This was expected as the proposed SDOF method is purely based on the fundamentals of dynamics, however, the AISC's SDOF method is calibrated using a limited number of experimental tests. The proposed SDOF method can be considered as a reliable and simple vibration assessment method that can be implemented in the future editions of design codes.

6.3 Future Work

The following recommendations for future research and improvements on the proposed SDOF method for floor vibration assessment are suggested:

- The proposed SDOF method was developed for floors subjected to walking due to a single person. However, work is needed to extend the application of the proposed method for the vibration assessment of floors subjected to multi-person walking.

- More floor vibration experimental tests are needed to further verify the performance of the proposed SDOF method, especially for very high-frequency floors that are typically used for modular construction. Currently there has been no experimental data available for such highly stiff floors as the main focus of current design codes is on low-frequency floors in which resonance occurs. However, for sensitive areas like hospitals, even high-frequency floors can cause serious serviceability issues because of the stringent code requirements.
- Various techniques of floor stiffening to reduce the vibration level like increasing the moment capacity of the connections between the slab, joists and girders or using pre-tensioned or post-tensioned girders and joists need be investigated. Future research is needed to quantify the effect of each stiffening method on the vibration response of floors.
- In this research study hospital, the layout and design of modules are proposed that can be easily adapted in different layout configurations to meet the various functional requirements of hospitals. Further study is needed to investigate the design and performance of modular hospitals that were beyond the scope of this study.
- This research study focused on the development of layout and main aspects of design of modular hospitals based on Canadian codes as well as the vibration response of modular floors. Further study is needed to investigate other aspects of the design including lateral stability and design of other structural components such as connections, foundation, walls and ceilings.

References

Allen, D.E. and Murray, T.M. (1993), *"Design Criterion for Vibrations Due to Walking"*, Engineering Journal, AISC, Vol. 30, No. 4, pp. 117–129.

Annan, C.D. (2008), *"Applicability of Traditional Design Procedures to Modular Steel Buildings"*, Ph.D. Thesis, The University of Western Ontario, London, Ontario, Canada.

Annan, C.D., Youssef, M.A. and Naggar, E.N. (2009), *"Effect of Directly Welded Stringer-to Beam Connections on the Analysis and Design of Modular Steel Building Floors"*, Advanced Struct. Eng., Vol.12, pp. 373–383, https://doi.org/10.1016/j.jobe.2017.12.008.

Ansary, M.A., Reja, M.Y. and Jahan, I. (2010), *"Rethinking the Public Building as Post Disaster Shelters -In the Context of Old Dhaka"*, Proceedings of the 9th U.S. National and 10th Canadian Conference on Earthquake Engineering, Canada.

Bachmann, H. and Ammann, W. (1987). *"Vibrations in Structures, Induced by Man and Machines"*, No. 3, IABSE, Switzerland.

Betram, N., Fuchs, S., Mischke, J., Palter, R., Strube, G., and Woetzel J. (2019), *"Modular Construction: From Projects to Products"*, Capital Projects and Infrastructure, Mckinsey and Company.

Biggs, J.M. (1964), *"Introduction to Structural Dynamics"*, Mcgraw-Hill, Inc, United States of America.

Casagrande, D., Giongo, I., Pederzolli, F., Franciosi, A. and Piazza, M. (2018), *"Analytical, Numerical and Experimental Assessment of Vibration Performance in Timber Floors"*, Engineering Structures, Vol. 168, pp. 748-758, http://dx.doi.org/10.1016/j.engstruct.2018.05.020.

Chen, L.K., Yuan, R.P., Ji, X.J., Lu, X.Y., Xiao, J., Tao, J.B, Kang, X., Li, X., He, Z.H., Quan, S. and Jiang L.Z. (2021), *"Modular Composite Building in Urgent Emergency Engineering Projects: A Case Study of Accelerated Design and Construction of Wuhan Thunder God Mountain/ Leishenshan hospital to COVID-19 Pandemic"*, Automation in Construction, Elsevier, Vol. 124. https://doi.org/10.1016/j.autcon.2021.103555

Chen, S., Zhang, Z., Yang, J., Wang, J., Zhai, X., Barnighausen, T. and Wang, C. (2020), *"Fangcang Shelter Hospitals: A Novel Concept for Responding to Public Health Emergencies"*, Lancet, Vol. 395, https://doi.org/10.1016/S0140-6736(20)30744-3.

Chen, Z., Li, H., Chen, A., Yu, Y. and Wang, H. (2017), *"Research on Pretensioned Modular Frame Test and Simulations"*, Eng. Struct., Vol. 151, pp. 774–787, http://dx.doi.org/10.1016/j.engstruct.2017.08.019.

Chopra, A.K. (2011), *"Dynamics of Structures, Theory and Applications to Earthquake Engineering"*, No. 4, Prentice Hall, United States of America.

CSA Committee A23.3 (2019), *"Design of Concrete Structures (CSA A23.3:19)"*, Canadian Standards Association.

CSA Committee O86 (2014), *"Engineering Design in Wood (CSA O86:14)"*, Canadian Standards Association.

CSA Committee S16 (2019), *"Design of Steel Structures (CSA S16:19)"*, Canadian Standards Association.

CSA Committee Z8000 (2018), *"Canadian Health Care Facilities (CSA Z8000:18)"*, Canadian Standards Association.

CSI (2018), *"Analysis Reference Manual for SAP2000, ETABS, SAFE, and CSI-Bridge"*, Computers and Structures Inc., Berkeley, C.A., United States of America.

CAE (2020), *"Abaqus/ CAE User's Manual"*, Dassault Systems Simulia Corp., Providence, RI, United States of America.

Davis, D.B. (2008), *"Finite Element Modeling for Prediction of Low Frequency Floor Vibrations Due to Walking"*, Ph.D. Thesis, Virginia Polytechnic Institute and State University, Blacksburg, Virginia, United States.

Davis, D.B. and Murray, T.M. (2007), *"Comparisons of Measured Natural Frequencies Method"*, M.S. Thesis, Virginia Polytechnic Institute and State University, Blacksburg, Virginia, United States.

EN 1995-1-1 (2004), *"A2, Eurocode 5: Design of Timber Structures – Part 1–1: General–Common Rules and Rules for Building"*, CEN, European Committee for Standardization, Brussels Belgium.

Fathieh, A. (2013), *"Nonlinear Dynamic Analysis of Modular Steel Buildings in Two and Three Dimensions"*, Master's Thesis, University of Toronto, Canada.

Fathieh, A. and Mercan, O. (2016), *"Seismic Evaluation of Modular Steel Buildings"*, Eng. Struct., Vol.122, pp. 83–92, http://dx.doi.org/10.1016/j.engstruct.2016.04.054.

Galbraith, F.W. and Barton, M.V. (1970), *"Ground Loading from Footsteps"*, Journal of Acoustical Soc. of America, Vol. 48, No.5, https://doi.org/10.1121/1.1912271.

Gallagher, K.A. (2013), *"Modular Construction: Hidden Hazards Within",* Fire Engineering, PennWell Corporation, Tulsa, pp. 73–78.

Giriunas, K., Sezen, H. and Dupaix, R.B. (2012), *"Evaluation, Modeling, and Analysis of Shipping Container Building Structures"*, Eng. Struct., Vol. 43, pp 48–57, http://dx.doi.org/10.

Gorgolewski M.T., Grubb, P.J. and Lawson, R.M. (2001), *"Modular Construction Using Light Steel Framing: Design of Residential Buildings"*, The Steel Construction Institute, Ascot, Berkshire, England.

Gunawardena, T. (2016), *"Behaviour of Prefabricated Modular Buildings Subjected to Lateral Loads"*, Ph.D. Thesis, The University of Melbourne, Melbourne, Australia.

Gunawardena, T., Ngo, T.D., Mendis, P., Aye, L. and Alfano, J. (2013), *"Structural Performance under Lateral Loads of Innovative Prefabricated Modular Structures"*, in: Samali, Song Attard (Eds.), Materials to Structures: Advancement Through Innovation, Taylor & Francis, London.

Ha, T.H., Cho, B.H., Kim, H. and Kim, D.J. (2016), *"Development of an Efficient Steel Beam Section for Modular Construction based on Six-Sigma"*, Adv. Material Science Eng., Vol. 2016, Article ID. 9687078, http://dx.doi.org/10.1155/2016/9687078.

Harper, F.C., (1962), *"The Mechanics of Walking"*, Research Application in Industry, Vol. 15, No.1.

Harrison, B.F. (2003), *"Blast Resistant Modular Buildings for the Petroleum and Chemical Processing Industries"*, J. Hazard. Mater., Vol. 104, pp. 31–38, http://dx.doi.org/10.1016/s0304-3894(03)00232-2.

Hicks, S. (2004), *"Vibration Characteristics of Steel-Concrete Composite Floor Systems"*, Progress in Structural Engineering and Materials, Vol. 6, pp. 21-38, https://doi.org/10.1002/pse.163.

Highway Traffic Act Ontario (2020), R.S.O. 1990, c. H.8.

Hong, S.G., Cho, B.H., Chung, K.S. and Moon, J.H. (2011), *"Behavior of Framed Modular Building System with Double Skin Steel Panels"*, J. Constr. Steel Res., Vol. 67, pp. 936–946, http://dx.doi.org/10.1016/j.jcsr.2011.02.002.

Hu, L. and Gagnon, S. (2012), *"Controlling Cross-Laminated Timber (CLT) Floor Vibrations: Fundamentals and Method"*, In: Proceedings of World Conference Timber Engineering – Institute (SCI) Entitled, New Zealand.

Smith, A.L., Hicks, S.J. and Devine, P.J. (2009), *"Design of Floors for Vibration: A New Approach"*, SCI Publication P354, The Steel Construction Institute, Silwood Park, Ascot, Berkshire, England.

Kerr, S.C. (1998), *"Human Induced Loading on Staircases"*, Ph.D. Thesis, University of London, London, United Kingdom.

Knippers, J. and Gabler, M. (2006), *"New Design Concepts for Advanced Composite Bridges - The Friedberg Bridge in Germany"*, IABSE Symposium Report, Vol. 92, No.10, pp. 16-23, 0.2749/222137806796185012.

Lacey, Chen, Hao, Bi (2018), *"Structural Response of Modular Buildings – An overview"*, Journal of Building Engineering, Vol. 16, pp. 45-56, https://doi.org/10.1016/j.jobe.2017.12.008.

Lawson (2017), *"AFCEC Conducts CONEX Dorm Field Testing"*, News Article. ⟨http://www.afcec.af.mil/News/Article-Display/Article/1157092/afcec-conducts-conex-dorm-field-testing/⟩.

Lawson, R.M and Ogden, R.G. (2008), *"Hybrid Light Steel Panel and Modular Systems"*, Thin Wall Struct. Vol. 46, pp. 720–730, http://dx.doi.org/10.1016/j.tws.2008.01.042.

Lawson, R.M., Ogden, R.G. and Goodier, C. (2014), *"Design in Modular Construction"*, CRC Press, Boca Raton, FL, USA.

Lawson, R.M., Ogden, R.G., Pedreschi, R., Grubb, P.J. and Popo-Ola, S.O. (2005), *"Developments in Prefabricated Systems in Light Steel and Modular Construction"*, Struct. Eng., Vol. 83, pp. 28–35.

Lawson, R.M. and Richards, J. (2010), *"Modular Design for High-Rise Buildings"*, Proc. Inst. Civ. Eng. Struct. Build., Vol. 163, pp. 151–164.

Li, Y. and Yang, X. (2021), *"Study on hospital design and its transition during pandemic situation"*, M. S. Thesis, Politecnico di Torino, Turin, Italy.

Liu, Davis (2015), *"Walking Vibration Response of High-Frequency Floors Supporting Sensitive Equipment"*, J. Struct. Eng., ASCE, Vol. 141, No. 8, https://doi.org/10.1061/(ASCE)ST.1943-541X.0001175.

Manalo, A., Aravinthan, T., Fam, A. and Benmokrane, B. (2017), *"State-of-the-Art Review on FRP Sandwich Systems for Lightweight Civil Infrastructure"*, J. Compos. Constr. Vol. 21, http://dx.doi.org/10.1061/(asce)cc.1943-5614.0000729.

Mohr, B. (1999), *"Floor vibrations. In: Proceedings of international council for research and innovation in building and construction"*, Working Commission W18 Timber Structures– CIB W18, Graz, Austria.

Murray, T.M, Allen, D.E., Ungar, E.E. and Davis, D.B. (2016), *"Design Guide 11 Vibration of Steel-Framed Structural Systems Due to Human Activity"* AISC, Vol. 11, No. 2.

Ngo, T.D., Nguyen, Q.T. and Tran, P. (2016), *"Heat Release and Flame Propagation in Prefabricated Modular Unit with GFRP Composite Facades"*, Build. Simululation, Vol. 9, pp. 607–616, http://dx.doi.org/10.1061/(asce)ae.1943-5568.0000214.

Nilsson (1976), *"Impact Loads Produced by Human Motion, Part 1"*, Document D13, Swedish Council for Building Research, Stockholm, Sweden.

Nilsson (1980), *"Impact Loads Produced by Human Motion, Part 2"*, Document D20, Swedish Council for Building Research, Stockholm, Sweden.

Ohlsson (1998), *"Springiness and Human Induced Floor Vibrations – A Design Guide"*, Swedish Council for Building Research, Stockholm, Sweden.

Ohlsson, S.V., (1982), "*Floor Vibration and Human Discomfort"*, Chalmers University of Technology, Goteborg, Sweden.

Owens, P.J, Forgione A. and Briggs, S. (2005), *"Challenges of International Disaster Relief: Use of a Deployable Rapid Assembly Shelter and Surgical Hospital"*, Emergency Nurses Association, https://doi.org/10.1016/j.dmr.2004.10.004.

Park, Moon, Lee, Bae and Roeder (2016), *"Embedded steel column-to foundation connection for a modular structural system"*, Eng. Struct., Vol. 110, pp. 244–257, http://dx.doi.org/10.1016/j.engstruct.2015.11.034.

Petrova, E., Farinholt, T., Joshi, T.P., Moreno, H., Mohajer, M.A., Patel, S.M., Petrosino, J. and Anandasabapathy, S. (2021), *"A Community-Based Management of COVID-19 in a Mobile Container Unit"*, MDPI, Basel, Switzerland, https://doi.org/10.3390/vaccines9111362.

Rainer, J.H., Pernica, G. and Allen, D.E. (1988), *"Dynamic Loading and Response of Footbridges"*, Structures Section, Institute for Research in Construction, National Research Council of Canada, Vol. 15, pp. 66-71.

Ratti, C. (2021), *"Converts Shipping Containers into Intensive-Care Pods for the Covid-19 Pandemic"*, from https://www.archdaily.com/936247/ carlo-ratti-converts-shipping-containers-into-intensive-care-pods-for-the-covid-19-pandemic, News Article.

Sladki, M.J. (1999). *"Prediction of Floor Vibration Response Using the Finite Element"*, Wood Science and Technology Centre, Fredericton, Canada, http://hdl.handle.net/10919/36023.

Styles, A.J., Luo, F.J., Bai, Y. and Murray-Parkes, J.B. (2016), *"Effects of joint rotational stiffness on structural responses of multi-story modular buildings"*, Proceedings of the International Conference on Smart Infrastructure and Construction, ICE Publishing, London, pp. 457–62.

Summers, P.B. (2008), *"Design of modular blast-resistant steel-framed buildings in petrochemical facilities"*, Structures Congress: Crossing Borders, Canada, American Society of Civil Engineers, Vancouver, pp. 1557–1563.

Timoshenko, S. and Woinowsky-Krieger, S. (1989), *"Theory of Plate and Shells"*, No. 2, McGraw-Hill, United States of America.

Tuan, C. Y. and Saul, W. E. (1985), *"Loads due to Spectator Movements"*, ASCE Journal of Structural Engineering, Vol. 111, pp. 418- 434, https://doi.org/10.1061/(ASCE)0733-9445(1985)111:2(418).

Willford, M., Field, C. and Young, P. (2007), *"Improved Methodologies for the Prediction of Footfall-Induced Vibration"*, ASCE.

Willford, M. and Young, P. (2006), *"A Design Guide for Footfall Induced Vibration of Structures"*, The Concrete Center.